Solitons, vortices and shell structure in ultracold atomic quantum systems

Eriksson, Gunnar

2020

Document Version:
Publisher's PDF, also known as Version of record

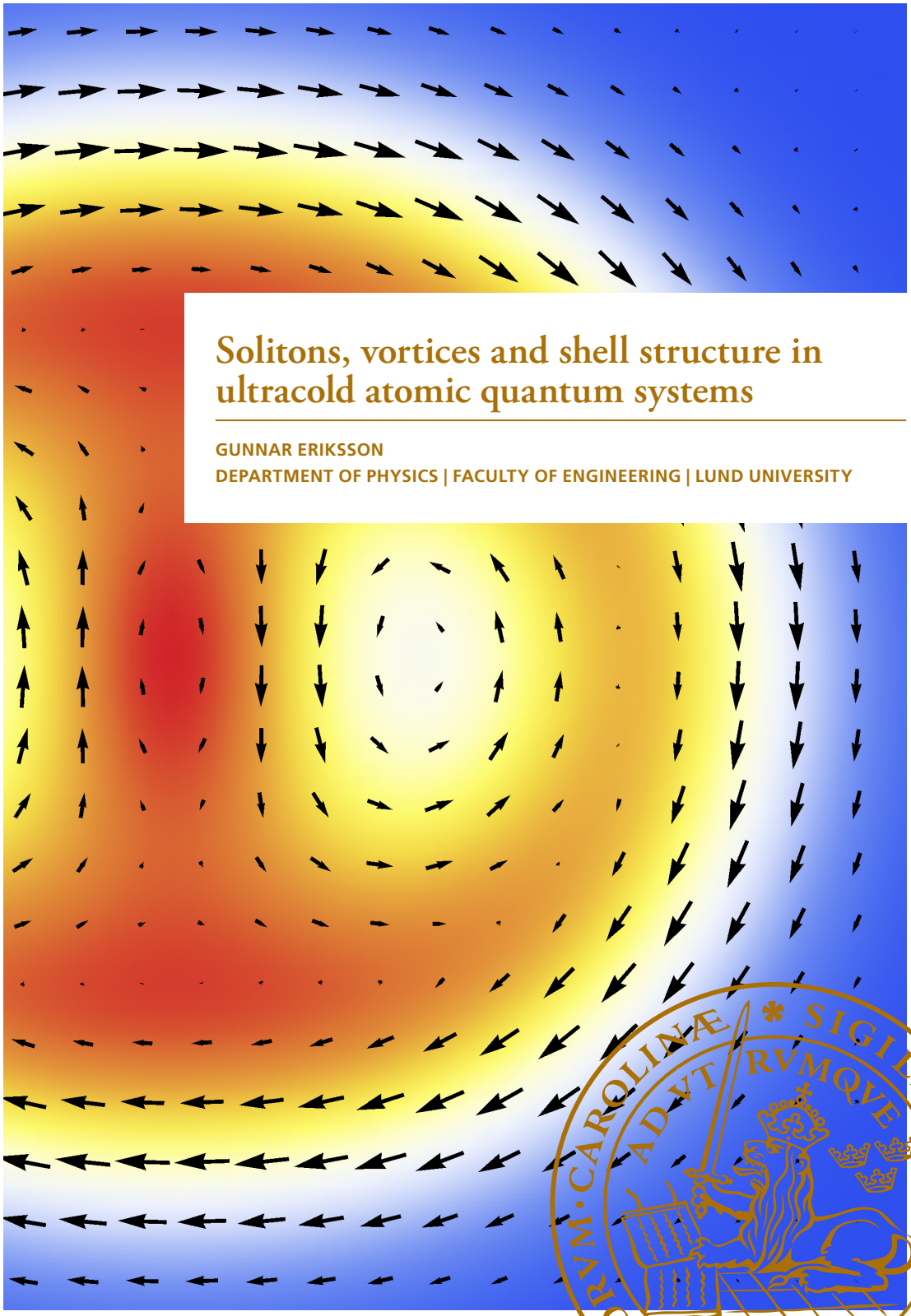

Solitons, vortices and shell structure in ultracold atomic quantum systems

GUNNAR ERIKSSON
DEPARTMENT OF PHYSICS | FACULTY OF ENGINEERING | LUND UNIVERSITY

Printed by Media-Tryck, Lund 2020 NORDIC SWAN ECOLABEL 3041 0903

Faculty of Engineering
Department of Physics
Division of Mathematical Physics

ISBN 978-91-7895-452-0

Solitons, vortices and shell structure in ultracold atomic quantum systems

Solitons, vortices and shell structure in ultracold atomic quantum systems

by Gunnar Eriksson

LUND
UNIVERSITY

Dissertation for the degree of
Doctor of Philosophy in Engineering
Thesis advisors: Stephanie Reimann, Sven Åberg and Jakob Bengtsson
Faculty opponent: Anna Minguzzi

Academic dissertation which, by due permission of the Faculty of Engineering at Lund University, will be publicly defended on Thursday, March 26th, 2020, at 9:00 in Lundmarksalen at Lund Observatory, Sölvegatan 27, Lund, for the degree of Doctor of Philosophy in Engineering.

Organization
LUND UNIVERSITY

Department of Physics
Division of Mathematical Physics
Box 118, 221 00 LUND,
Sweden

Document name
DOCTORAL DISSERTATION

Date of issue
2020-03-26

Sponsoring organization

Author(s)
Gunnar Eriksson

Title
Solitons, vortices and shell structure in ultracold atomic quantum systems

Abstract
This dissertation deals with finite-size effects in a few different quantum many-body phenomena in ultracold atomic systems. The finite-sized systems were simulated numerically using both mean-field methods and methods beyond mean-field, e.g. quadratic configuration interaction and exact diagonalization. The thesis is based on five scientific papers:

Paper I is about the finite-size effects in the dynamics of a few-body soliton-like state. The collapses and revivals of the solitary wavefront in the particle density is characterized both analytically and numerically in the limit of weak interactions.

Paper II analyzes a scheme to renormalize the contact interaction when used for exact diagonalization in a two-dimensional space. By relating the coupling strength in the diagonalization using the two-particle system, for which regularized solutions exists, converged results are obtained.

Paper III deals with the formation of quantized vortices when stirring a harmonically trapped finite-sized system with a quadrupole deformation. I the energy spectrum the avoided crossing is found to be described by either of two types of correlated states. The type of avoided crossing can be controlled by the inclusion of an extra quartic deformation. Hysteresis in the mean-field description is found to be related to the types of avoided crossings exhibited and the full many-body time-evolution is compared to mean-field results.

Paper IV investigates vortices in rotating fermionic droplets with dipole-dipole interactions. The vortex structure is found to still be present after the interaction is made anisotropic by having the dipoles tilt.

Paper V contains an investigation of the effects on shell structure in fermionic droplets with dipole-dipole interactions. For a anisotropic harmonic oscillator, by tilting the dipoles, the shell structure of an isotropic oscillator can be restored.

Key words
few-body physics, finite-size effects, solitary waves, quantized vortices, quantum hysteresis, shell structure, dipolar interactions

Classification system and/or index terms (if any)

Supplementary bibliographical information

Language
English

ISSN and key title

ISBN
978-91-7895-452-0 (print)
978-91-7895-453-7 (pdf)

Recipient's notes

Number of pages
170

Price

Security classification

Distributor
Gunnar Eriksson, Division of Mathematical Physics, Department of Physics, Sölvegatan 14, S-223 62 Lund, Sweden

Signature 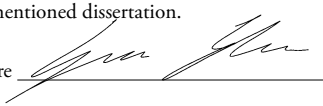 Date 2020-02-18

Solitons, vortices and shell structure in ultracold atomic quantum systems

by Gunnar Eriksson

LUND
UNIVERSITY

A doctoral thesis at a university in Sweden takes either the form of a single, cohesive research study (monograph) or a summary of research papers (compilation thesis), which the doctoral student has written alone or together with one or several other author(s).

In the latter case the thesis consists of two parts. An introductory text puts the research work into context and summarizes the main points of the papers. Then, the research publications themselves are reproduced, together with a description of the individual contributions of the authors. The research papers may either have been already published or are manuscripts at various stages (in press, submitted, or in draft).

Cover illustration: Particle density and probability current for the state with two vortices in a fermionic droplet with dipole-dipole interactions. Adapted from Figure 3 in Paper IV.

Faculty of Engineering, LTH, Department of Physics
Division of Mathematical Physics

ISBN: 978-91-7895-452-0 (print)
ISBN: 978-91-7895-453-7 (pdf)

Printed in Sweden by Media-Tryck, Lund University, Lund 2020

Contents

List of publications and author's contributions

This thesis is based on the following publications, referred to by their Roman numerals:

I Finite-size effects in the dynamics of few bosons in a ring potential

G. Eriksson, J. Bengtsson, E. Ö. Karabulut, G. M. Kavoulakis, and S. M. Reimann

J. Phys. B: At. Mol. Opt. Phys. 51 (2018) 035504

For this paper, I derived the formula for the time-evolution of the many-body state. I wrote all the computer code and performed all simulations for many-body time-evolution. I also produced all figures, participated in the analysis of the data and helped in the preparation of the manuscript.

II On the renormalization of contact interactions for the configuration-interaction method in two- dimensions

M. Rontani, **G. Eriksson**, S. Åberg and S. M. Reimann

J. Phys. B: At. Mol. Opt. Phys. 50 (2017) 065301

I wrote the computer code and performed the simulations for the systems with $N = 4$ and 5. I produced Figures 4, 5, 8 and 9, participated in the analysis of the data and helped in the preparation of the manuscript.

III Two-state model for vortex nucleation in a rotating Bose-Einstein condensate

G. Eriksson, J. Bengtsson, G. M. Kavoulakis, and S. M. Reimann

Physical Review A 100 (2019) 063638

I wrote the computer code and performed all numerical simulations for this paper. I produced all figures, participated in the analysis and wrote parts of the manuscript. I produced and performed all the simulations and analysis for the additional study of hysteresis in this system presented in this thesis.

IV Vortices in fermion droplets with repulsive dipole-dipole interactions

G. Eriksson, J. C. Cremon, M. Manninen, and S. M. Reimann

Physical Review A 86 (2012) 043607

I produced the computer code and ran all simulations for this paper. I made all figures, participated in the analysis and wrote a first version of the manuscript.

V Interplay between shell structure and trap deformation in dipolar fermi gases

J. Bengtsson, **G. Eriksson**, J. C. Cremon, J. Josefi and S. M. Reimann

Manuscript

I wrote the initial computer code that was later used in parallel for testing and validation of the final code. I participated in the analysis and helped with producing the figures and writing the manuscript.

Populärvetenskaplig sammanfattning

En samling av partiklar som interagerar med varandra är ett komplicerat system att försöka beskriva. Hur en enskild partikel uppför sig beror på hur de resterande partiklarna beter sig. Detta gör att det blir väldigt svårt att förutbestämma vad som kommer att hända med hela systemet även om vi har en mycket god uppfattning om hur de fundamentala rörelseekvationerna ser ut. Särskilt komplicerat blir kvantmekaniska system där vi, till skillnad från i klassisk mekanik, i någon mening måste ta hänsyn till alla möjliga händelser samtidigt. Det är dock viktigt att studera hela samlingen av dessa växelverkande partiklar då mycket av deras beteende kommer från just växelverkan. Nya fenomen kan uppkomma som inte alltid inses direkt från rörelseekvationerna för de enskilda partiklarna och vars behandling kan kräva nya koncept, regler och angreppssätt. Helheten kan helt enkelt vara mer än summan av dess delar.

Det finns många system av växelverkande partiklar i naturen som måste beskrivas med hjälp av kvantmekanik och vars beteende påverkar oss dagligen. Atomkärnor, elektroner som är bundna till kärnan, molekyler och metaller är några exempel. Vi människor har även skapat våra egna kvantsystem, både för att lättare kunna undersöka de naturliga motsvarigheterna, men även dess tekniska tillämpningar. Exempel är bland annat små kluster av metallatomer som uppför sig liknande atomkärnor och nanometerstora strukturer av halvledarmaterial som fångar in ett fåtal elektroner vilka kan fås att efterlikna elektronerna i en atom.

Ett annat artificiellt mångpartikelsystem som på senare tid blivit mycket populärt att undersöka är atomer som hålls infångade med hjälp av laserljus. Det har visat sig, kanske något överraskande, att atomerna i en gas går att stoppa och hålla kvar

på en specifik plats genom att lysa med en väl vald laser på dem. Några fördelar med dessa ljusbaserade infångningsmetoder är bland annat att atomerna är väldigt isolerade från omgivningen och att de kan kylas ner till otroligt låga temperaturer, så att de kvantmekaniska aspekterna blir direkt synliga. De kalla atomsystemen är dessutom väldigt anpassningsbara så till den grad att det nästan bara är fantasin hos forskarna som sätter gränsen. Än så länge saknas vardagliga tillämpningar av de kalla atomsystemen. Istället har de används till att öka den grundläggande förståelsen av kalla atomsystem i synnerhet och mångpartikelsystem i allmänhet. En möjlig framtida tillämpning är att med hjälp av kalla atomer bygga komponenter som använder något mångapartikelfenomen för att efterlikna dagens elektronik, men som kan användas snabbare och mer effektivt. Då dagens elektronik inte verkar gå att skala upp så mycket mer kan detta vara en möjlig väg för fortsatt teknisk utveckling.

I den här avhandlingen har vi studerat hur några fenomen som är välkända i laserinfångade gaser av många atomer påverkas av antalet partiklar i gasen. Vi har i många fall jämfört egenskaper hos gaser med väldigt många partiklar mot en gas med färre atomer. I gasen med väldigt många partiklar är det rimligt att bara använda medelvärdet av påverkan mellan partiklarna, medan de exakta kvantmekaniska rörelseekvationerna kan lösas för systemet med få partiklar. Vi härledde bland annat en exakt formel för hur en ensam vågfront i partikeltätheten färdas runt i en ring. Utifrån det bestämde vi olika tidsskalor för hur vågfronten försvinner och sedan dyker upp igen, samt hur dessa tidsskalor beror på antalet partiklar i ringen.

Kvantiserade virvlar är en annan karaktäristisk egenskap hos ett kvantmekaniskt system och vi har studerat dessa på flera olika sätt. En av undersökningarna gällde hur virvlarna skapas när en samling partiklar roteras. Beroende på formen av behållaren som innesluter partiklarna kunde vi observera två olika sätt som dessa virvlar uppstår. Det krävs dock ett större antal partiklar innan de olika sätten kan särskiljas och beteendet är då mycket annorlunda från fallet när antalet partiklar är väldigt litet. Vi fann också att dessa två typer av virvelbildningar bestämmer om systemet uppvisar hysteres, fenomenet att övergången inte sker på samma plats beroende på om man ökar eller minskar rotationen, eller inte. Virvlar kan också skapas när partiklarna växelverkar som dipoler, vilket vi visade i en annan studie. Dessa dipoler kan liknas vid små stavmagneter som repellerar eller attraherar varandra beroende på deras orientering. En sådan växelverkan har nyligen blivit möjlig att ha i experiment med kalla atomgaser.

Kalla atomer kan också uppvisa skalstruktur, ett fenomen som kommer från en underliggande symmetri hos systemet och är känt från många naturliga system såsom hur atomernas elektroniska struktur samt atomkärnan är uppbyggda. Vi undersökte hur denna skalstruktur påverkades av växelverkan mellan dipoler och hur egenskaperna hos systemet kunde ändras med hjälp av egenskaper hos denna växelverkan.

Popular science summary

A collection of particles that interacts with each other is a complicated system to try to describe. How a single particle behaves depends on how the remaining particles behave. This makes it very difficult to predict what will happen with the whole system even if we have a very good understanding of how the fundamental equations of motion look like. Especially complicated becomes quantum mechanical systems where we, unlike in classical mechanics, in some sense need to take into account all possible events at the same time. It is however important to study the whole collection of these interacting particles as much of their behavior precisely comes from the interactions. New phenomena can arise that can not always be realized directly from the equations of motion and whose treatment can demand new concepts, rules and approaches. The whole can simply be more than the sum of its parts.

There exist many systems of interacting particles in nature that have to be described with the help of quantum mechanics and whose behavior affects us daily. Atomic nucleus, electrons that are bound to the nuclei, molecules and metals are some examples. We humans have also created our own quantum systems, both to easier be able to investigate the natural counterparts, but also their technical applications. Examples are among other small clusters of metal atoms that behave like atomic nucleus and nanometer sized structures of semiconductors that traps a few electrons which can be made to mimic the electrons in an atom.

Another artificial many-particle system that lately has become very popular to study is atoms that are trapped with the help of laser light. It has been shown, maybe somewhat counterintuitively, that the atoms in a gas can be stopped and kept at a specific place by shining a cleverly chosen laser on them. Some advantages with these light based trapping methods are among other that the atoms are

very isolated from the environment and that they can be cooled down to incredibly low temperatures, such that the quantum mechanical aspects become directly observable. The cold atom systems are also very customizable to such a degree that only the scientist's imagination sets the limit. So far no everyday application exists for these cold atomic systems. Instead, they have been used to advance the basic knowledge of cold atoms systems in particular and many-particle systems in general. A possible future application is with the help of cold atoms to build devices that utilize some many particle phenomenon to imitate todays electronics, but can be used faster and more efficient. As todays technology does not seem to be able to scale up much more this can be a possible way for continued technological advancement.

In this thesis we have studied how some phenomena that are well known in laser trapped gases of many atoms are affected by the number of particles in the gas. We have in many cases compared properties of the gases with very many particles to a gas with less atoms. In the gas with very many particles it is reasonable to only use the mean value of the influence between the particles, while the exact quantum mechanical equations of motion can be solved for the system with few particles. Among other we derived an exact formula for how a solitary wavefront in the particle density traveled around in a ring. From this we determined different time scales for how the wavefront disappears and then comes back, as well as how these time scales depend on the number of particles in the ring.

Quantized vortices is another characteristic property of a quantum mechanical system and we have studied these in a number of different ways. One of the investigations were concerned about how vortices are created when a collection of particles is rotated. Depending on the shape of the container that encloses the particles we could observe two different ways these vortices can be created. However, it requires a larger number of particles before the different ways can be distinguished and the behavior is then much different from the case when the number of particles is very small. We also found that these two types of vortex formations determine if the system exhibit hysteresis, the phenomenon that the transition does not happen at the same place depending on if one increases or decreases the rotation, or not. Vortices can also form when the particles interact as dipoles, which we showed in another study. These dipoles can be seen as small bar magnets that repel or attract each other depending on their orientation. Such an interaction has recently become possible to attain in experiments with cold atomic gases.

Cold atoms can also exhibit shell structure, a phenomenon that comes from an underlying symmetry of the system and is known from many natural systems such as the electronic structure of atoms as well as how atomic nuclei are structured. We investigated how this shell structure was affected by the interaction between dipoles and how the properties of the system could be changed with the help of properties of this type of interactions.

Acknowledgments

For this thesis I would first like to thank my supervisors Stephanie, Sven and of course Jakob, with whom I have probably spent the most hours discussing. I would also like to thank Jonas for all the help at the beginning of my studies. A special thank you to Georgios, whose collaborations have been very important during this time. Together with my other collaborators Massimo, Elife and Josef, these are the main responsible for the completion of this thesis.

I am also very grateful for all the help from Katarina. No matter if the problem is big or small, professional or private, one can always count on your support. My roommates have also contributed to a good environment. I would like to give a special thank you to Fikeraddis and Emil with whom I have spent the most time and had the most discussions. Then there are all the other great people I have met at the division over the years. I would have liked to list you all and give you an individual thank you, but unfortunately the list would just be too long.

Without all the friends outside of physics I had before starting my studies, and all the ones I have made along the way, coming this far would have been much harder. I would especially like to thank Gustav and Stefan for all the adventures we have been to, and to the gang at Gerdahallen that have made me think of other things than my research. Finally, I would like to thank Carin, Göran and Erik. Your support over all these years have been invaluable.

Chapter 1

Introduction

In our quest to better understand the world around us we encounter many situations where we have to study how interacting bodies behave together. The scale of such systems can be very large, e.g. astronomical objects orbiting each other. On this scale classical mechanics and the theory of general relativity can be used to make predictions with good accuracy. Interacting systems can also be found on the very small scale, necessitating a quantum mechanical treatment instead. The governing equations for such systems are by now well established. However, these equations are notoriously difficult to solve for interacting systems with more than two particles, as the complexity grows extremely fast when their number increases. Thus, to understand large systems new concepts and perspectives often need to be used, as the behavior many times cannot be feasibly inferred from the basic laws that govern the microscopic constituents. The collective phenomena that emerge for large interacting systems can be seen as being equally fundamental as these basic laws [1]. To get a proper understanding of the world, we thus need to not only study the fundamental equations, but also the complete many-body systems. The phenomena they exhibit together with how the collective behavior is altered as the number of particles is changed is also important to investigate.

One may also go the other way around. Due to the macroscopic behavior and properties mentioned above, often when modeling a quantum mechanical many-body system one assumes it contains an infinite number of particles and extends over all of space. This is however only an approximation to the natural systems. At very large particle numbers the difference is usually negligible, but as the parti-

cle number is decreased these finite-size effects might become important, or even dominant. Another scientific challenge is thus to quantify these effects and understand how they alter the overall behavior.

Finite-sized quantum many-body systems of interacting particles can be found in many places in nature such as atomic nuclei, atoms and molecules. These systems, that in many ways could have direct implications on our lives, exhibit a vast collection of different behavior and phenomena, e.g. shell structure, non-linear effects, irrotational flow and strongly correlated states. In addition to the few-body systems found directly in nature, during the last couple of decades, several possibilities for creating artificial ones have been developed. Clusters of metallic atoms e.g. show many similarities to atomic nuclei [2, 3] and by confining electrons in semiconductor structures so called artificial atoms can be created [4]. Due to their similarities to the natural systems the artificial ones can be used to perform experiments that would be very difficult if done using real atoms or atomic nuclei.

This thesis will however focus on few-body systems in ultracold gases of atoms trapped and cooled by laser light. This is another type of a man-made collection of interacting particles that has matured in the last couple of decades. Now they are routinely used to study many-body effects in quantum-mechanical systems where they have many advantages compared to other types of artificial systems, such as being well isolated from their environment and the ability to observe and manipulate them using the precise tools of laser physics [5]. We have here examined how some phenomena known to appear in large, infinite, collections of atoms behave when the number of particles is reduced, but also how few-body systems that could be realized in atomic gases transition into their larger versions.

In Chap. 2 ultracold atomic gases and their basic properties will be introduced together with the basic concepts of many-body quantum mechanics. The numerical methods used to investigate these system will then be presented in Chap. 3. The main results of the studies will be given in Chap. 4 together with a brief outlook in Chap. 5. This is then followed by the papers this thesis is based on that are included at the end.

Chapter 2

Many-body quantum physics with ultracold atoms

This chapter introduces the many-body systems realizable with ultracold atoms that will be considered in this thesis. First, in Sec. 2.1, the trapping and cooling of the atoms using light and magnetic fields is discussed. Techniques for detection and manipulation will briefly be mentioned as well. The basic concepts of many-body quantum mechanics using the formalism of second quantization needed to describe these systems will be touched upon in Sec. 2.2. Here rotating systems will also be discussed. Many of the complicated phenomena that arise in ultracold atomic systems come from interactions between the particles, we thus describe those in more detail. The short range interactions present in most ultracold atomic gases will be discussed first in Sec. 2.3. This is followed by a short introduction to long-range dipole-dipole interactions which have also been realized in experiments. Gases of ultracold atoms have also become a well-used platform to study degenerate quantum gases, a regime where quantum mechanical effects are prevalent. The basic principles of such degenerate gases will be briefly discussed in Sec. 2.4, especially the case of Bose-Einstein condensates for bosonic gases. This finally leads up to Sec. 2.5 where the recent progress in realizing few-body systems with a low and controllable number of particles will be discussed. Such few-body systems will be the main topic of the rest of the thesis.

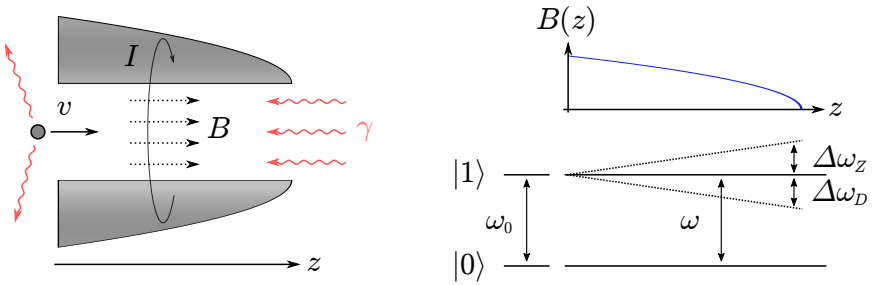

Figure 2.1: The left part shows a sketch of a Zeeman slower. The gray part is a solenoid through which the current I is running as indicated by the arrow. This creates a magnetic field B such that the intensity is varying along the z axis. If atoms are traveling with velocity v along the same axis, the varying magnetic field alters the transition frequency between two states $|0\rangle$ and $|1\rangle$ in the atoms by the amount $\Delta\omega_Z$. The solenoid is shaped such that this is the same frequency shift $\Delta\omega_D$ for the laser light photons γ due to the Doppler shift, as depicted to the right. This keeps the laser light with a fixed frequency ω in resonance with the transition along the whole solenoid. As the atoms absorb photons from the forward direction but emit in a random direction they experience a force slowing them down. Adapted from figures in [7, 8].

2.1 Trapping, cooling and detection of atoms

The cross-section for a collision between a photon and an atom has a large resonant enhancement if the energy of the incoming photon is matched to a transition in the atom. If the atom absorbs a photon, the change in momentum will result in a force opposite to the incoming light. The atom will eventually deexcite and send out another photon, but it will be in a random direction, such that the force from this process averages to zero. If a laser is tuned to a frequency slightly lower than an atomic transition it will slow down the atoms going towards the light source due to the Doppler shift bringing it into resonance. Because of the generated reduction in the average speed of the atoms in the gas, the temperature is also reduced. Using the Doppler shift to cool and slow down the motion of atoms is now a widely used technique and is described in more detail in many textbooks on the subject, e.g. see [6, 7]. The development of these techniques was first driven by the desire to improve atomic clocks and atomic spectroscopy, but it was soon realized that they could also be used to realize and probe very controlled quantum many-body systems [8].

The technique of laser cooling was first used to cool Mg ions in 1978 [9], but was later extended to a beam of neutral Na atoms in 1982 [10]. Here a varying magnetic field was used to keep the atoms in resonance with the laser as their

velocities continued to decrease. Such a device is called a Zeeman slower and Fig. 2.1 sketches how it works. A Zeeman slower can be used to initially slow down a beam of atoms, but it only operates in one direction and it does not produce a trapping potential.

By employing pairs of counter-propagating lasers in each of the three spatial directions, (x, y, z), one may create a region in which the atoms experience a significant damping of their velocities and hence the atoms stay in this region for a considerable amount of time. This is called the optical molasses technique and it can be used to further cool the gas before the atoms diffuse out of the central region [6, 7]. The optical molasses technique, however, does not provide a restoring force and hence does not actually trap the atoms. One way of creating a trap for the atoms is to add a pair of coils to the setup, producing a small magnetic field with a magnitude that is linear for small distances away from the origin. Together with using circularly polarized light such a magnetic field will result in an imbalance of the scattering force from the photons that depends on the distance from the center [6, 7]. Thus a restoring force is created, such that the particles feel a trapping potential with an approximately harmonic shape. This type of trap is called a magneto-optical trap and has become a widely used tool in atomic physics. The set-up of both the optical molasses technique and a magneto-optical trap is shown in Fig. 2.2.

Other ways of producing a trap for the atoms include using a magnetic field that is varying in space. Some of the hyperfine states of the atom, the so called low-field-seekers, increase in energy as the strength of the magnetic field is increased. As the name suggests, this will result in a restoring force to a region where the field has a minimum [7]. However, if one uses a quadrupole field, as in the magneto-optical trap, the minimum is a zero field and the levels can mix into a state that is not trapped and hence the atoms can escape. The hole in the middle of the trap has to be plugged in some way and this can be done by e.g. adding a time-varying magnetic field to the trap, or adding a static field in the perpendicular direction. Adding such fields to the trap will, for small distances from the center, produces a harmonic potential [6, 7]. In the left part of Fig. 2.3 the resulting magnetic field for a commonly used set-up is shown.

There are however some reasons for not using a magnetic field to trap the atoms, e.g. wanting to use the magnetic field to tune the interactions which will be briefly mentioned in Sec. 2.3. Fortunately there are techniques where one uses only laser

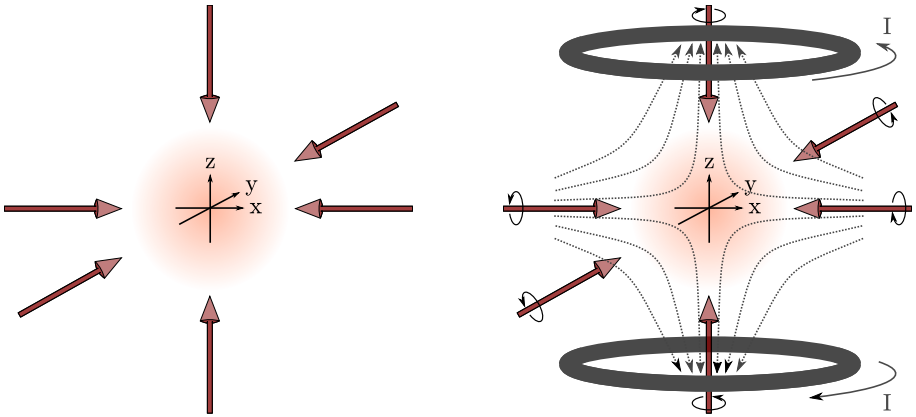

Figure 2.2: The left part shows the setup of the six lasers used in the optical molasses technique. Similar to the Zeeman slower in Fig. 2.1 this causes the atoms to experience a force F proportional to, and in the the opposite direction of, their velocity v. Here α is the proportionality constant. Adding a pair of coils carrying a current I as the arrows indicate on the right side creates a magnetic field. Together with making the laser light circularly polarized this results in a restoring force on the atoms, trapping them in the center. The force exerted on the atoms in the z direction now includes a term $-\beta z$, where β is the spring constant, and similarly in the other directions. Such a device is called a magneto-optical trap. Adapted after figures in [7].

light to trap the atoms. Due to the Stark shift of the energy levels of the atom when perturbed by an oscillating electric field, the atoms will feel a potential that is proportional to the intensity of the light [7]. This is sketched in the right part of Fig. 2.3. By focusing a laser beam, one can make the intensity vary in space and thus create an optical dipole trap for the atoms. As the shape of the optical dipole traps is basically only limited to the shape of the intensity, a large number of different geometries have been realized. Examples ranging from harmonic traps with possibly different trapping frequencies in the different directions, creating quasi-two or one-dimensional systems, to more exotic configurations such as tori [11], double wells [12] or small tunnel constrictions between bigger particle reservoirs [13]. One may also use this technique to obtain a periodic potential by producing a standing wave with the lasers. For such light fields the intensity obviously vary in space. The resulting periodic potentials are called optical lattices [6, 7] and has been used extensively in experiments with ultracold atoms [5].

Even though the optical molasses technique for alkali atoms cooled the gas to a temperature lower than was expected to be possible with Doppler cooling [14],

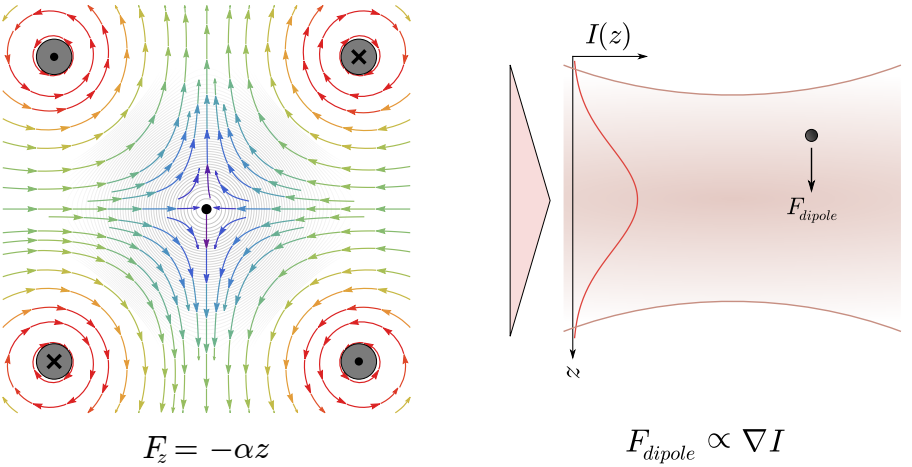

Figure 2.3: The resulting magnetic field of the four perpendicular conductors in gray, carrying current as indicated, is shown to the left. Field intensity is indicated by the colors of the field lines. Close to the center of the trap the resulting force on the atoms, given for the z direction in the figure, is approximately linear with respect to the distance from the center and with proportionality constant α. This results in a harmonic trap for the atoms. The resulting dipole force from the spatially varying light field intensity I is sketched in the right part of the figure. Here the force will be proportional to the gradient of the intensity. Adapted after [7].

it is possible to cool the gas to even lower temperatures. This is usually done by evaporative cooling, a technique that can be used for both magnetic and optical dipole traps. Schematically, this is done by cutting off the trap at some height and thus letting high energy atoms escape [6, 7]. The remaining atoms have a lower mean energy and thus, after thermalization, a lower temperature. In a magnetic trap one may instead use radio-frequency radiation to make the high-energy atoms escape the trap. As the magnetic field is varying with distance from the center, the transition between trapped and untrapped states of the atoms will also depend on the distance. Hot atoms will reach further from the center, so by tuning the radiation to match this distance these atoms will be made to escape the trap. In an optical dipole trap one has to lower the trap strength instead. Evaporative cooling has been successfully used to obtain temperatures of the order of nK in atomic gases [7]. Some parts of the history behind the breakthroughs of trapping and cooling neutral atoms can be found in the Nobel prize lectures from 1997 [8, 15, 16].

Once the atoms are cooled and trapped they can also be manipulated by the same techniques used to trap them, both by magnetic fields and optical dipole forces. The trap can e.g. be modulated in time to induce excitations in the gas. Another way to produce excitations is to use radio-frequency radiation to induce transitions

in the atoms that could affect the collective behavior of the gas. Most experiments rely on the imaging of the particle density. By turning off the trap and releasing the particles, as the particle cloud expands one can observe features too small to resolve directly. If one waits long enough after turning off the trap, distribution of particles will correspond to the momentum distribution of the system instead, due to the ballistic expansion of the cloud. This can thus be used to get more insight into the system. Performing a sequence of non-destructive measurements, or performing several release experiments after different times one may follow the time-evolution of the system. For a review of manipulation and detection techniques for ultracold atomic gases, see e.g. [17]. Recently there has been a lot of progress towards single-atom imaging, especially in optical lattice systems [18].

The systems realized using optical and magnetic trapping of neutral atoms are very isolated from the environment compared to e.g. semiconductor based electronic devices [19]. Combined with the very low temperatures obtainable, this makes them an excellent platform to investigate quantum mechanical many-body effects. Furthermore, these systems offer a wide range of powerful manipulation and detection techniques that are not available for other types of systems. For a review of some many-body phenomena that have been studied in these systems see [5]. Optical lattices have e.g. been used extensively in ultracold atomic experiments mimicking condensed matter models [20], where one can produce physical systems that are much cleaner than the electronic counterparts. It also offers the possibility to vary dimensionality, geometry, depth of the potential and including effects such as disorder or artificial magnetic fields [21]. Using the different hyperfine states of the atoms as a pseudo spin offers the possibility to study multi-component mixtures and other phenomena associated with spin, e.g. spin-orbit coupling [22]. Ultracold atoms have also been an advantage for studying dynamics of many-body systems, such as e.g. thermalization of a many-body quantum system [23] or the transport of particles between reservoirs [24].

2.2 Many-body quantum systems

In non-relativistic quantum mechanics, the time-evolution of the state $|\Psi(t)\rangle$ is governed by the Schrödinger equation

$$i\hbar\frac{\partial}{\partial t}|\Psi(t)\rangle = \hat{H}(t)|\Psi(t)\rangle, \tag{2.1}$$

where $\hat{H}(t)$ is the Hamiltonian of the system. In the case of a time-independent Hamiltonian, the above equation can be recast into an eigenvalue equation and the problem becomes finding eigenstates to observables that commute with the Hamiltonian, as the time-evolution is a trivial phase factor depending on the corresponding eigenvalues [25]. For an interacting N-body system, the Hamiltonian typically has the form

$$\hat{H} = \sum_{n=1}^{N} \hat{h}_0(n) + \sum_{n<m} \hat{V}_{int}(n,m), \tag{2.2}$$

where the sums run over the particles n and m, $\hat{h}_0$ is the single-particle part including the operators only acting on each particle separately, and where $\hat{V}_{int}$ is the pairwise-interaction between two particles. For systems of identical particles it is convenient to use the formalism of second quantization, see e.g. [26, 27]. One then uses the so called Fock states $|\Psi\rangle = |n_0, n_1, n_2, \ldots\rangle$ where only the occupations n_i of some single-particle orbitals $|\varphi_i\rangle$ are specified. Introducing a basis of Fock states, one can work with the creation and annihilation operators, $\hat{a}_i^\dagger$ and $\hat{a}_j$, which create and annihilate particles in the orbital $|\varphi_i\rangle$ and $|\varphi_j\rangle$ respectively. These operators satisfy a set of commutation or anticommutation relations depending on if the particles are bosonic or fermionic respectively, in this way taking care of the identical-particle symmetry properties. In second quantization, the Hamiltonian in Eq. (2.2) is transformed into

$$\hat{H} = \sum_{i,j} h_{ij}\, \hat{a}_i^\dagger \hat{a}_j + \frac{1}{2} \sum_{i,j,k,l} v_{ijkl}\, \hat{a}_i^\dagger \hat{a}_j^\dagger \hat{a}_l \hat{a}_k, \tag{2.3}$$

where the sums now run over the different orbitals instead of the different particles. In Eq. (2.3) one also only needs to be concerned about the matrix elements $h_{ij} = \int \varphi_i^*(\mathbf{r}) \hat{h}_0 \varphi_j(\mathbf{r}) d^D r$ and $v_{ijkl} = \int \varphi_i^*(\mathbf{r}) \varphi_j^*(\mathbf{r}') \hat{V}_{int} \varphi_k(\mathbf{r}) \varphi_l(\mathbf{r}') d^D r\, d^D r'$ of the operators $\hat{h_0}$ and $\hat{V}_{int}$ with respect to the single-particle orbitals, and with D being the dimension of the space.

Using the position eigenstates $|\mathbf{r}\rangle$ as the single-particle basis give rise to the so called field operators, $\hat{\Psi}^\dagger(\mathbf{r}, t)$ and $\hat{\Psi}(\mathbf{r}, t)$, which create and annihilate a particle at the specific position $\mathbf{r}$ respectively. Written as a sum of the previously used single-particle orbitals $|\varphi_i\rangle$ together with their respective annihilation or creation operator for given particle statistics, the field operators are given by $\hat{\Psi}(\mathbf{r}) = \sum_i \varphi_i(\mathbf{r}) \hat{a}_i$ and similarly for $\hat{\Psi}^\dagger(\mathbf{r})$. The field operators offer a more convenient

way to express observables depending on the spatial position, such as an inhomogeneous particle density. At time t, for the state $|\Psi(t)\rangle$, the particle density is given by $\rho(\mathbf{r},t) = \langle\Psi(t)|\hat{\Psi}^\dagger(\mathbf{r})\hat{\Psi}(\mathbf{r})|\Psi(t)\rangle$ giving the probability to find a particle at position $\mathbf{r}$, normalized to N. When working with the full solution to the Schrödinger equation, the eigenstates to the Hamiltonian will simultaneously be eigenstates to the symmetry operators commuting with the Hamiltonian. Thus, the internal structure can be hidden in, e.g., ρ. In order to reveal those structures, one may break the symmetry by using the pair-correlated density $\rho_c(\mathbf{r},\mathbf{r}',t) = \langle\Psi(t)|\hat{\Psi}^\dagger(\mathbf{r})\hat{\Psi}^\dagger(\mathbf{r}')\hat{\Psi}(\mathbf{r}')\hat{\Psi}(\mathbf{r})|\Psi(t)\rangle$. This quantity gives the probability of finding a particle at $\mathbf{r}$ given that one particle is at $\mathbf{r}'$.

In Papers I, III, IV and Sec. 4.4 we will consider rotating systems. To model this, we will make a transformation to a frame of reference that is rotating around a symmetry axis, here taken to be in the z direction, with angular velocity Ω. Making such a transformation results in an extra single-particle operator in the Hamiltonian. This term arises when considering the Schrödinger equation for the rotated state $|\tilde{\Psi}(t)\rangle = \hat{R}(t)|\Psi(t)\rangle$ [28], where the operator $\hat{R}(t) = e^{-i\theta(t)\hat{L}_z/\hbar}$ rotates the state by an angle θ around the z axis [25]. The Hamiltonian will then get an extra term $i\hbar\frac{\partial\hat{R}}{\partial t}\hat{R}^\dagger(t)$. By assuming that θ is varying in time according to $\theta(t) = -\int_{t_0}^{t}\Omega(t')\mathrm{d}t'$ where t_0 is the initial time and $\Omega(t)$ is the instantaneous angular velocity of the rotation, the time derivative $\frac{\partial\hat{R}}{\partial t} = \frac{i}{\hbar}\Omega(t)\hat{L}_z\hat{R}(t)$, we end up with the extra term $-\Omega(t)\hat{L}_z$ where $\hat{L}_z$ is the angular momentum in z. Furthermore, if all the operators in the lab frame are rotating with the same constant frequency Ω, the problem becomes time-independent in the rotating frame.

In the systems considered in this thesis, the single-particle part $\hat{h}_0$ of the many-body Hamiltonian, Eq. (2.2), can be written in the form

$$\hat{h}_0(t) = \frac{\hat{\mathbf{p}}^2}{2m} + u(\hat{\mathbf{r}},t) - \Omega(t)\hat{L}_z, \tag{2.4}$$

where $\hat{\mathbf{p}}$ is the momentum operator, $\hat{\mathbf{r}}$ is the position operator, $u(\hat{\mathbf{r}})$ is the trapping potential and the last term is for rotation. The trapping potential is usually taken to be the here isotropic harmonic oscillator $u(\hat{\mathbf{r}}) = \frac{1}{2}m\omega^2\hat{\mathbf{r}}^2$, where m is the mass of the particles and ω is the trapping frequency, as it is a good approximation to many of the potentials produced by the trapping techniques described in Sec. 2.1. In addition, we will also consider deformed traps such as an anisotropic oscillator confinement along the different axes, as well as ring shaped potentials $u(\hat{\mathbf{r}}) = \frac{1}{2}m\omega^2(\hat{\mathbf{r}}-R)^2$ with radius R.

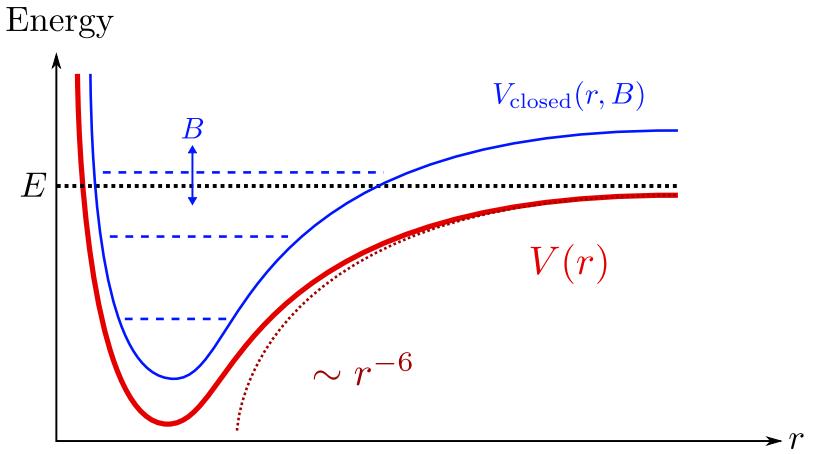

Figure 2.4: A schematic picture of the interaction potential for two atoms as a function of the relative distance r. The red curve shows the typical interaction potential in an open channel. The dotted red line shows the typical r^{-6} dependence of the long-range tail. The black-dotted line shows the energy E of the incident particle. The blue curve shows the closed channel used in a Feshbach resonance for which the energy of the bounded states, shown as dashed horizontal lines, is altered by the external magnetic field B. Adapted after [5].

2.3 Interactions in cold atomic systems

The interaction potential for particle-particle collisions in an ultracold gas of alkali atoms is usually rather complicated. Typically the atoms are strongly repulsive for very short distances, but the interaction have an attractive region for intermediate separations. As the relative distance approaches infinity the potential goes to zero with some power law dependence. A typical interaction potential $V(\mathbf{r})$, where $\mathbf{r}$ is the relative distance between the two particles, is sketched in Fig. 2.4. In a gas of atoms, the interaction potential is of van der Waals type and can be calculated using second order perturbation theory. It has the form $V_{\text{vdW}}(r) = -C_6/r^6$, where r is the magnitude of $\mathbf{r}$ between the two particles and C_6 is the strength of the interaction. See e.g. [29].

In principle one would need to solve the full time-dependent problem of the collision process. However, a time-independent treatment is sufficient to obtain the low-energy behavior [25, 30], which is usually what is important in ultracold atomic systems [5]. Consider a Hamiltonian $\hat{H}$ for the relative motion of two particles colliding assumed to be of the form $\hat{H} = \hat{H}_0 + \hat{V}$. Here $\hat{H}_0$ is the free

particle Hamiltonian with eigenstates $|\Phi_{\mathbf{k}}\rangle$ that are plane waves with momentum $\hbar\mathbf{k}$ and eigenenergy $E = \frac{\hbar^2 k^2}{2m_r}$, where $m_r = m/2$ is the reduced mass, and $\hat{V}$ is the interaction potential. The outgoing scattered state $|\Psi_{\mathbf{k}}^{(+)}\rangle$ of an elastic collision for such a system is given by the Lippmann-Schwinger equation [25], which in the spatial representation is

$$\langle \mathbf{r}|\Psi_{\mathbf{k}}^{(+)}\rangle = \langle \mathbf{r}|\Phi_{\mathbf{k}}\rangle + \int d^D r' \underbrace{\langle \mathbf{r}|\frac{1}{E-\hat{H}_0+i\epsilon}|\mathbf{r}'\rangle}_{\equiv(2m_r/\hbar^2)G_+(\mathbf{r},\mathbf{r}')}\langle \mathbf{r}'|\hat{V}|\Psi_{\mathbf{k}}^{(+)}\rangle, \tag{2.5}$$

where D is the dimension of the space. By inserting a complete set of plane wave states, which are eigenstates to the free particle Hamiltonian $\hat{H}_0$, the matrix elements $G_+(\mathbf{r},\mathbf{r}')$ can be evaluated for different dimensions as

$$G_+(\mathbf{r},\mathbf{r}') = \begin{cases} \frac{e^{ik|r-r'|}}{2ik} & D=1 \\ \frac{K_0(-ik|\mathbf{r}-\mathbf{r}'|)}{-2\pi} & D=2\,, \\ \frac{e^{ik|\mathbf{r}-\mathbf{r}'|}}{-4\pi|\mathbf{r}-\mathbf{r}'|} & D=3 \end{cases} \tag{2.6}$$

where K_0 is the zeroth order modified Bessel function of the second kind [31]. For a point far away from the region where the interaction potential has an appreciable strength we have that $|\mathbf{r}| \gg |\mathbf{r}'|$, and we can expand $|\mathbf{r}-\mathbf{r}'| \approx |\mathbf{r}| - \mathbf{r}\cdot\mathbf{r}'/|\mathbf{r}|$. Inserting this into Eq. (2.5), we get in a three-dimensional space

$$\langle \mathbf{r}|\Psi_{\mathbf{k}}^{(+)}\rangle = \langle \mathbf{r}|\Phi_{\mathbf{k}}\rangle + \frac{1}{(2\pi)^{3/2}}\frac{e^{ikr}}{r}\underbrace{\left(-\frac{1}{4\pi}(2\pi)^3\frac{2m_r}{\hbar^2}\right)\langle \mathbf{k}'|\hat{V}|\Psi_{\mathbf{k}}^{(+)}\rangle}_{\equiv f(\mathbf{k}',\mathbf{k})}, \tag{2.7}$$

where we have defined $\mathbf{k}' = k\,\mathbf{r}/|\mathbf{r}|$. See Fig. 2.5 for a schematic picture of the vectors used. We can then identify the important quantity f, called the scattering amplitude. The scattered state far away from the scattering region is thus the incoming wave plus a spherical wave with amplitude $f(\mathbf{k}',\mathbf{k})$. Similar results are obtained in the other dimensions, with their respective type of spherical wave.

One may also expand the scattered state using partial waves with angular momentum l according to $\langle \mathbf{r}|\Psi_{\mathbf{k}}^{(+)}\rangle = \sum_{l=0}^{\infty} P_l(\cos\theta)\chi_{kl}(r)/kr$ where P_l are the Legendre polynomials. At large distances the radial equation has solutions $\chi_{kl}(r) =$

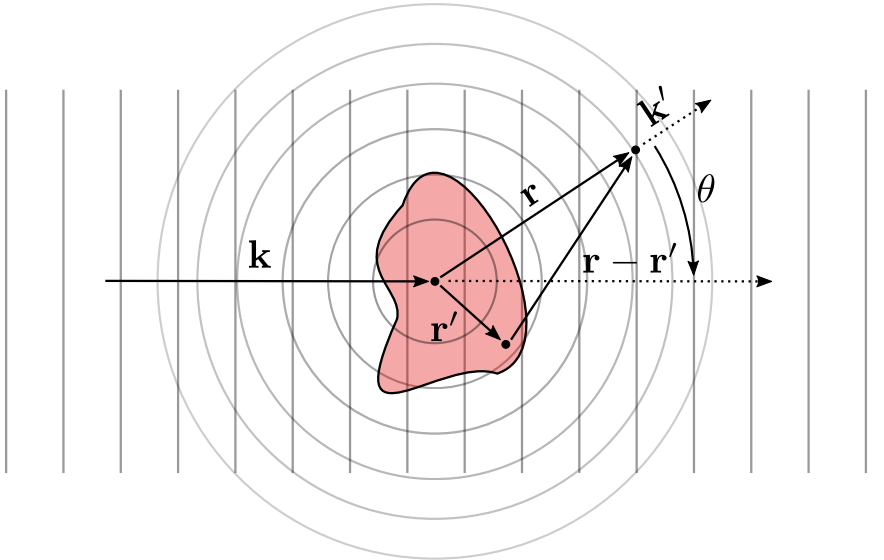

Figure 2.5: A sketch of the different vectors involved in the Lippmann-Schwinger equation at long distances, Eq. (2.7), where the red shaded area represents the spatial extent of the scattering potential $\hat{V}$. The free particle plane wave state has momentum $\hbar\mathbf{k}$ and the vector $\mathbf{k}'$ forms an angle θ with the direction of $\mathbf{k}$. Adapted after [25].

$A_l \sin(kr - \pi l/2 + \delta_l)$ where δ_l is called the phase-shift and is generally a function of k [32]. Comparing to Eq. (2.7) one may derive that the scattering amplitude f, which, due to the spherical symmetry, here only depends on the magnitude of $\mathbf{k}$ and the angle θ between $\mathbf{k}$ and $\mathbf{k}'$, can be written as $f(k,\theta) = \sum_{l=0}^{\infty}(2l+1)P_l(\cos\theta)f_l(k)$ with, the partial-wave amplitude

$$f_l(k) \equiv \frac{(e^{2i\delta_l} - 1)}{2ik} = \frac{1}{k\cot\delta_l - ik}. \tag{2.8}$$

For collisions of slow particles, i.e. when $k \to 0$, with a finite-range potential, it can be shown that the phase-shifts vary as k^{2l+1} [33]. If the potential goes as r^{-n} at large distances r, the phase-shifts for partial waves with l above $(n-3)/2$ vary as k^{n-2}. Thus, in the limit $k \to 0$, since $f_l \approx \delta_l/k$, only the term for $l = 0$ survives. When this is the case it is said that we have s-wave scattering. The term $k\cot\delta_0$ in Eq. (2.8) can furthermore be expanded using the effective range expansion [34]. For ultracold atoms it turns out that all terms in the expansion except the first one

are negligible [5]. Eq. (2.8) for $l = 0$ can then be written as

$$f_0(k) = -\frac{a}{1 + ik}. \tag{2.9}$$

In the limit $k \to 0$ this expression becomes constant, $f_0 = -a$, i.e. the two-particle scattering at low energies is determined by only a single parameter of the interaction potential, the scattering length a.

In many cases for ultracold atomic gases one may use a Feshbach resonance to change the scattering length by tuning an external magnetic field [5, 29, 35]. This can be performed when the scattering process has an open and a closed channel. The situation for such a scattering process is depicted in Fig. 2.4. In the open channel, the energy of the system is high enough such that this state can be the asymptotic result of the process. For the closed channel this is not the case. However, if there are bound states for the closed channel and these states are coupled to the open channel, the scattering length for the open channel can effective be altered. A very pronounced effect can be seen if a bound state of the closed channel is very close to the incident energy E of the collision where the scattering length diverges. In ultracold gases the different channels can have different magnetic moments and thus the relative energy can be altered by an external magnetic field. By carefully tuning the strength of the magnetic field the scattering length can be made to take almost any value. A Feshbach resonance in a Bose-Einstein condensate was first observed in 1998 [36]. Since then it has become an important tool in investigating many-body effects in ultracold atoms as it allows for the possibility to effectively alter the strength of the interactions in the system by tuning an external parameter. For a review of Feshbach resonances in ultracold atoms see [35].

If the scattering potential is not very strong one may use the Born approximation in order to determine the scattering length [25]. In the Born series the scattering amplitude is expanded in orders of V as a series $f = f^{(1)} + f^{(2)} \dots$ and to get the first-order Born amplitude $f^{(1)}$ one assumes that the incoming scattering state $|\Psi^{(+)}\rangle$ is not very different from a plane-wave. On the right hand side of Eq. (2.5) the state $|\Psi^{(+)}\rangle$ is then replaced by a plane-wave state. At large distances, the scattering amplitude becomes

$$f^{(1)}(\mathbf{k}, \mathbf{k}') = -\frac{1}{4\pi}\frac{2m_r}{\hbar^2}\int d^3r' e^{i(\mathbf{k}-\mathbf{k}')\cdot\mathbf{r}'} V(\mathbf{r}'). \tag{2.10}$$

From this we get that when $|\mathbf{k} - \mathbf{k}'| \to 0$ the scattering length is given by

$$a = \frac{m_r}{2\pi\hbar^2} \int V(\mathbf{r}) \mathrm{d}^3 r. \tag{2.11}$$

One may then substitute the complicated true interaction potential $V(\mathbf{r})$ with an effective pseudopotential $V_{\mathit{eff}}(\mathbf{r})$ with the same scattering length. Utilizing a pseudopotential that gives the same scattering length already in the first-order Born approximation can be seen as an effective interaction where effects of the short-range correlations from the interactions have already been incorporated. This works well when combined with a mean-field treatment, where only long-wavelength effects are considered, and is then expected to give correct low-energy results [29].

A simple pseudopotential for which a is easily calculated through Eq. (2.11) is

$$V_{\mathit{eff}}(\mathbf{r}) = g\,\delta(\mathbf{r}), \tag{2.12}$$

where δ is the Dirac delta function. This contact pseudopotential has been used extensively, and with much success, in the context of ultracold atoms [5, 29, 32]. However, in treatments beyond mean-field it must be used with caution as it is not a proper physical interaction potential in two or higher dimensional spaces. The resulting Hamiltonian operator is not self-adjoint [37]. This issue can actually be seen directly in the scattering problem by considering Eq. (2.5) for such a local potential [38],

$$\Psi^{(+)}_{\mathbf{k}}(\mathbf{r}) = \Phi_{\mathbf{k}}(\mathbf{r}) + g\,G_+(\mathbf{r}, 0)\Psi^{(+)}_{\mathbf{k}}(0), \tag{2.13}$$

where the singular behavior of $G_+(0, 0)$, as can be seen in Eq. (2.6), prohibits a consistent solution for the point $\mathbf{r} = 0$. In Paper II we have analyzed a simple way to anyway use the contact-type interactions for higher dimensions when performing exact diagonalization calculations, a numerical method that will be discussed in Sec. 3.3, on few-particle systems.

Recently there has been a lot of progress in realizing laser cooled gases of atoms and molecules with large permanent dipole moments. In such gases the interactions between the particles would be dominated by the dipole-dipole interaction, a type of interaction that can not be described by only the contact pseudopotential and gives rise to new behavior and phenomena in these gases. For reviews see [39–41].

The interaction potential V_{DD} of two dipoles with dipole moments $\mathbf{d}_1 = d\hat{\mathbf{e}}_1$ and $\mathbf{d}_2 = d\hat{\mathbf{e}}_2$ with the same magnitude d and separated by $\mathbf{r}$ is given by

$$V_{\mathrm{DD}}(\mathbf{r}) = \frac{C}{4\pi}\frac{(\hat{\mathbf{e}}_1 \cdot \hat{\mathbf{e}}_2)\, r^2 - 3\,(\hat{\mathbf{e}}_1 \cdot \mathbf{r})\,(\hat{\mathbf{e}}_2 \cdot \mathbf{r})}{r^5}, \tag{2.14}$$

where $C = d^2/\epsilon_0$ for electric dipoles and $C = d^2\mu_0$ for magnetic dipoles, with ϵ_0 and μ_0 being the permittivity and permeability of free space respectively [42]. In principle there would be an additional term proportional to $\delta(\mathbf{r})$, but as we here will only use this potential for spin polarized fermions it can be disregarded. If the dipoles are of the same magnitude and aligned along the same direction, i.e. $\hat{\mathbf{e}}_1 = \hat{\mathbf{e}}_2$ and $\mathbf{d} = \mathbf{d}_1 = \mathbf{d}_2$, then Eq. (2.14) reduces to

$$V_{\mathrm{DD}}(\mathbf{r}) = \frac{C}{4\pi}\frac{1 - 3\cos^2\theta_{rd}}{r^3}, \tag{2.15}$$

where θ_{rd} is the smallest angle between $\mathbf{r}$ and $\mathbf{d}$, such that $\mathbf{r} \cdot \mathbf{d} = |\mathbf{r}||\mathbf{d}|\cos\theta_{rd}$. Fig. 2.6 shows the constituent vectors for the different configurations.

At large distances the dipole-dipole potential goes as r^{-3} and thus extends much longer than the normal van der Waals type interactions previously discussed. Due to this slow decay at large distances, for scattering with the dipole-dipole interaction, other partial waves other than the s-wave also give a significant contribution to the scattering amplitude. Furthermore, the dipole-dipole interaction does not just depend on the relative distance, but also on the angles between the dipole moments. This anisotropy allows the mixing of different partial waves. Thus, the scattering problem is more complex and one can not substitute the true interaction potential with a contact pseudopotential [39].

Since the experimental realization of a Bose-Einstein condensate with a significant dipolar character of ^{52}Cr in 2005 [43], condensates of other atomic species with large permanent magnetic dipole moments, such as ^{164}Dy [44] and ^{168}Er [45], have also been realized. Fermi gases with strong dipole-dipole interactions, e.g. of ^{167}Er [46], have also been reported. Another type of laser-cooled and trapped gases with dipolar interactions that has recently seen major experimental progress is gases of polar molecules, where experimental realization has been reported for e.g. KRb [47], Cs_2 [48], RbCs [49, 50], NaK [51] and NaRb [52]. A third possible candidate for a gas with long-range interactions is to use Rydberg atoms [53]. Dipolar condensates have e.g. been observed forming self-bound droplets [54], a system that has demonstrated signatures of supersolidity [55–57].

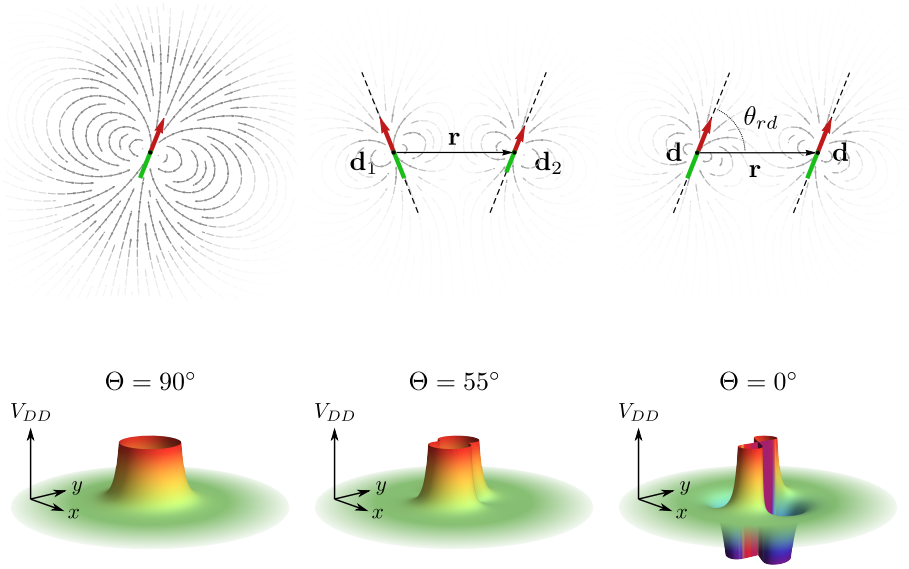

Figure 2.6: A sketch of the different vectors involved in the dipole-dipole interaction is shown in the upper part of the figure. The left upper panel shows the dipole field generated by the dipole in the middle. The middle upper panel depicts a situation where two dipoles point in different directions. In the panel to the upper right the two dipole moments are pointing in the same direction. The vector $\mathbf{r}$ between the different positions of the dipole moments and the angle θ_{rd} between the dipole moments $\mathbf{d}$ and the separation vector $\mathbf{r}$ is also shown. In the lower part of the figure the interation potential $V_{\mathrm{DD}}(\mathbf{r})$ of Eq. (2.15) for two dipolar particles with dipole moments pointing in the same direction is shown for three different angles Θ between $\mathbf{d}$ and the xz axis. Below the so called magical angle $\arccos 1/\sqrt{3} \approx 54.7°$ attractive regions are formed.

2.4 Degenerate quantum gases

When cooled down to extremely low temperatures, the quantum statistics of the particles making up a gas will start to become important. After reaching such low temperatures, the gas would have properties that differ substantially from a classical gas, and is therefore referred to as a degenerate quantum gas [58]. The most striking example is probably for bosons. In a series of seminal works in 1924-1925 by Bose and Einstein [59–61], for which translations to English can be found in [62], it was realized that below a certain critical temperature a gas of ideal and massive bosonic particles would undergo a transition into a new type of phase, nowadays well known as a Bose-Einstein condensate. In this phase, a large fraction of the total number of particles macroscopically occupy a single-particle orbital.

The concept of Bose-Einstein condensation can be generalized to interacting systems, where a priori the single-particle orbitals do not have a direct physical meaning, with the help of the one-particle density matrix [63]. In position representation, the one-particle density matrix is defined as

$$\rho_1(\mathbf{r}, \mathbf{r}', t) = \langle \hat{\Psi}^\dagger(\mathbf{r}', t)\hat{\Psi}(\mathbf{r}, t)\rangle, \tag{2.16}$$

where $\hat{\Psi}^\dagger(\mathbf{r}, t)$ and $\hat{\Psi}(\mathbf{r}, t)$ are the field operators. As ρ_1 is an Hermitian matrix, it can be diagonalized with real, possibly time-dependent, eigenvalues $n_i(t)$ [32, 64]. It can then be written as

$$\rho_1(\mathbf{r}, \mathbf{r}', t) = \sum_i n_i(t)\chi_i(\mathbf{r}, t)\chi_i^*(\mathbf{r}', t), \tag{2.17}$$

where the orthonormal eigenfunctions χ_i, called the natural orbitals, fulfill the eigenvalue equation

$$\int \rho_1(\mathbf{r}, \mathbf{r}', t)\chi_j(\mathbf{r}', t)\mathrm{d}\mathbf{r}' = n_j(t)\chi_j(\mathbf{r}, t). \tag{2.18}$$

These orbitals need not be eigenfunctions to the single-particle part of the Hamiltonian, but they will give the orbital with the largest possible occupation, even in the presence of interactions. The maximum occupation is given by the largest eigenvalue. In the limit of vanishing interactions, these orbitals reduce to the eigenstates of the single-particle part of the Hamiltonian. The system is said to be a simple Bose-Einstein condensate if all eigenvalues $n_i(t)$ are of order unity except one which is of order N [64]. If there are several eigenvalues that are of order N, the system has condensed into several condensates and is said to be fragmented [65].

If one uses the natural orbitals in the expansion of the field operators and if we take the orbital $|\chi_0\rangle$ to be the macroscopically occupied orbital, it is convenient to single it out in the form

$$\hat{\Psi}(\mathbf{r}, t) = \chi_0(\mathbf{r}, t)\hat{a}_0 + \delta\hat{\Psi}(\mathbf{r}, t), \tag{2.19}$$

where, due to the asymmetric occupations, the effect of $\delta\hat{\Psi} \equiv \sum_{i\neq 0}\chi_i(\mathbf{r}, t)\hat{a}_i$ on the Fock states is negligible compared to the one by $\hat{\Psi}_0 \equiv \chi_0(\mathbf{r}, t)\hat{a}_0$. This form can then be used as the starting point for a mean-field approximation, which will be covered in Sec. 3.1 [32].

The possibility for an interacting bosonic system to form a condensate comes has statistical and energetical reasons. For classical particles, due to their distinguishability, many-particle states with most particles in one specific single-particle orbital are heavily out-numbered compared to the states with a roughly equal distribution of the occupancies. If it is a system of indistinguishable bosons the states with macroscopic occupations are instead equally numerous as the states with a uniform distribution, and thus they are not statistically unfavored. Due to the symmetric nature of the state, it is also, perhaps counter-intuitively, most likely energetically favorable for the bosonic system to have all particles in the same natural orbital [64]. As one of these states with macroscopic occupation is likely to be the ground state at zero temperature, when lowering the temperature below some critical temperature T_c the system will start to exhibit properties coming from the exceptional occupations.

A characteristic property of a condensate is the occurrence of a non-classical moment of inertia when it is set rotating [64]. The response to rotation is not an immediate and smooth increase in angular momentum. Instead, one has to rotate the system above a certain rotational frequency for it to pick up a substantial amount of angular momentum, that keeps increasing in distinct steps at specific frequencies. Similarly, a condensate rotating in a vessel will usually continue rotating even when the vessel stops, a so called persistent current. These two phenomena can be taken as defining properties of a superfluid [64], a fluid with zero viscosity, and can be related to the formation of quantized vortices [32, 64], to be introduced in Sec. 4.3.

Although it has been suggested that Bose-Einstein condensation is the reason for superfluidity in liquid helium since 1938 [66], it has been difficult to confirm this by experiments [64]. Due to the advances in atomic cooling and trapping from the 1970's and onwards it was speculated that a gas of hydrogen atoms would be the first system to be experimentally confirmed to exhibit Bose-Einstein condensation [67, 68]. Instead, it turned out to be the alkali atoms that offered the best possibilities. The experimental signal from a gas of ^{87}Rb obtained in 1995 was very clear, distinct from the normal thermal velocity distribution was a sharp peak coming from a macroscopic occupation of the zero-momentum state [69]. More of the history by the pioneers in the field of Bose-Einstein condensates in systems of ultracold alkali atoms can be found in the Nobel lectures from 2001 [70, 71]. More thorough discussions of the phenomenon of Bose-Einstein condensation and its consequences, in general and in the special case of ultracold atoms, can be found

in specialized textbooks on the subject, e.g. [29, 32, 64].

A Bose-Einstein condensate is a consequence of the indistinguishability of the bosonic particles, and it can be considered a quantum liquid, a system where both quantum mechanical effects and the quantum statistics of the particles are important [64]. Fermionic particles as long as there is no pairing involved, are forbidden by the Pauli exclusion principle to form a condensate. However, at sufficiently low temperatures, due to the quantum statistics of the particles, the properties of the gas will anyway start to deviate from the classical behavior. For an ideal Fermi gas this can be seen as a consequence of the filling of the single-particle energy levels according to the Fermi-Dirac distribution, creating a Fermi sea of inert particles [72].

As most of the optical and magnetical trapping and cooling mechanisms discussed in Sec. 2.1 do not depend on the particle statistics, it is possible to reach quantum degeneracy using such techniques also with fermionic isotopes of the atoms. The first experimental realization of such a degenerate Fermi gas in ultracold atomic systems was reported in 1999 [73]. Fermi gases have also been realized with weak attractive interactions, where the particles form very loosely bound pairs, well described by the Bardeen-Cooper-Schrieffer theory of superconductivity [74]. Such ultracold Fermi gases have been used to study the crossover from the loosely bound pair to a gas of tightly bound dimers forming a Bose-Einstein condensate. For a review on ultracold fermionic gases see [75].

2.5 Few-particle systems

Magneto-optical traps have also earlier been used for single-atom trapping [76]. However, due to the continuous absorption and emission of photons, the control of the quantum state of the atom is troublesome. To mitigate this problem one can use an optical dipole trap created by a highly focused laser beam, such that only one atom can fit in the trap. Such a setup was demonstrated in 2001 [77]. Confining one atom this way does however not allow for the control of the system's quantum state in a simple way. For larger numbers of bosons, it has also been difficult to tune the chemical potential of the system such that the trap contains a pre-determined number of them, although experiments with as few as 60 bosonic atoms have been reported [78]. In experiments with optical lattices one can control the filling of the different sites by altering the lattice parameters [5]. However, in such experiments

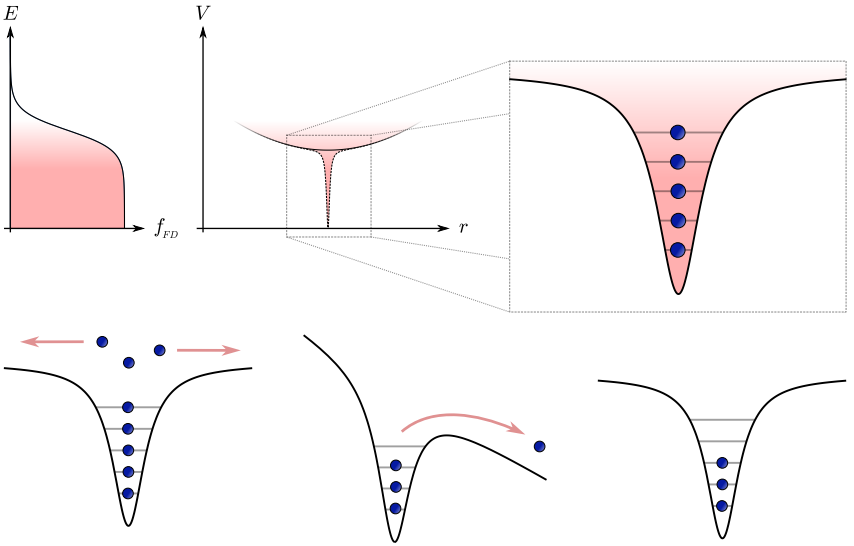

Figure 2.7: A sketch of the microtrap method used to prepare a fermionic few-body system according to [79]. The top part shows the additional microtrap on top of the usual harmonic confinement. The shading represents the filling of the states according to the Fermi-Dirac distribution, sketched on the left side. On the right, the microtrap is shown in greater detail, depicting how all the levels are occupied. The lower part of the figure depicts the spilling mechanism used to prepare the few-body system with a specific number of atoms. As the large trap is turned off only the particles trapped in the microtrap are left, as shown in the panel to the left. Adding a linear potential as in the middle panel, the particles close to the top edge can tunnel out of the microtrap in a controllable way. Removing the linear one is left with a few-body system, depicted to the right. Adapted after [79, 80].

one then has a lot of small systems next to each other, and possibly also coupled. This could create problems if one is interested in isolated few-body systems. In order to also be able to study a single few-particle system using ultracold atoms, the number of particles in the trapped gas has to be controlled much more precisely than what most of the setups commonly employed allow.

However, if one is interested in fermionic systems this problem can be overcome. Here one can use the Pauli exclusion principle to prepare a few-particle system [79]. By superimposing a smaller and narrower dipole trap on top of an ordinary, larger, trap and cool the gas well below the critical temperature for fermionic degeneracy, for weakly or non-interacting particles, all the single-particle levels in the smaller trap will be occupied. Such a situation is shown in the upper portion of Fig. 2.7. Turning off the larger trap will then leave only the particles in the small dimple still trapped by the lasers. Now, if a magnetic field that is varying linearly in space is a applied, one can tilt the trapping potential such that it spills out most of the

particles left in the trap in a controlled way [79]. A schematic picture of this process is shown in the lower part of Fig. 2.7. Using such a technique, the deterministic preparation of few-fermion systems ranging from one to ten particles was reported in 2011 [79]. Since then, this technique has been used to e.g. study the pairing of a few fermions with attractive interactions [81], investigating the crossover from few- to many-body physics [82], create a two-well Hubbard-like system [12] and realize Heisenberg spin chains [83].

Currently, this technique has mainly been used for a quasi-one-dimensional fermionic gas, but extension to higher dimensions is possible. However, there are still experimental challenges in order to be able to control the shape and simultaneously the number of particles in smaller traps. This scheme could possibly be extended to be used for bosons as well [84]. One could first fermionize the bosonic particles by increasing the scattering length, and hence the strength of the interactions, to a very high value using a Feshbach resonance. The strong repulsive interactions keep the particles from not being close to each other, creating an artificial exclusion principle and making the bosons behave more like fermions [85]. This has been done experimentally for two distinguishable fermions [86]. The number of particles trapped can now be controlled in the same way as for real fermions. After the spilling is completed the interaction strength would be ramped down to recover the bosonic behavior again. However, such a scheme might induce unwanted excitations in the system or be difficult to control with enough precision. Thus, for obtaining isolated general few-body quantum systems using ultracold atoms there still exists many experimental hurdles to overcome before the theoretical predictions can be tested.

Chapter 3

Approximate and numerical methods

Solving the Schrödinger equation for an interacting many-body system is usually very cumbersome. The interaction term induces direct correlations between the motion of the different particles, such that the Schrödinger equation can not be separated. Consequently, many different methods to find approximate solutions to these problems have been developed over the years. In this chapter the methods used in this thesis will be briefly introduced.

Sec. 3.1 discusses the method of approximating the effects of interaction in a system by replacing them with an averaged mean-field potential. Applied to fermionic systems and Bose-Einstein condensates, this method leads to the widely used Hartree-Fock approximation and the Gross-Pitaevskii equation respectively. For a fermionic system the Hartree-Fock state can be the starting point for many-body perturbation theory, where correlations are added to the reference state successively to different order of the perturbation. The basic concepts for this method will be introduced in Sec. 3.2. In Sec. 3.3 the method of quadratic configuration interaction will be introduced. This is a method similar to perturbation theory, but where the corrections are instead ordered by the type of substitutions made compared to the reference state. Including all correlations leads to the method of exact diagonalization, discussed in Sec. 3.3. Using this method the full many-body problem can in principle be solved exactly, although at a substantial computational cost, limiting it to only very small systems with moderate interaction strengths. Finally, in order

to study the dynamical behavior of a quantum system, two methods to perform time-propagation will be briefly discussed in the last section, Sec. 3.4.

3.1 Mean-field approximation

One of the simplest ways to try to account for the interactions in a system is to map the interacting problem on single-particle motion in an effective mean-field potential. Replacing the actual interaction term in the many-body Hamiltonian $\hat{H}$ in Eq. 2.2 with $\hat{V}_{MF}$, we get a new approximate Hamiltonian $\hat{H}_{MF}$ according to

$$\hat{H} = \sum_{i=1}^{N} \hat{h}_0(i) + \sum_{i<j} \hat{V}_{int}(i,j) \quad \rightarrow \quad \hat{H}_{MF} = \sum_{i=1}^{N} \underbrace{\left(\hat{h}_0(i) + \hat{V}_{MF}(i)\right)}_{\hat{h}_{MF}^{(i)}}. \tag{3.1}$$

Using $\hat{H}_{MF}$ instead of $\hat{H}$, the many-body problem now conveniently turns into N single-particle problems that are more easily solved. Depending on how the mean-field potential is constructed and what type of states are considered, this scheme leads to many methods that have been and are still being widely used, e.g. Hartree, Hartree-Fock and density functional theory [27, 87–89].

In a dilute system of condensed bosons, as described in Sec. 2.4, the Hartree mean-field equation takes on a rather simple form. Due to the large number of particles in the same quantum state, it is possible to derive a classical field equation that governs the behavior of the system - much like Maxwell's equations are a good description of a large number of photons. If the condensate fraction is large enough, i.e. $\hat{\Psi}$ in Eq. (2.19) is dominated by $\hat{\Psi}_0$, we can neglect the contribution from the other orbitals and follow the Bogoliubov approximation [32]. This amounts to replacing the field operator $\hat{\Psi}(\mathbf{r},t)$ with the complex function $\Psi_0(\mathbf{r},t) = \sqrt{n_0}\,\psi_0(\mathbf{r},t) \approx \sqrt{N}\psi_0(\mathbf{r},t)$, called the order parameter or condensate wave function. Starting from the time-evolution of $\hat{\Psi}$ in the Heisenberg picture, one may obtain a non-linear equation of motion

$$i\hbar\frac{\partial}{\partial t}\psi_0(\mathbf{r},t) = \left(\hat{h}_0(\mathbf{r},t) + gN|\psi_0(\mathbf{r},t)|^2\right)\psi_0(\mathbf{r},t) \tag{3.2}$$

for the macroscopically occupied orbital ψ_0 [29, 32, 64]. Here $\psi_0(\mathbf{r},t)$ is normalized to unity and $g = \int V_{\text{eff}}(\mathbf{r})\mathrm{d}\mathbf{r}$, which can be expressed in terms of the

s-wave scattering length a according to $g = \frac{4\pi\hbar^2 a}{m}$. Equation (3.2) is the Gross-Pitaevskii equation, proposed in 1961 [90, 91], which is valid for a dilute gas for which $na^3 \ll 1$ [29], where n is the particle density. It has since then been successfully applied to a large variety of experiments involving ultracold atomic systems. See e.g. the books [29, 32, 64].

As the Gross-Pitaevskii equation is the Hartree equation for condensed bosons, the corresponding many-body state is given by the simple product state where all bosons are in the orbital ψ_0 [64]. In the second quantized form, this many-body state is written as

$$|\Phi_{GP}\rangle = \frac{(\hat{a}_0^\dagger)^N}{\sqrt{N!}}|0\rangle, \tag{3.3}$$

where $\hat{a}_0^\dagger$ is the bosonic creation operator for the state ψ_0. The state in Eq. (3.3) is usually not an eigenstate to, and will in general also not have the same symmetries as, the full Hamiltonian. For the product state the energy functional $E[\Psi_0] = \langle\Psi_0|\hat{H}|\Psi_0\rangle$ is given by

$$E[\Psi_0] = N\int\left(\psi_0^*(\mathbf{r},t)\hat{h}_0(\mathbf{r},t)\psi_0(\mathbf{r},t) + \frac{1}{2}g(N-1)|\psi_0(\mathbf{r},t)|^4\right)\mathrm{d}r. \tag{3.4}$$

Equation (3.2) can also be obtained by taking the functional derivative of Eq. (3.4) [32], resulting in the difference of the factor $1/2$ in front of the interaction terms. This shows that it is actually not the energy, but instead the chemical potential $\mu = \partial E/\partial N$, that governs the time-evolution of the condensate [32, 64]. This type of time-evolution is reflecting the reservoir character of the condensate. As Ψ_0 can be seen as the expectation value of $\hat{\Psi}$, $\langle\alpha|$ in $\langle\alpha|\hat{\Psi}|\alpha\rangle$ has to have one particle less than $|\alpha\rangle$. Thus, if the states time-evolve by a phase factor $e^{-iE(N)t/\hbar}$ the time-dependence of the order parameter will be determined by the difference $E(N) - E(N-1) \approx \mu$. One can also see that the dependence of the interaction energy on the particle number in Eq. (3.2) should be $N(N-1)$. When N is large and when using the approximation $\Psi_0 \approx \sqrt{N}\psi_0$, the difference is assumed to be negligible.

The Hartree state in Eq. (3.3) is obviously not a good approximation for a fermionic state due to not being antisymmetric. This can be remedied by instead considering a state of the form of a Slater determinant. Optimizing the orbitals of a single determinant to give the lowest expectation value of the full Hamiltonian leads to

the Hartree-Fock equations [27, 87, 88, 92]

$$(\hat{h}_0 + \hat{V}_{HF})|\varphi_i\rangle = \epsilon_i|\varphi_i\rangle, \tag{3.5}$$

where $\hat{V}_{HF}$ is the Hartree-Fock potential. If the solution is expanded as $|\varphi_i\rangle = \sum_n c_n^{(i)}|\phi_n\rangle$ the matrix elements of the potential are given by

$$\langle\phi_m|\hat{V}_{HF}|\phi_n\rangle = \sum_{p=1}^{N}\left(\langle\phi_m\varphi_p|\hat{V}_{\text{int}}|\phi_n\varphi_p\rangle - \langle\phi_m\varphi_p|\hat{V}_{\text{int}}|\varphi_p\phi_n\rangle\right). \tag{3.6}$$

By solving this self-consistently one optimizes the N first orbitals, but if the number of basis functions in the expansion of $|\varphi_i\rangle$ is larger than the number of particles one also obtains a set of orbitals that are not used. These extra orbitals, called virtual orbitals, can be used to add correlations to the reference state with e.g. many-body perturbation theory.

3.2 Many-body perturbation theory

The Hartree-Fock approximation is uncorrelated, i.e. effects beyond exchange are said to be correlation effects [92]. A significant amount of work has been done to develop methods to try to account for these correlations, density functional theory being a well known example [89]. Another way of systematically adding these correlations is with many-body perturbation theory.

In perturbation theory one starts with the Schrödinger equation and tries to divide the Hamiltonian into two parts according to $\hat{H} = \hat{H}_0 + \hat{H}_p$, where the eigenstates $|\Psi_i^{(0)}\rangle$ to the Schrödinger equation for $\hat{H}_0$ are known and $\hat{H}_p$ is the perturbation. The correct energy and eigenstate is then expressed as a sum of the zero order solution $|\Psi_i^{(0)}\rangle$ together with corrections in orders of $\hat{H}_p$. Expanding the corrections in terms of the eigenstates to $\hat{H}_0$ leads to the Rayleigh-Schrödinger type of perturbation theory. We then get a series of equations for the different correction terms where the next order corrections are expressed in the previous one, such that they can be calculated systematically to any order. A full derivation of the perturbation expansion can be found in most textbooks on topics involving many-particle quantum physics, see e.g. [27, 87, 88, 92].

However, for perturbation theory to be useful, the sum of corrections needs to converge. In order for this to be the case no singularities to the operator $\hat{H}_0 + z\hat{H}_p$,

where z is a complex number, should exist for $|z| \leq 1$, i.e. the distance between the singularity and the unperturbed system is smaller than to the perturbed system [93]. Furthermore, for practical calculations the perturbation needs to be small enough such that the number of orders needed to be included for the desired precision is computationally feasible. In many-particle systems, the single-particle part can typically be solved easily, either exactly or numerically. The interactions are however usually too strong to be used directly as the perturbation. One way to try to come around this problem when dealing with fermionic systems is to take the Hartree-Fock solution to be the reference state from which we start the expansion. Thus, the perturbation is taken to be

$$\hat{H}_p = \hat{H} - \hat{H}_{HF} = \sum_{n<m} \hat{V}_{int}(n,m) - \sum_n \hat{V}_{HF}(n). \tag{3.7}$$

This is motivated by the assumption that the Hartree-Fock approximation has accounted for most of the effects of the interactions already. This type of many-body perturbation theory is called Møller-Plesset perturbation theory and was suggested in 1934 [94] and has been used extensively in e.g. quantum chemistry [87, 88, 92]. This form of the perturbation leads to particularly simple expressions for the energy corrections. It can also be shown that the Hartree-Fock energy, the expectation value of the Hartree-Fock solution with respect to the full Hamiltonian $\hat{H}$, is equivalent to perturbation theory to first order.

The corrections can furthermore be reduced to sums over two-body matrix elements. The second order energy correction becomes

$$E_{MP}^{(2)} = \frac{1}{4} \sum_{i,j}^{\text{occ}} \sum_{a,b}^{\text{vir}} \frac{|\langle \varphi_i \varphi_j | \hat{V}_{\text{int}} | \varphi_a \varphi_b \rangle - \langle \varphi_i \varphi_j | \hat{V}_{\text{int}} | \varphi_b \varphi_a \rangle|^2}{\epsilon_i + \epsilon_j - \epsilon_a - \epsilon_b}, \tag{3.8}$$

where the sums over i and j are over the orbitals that are occupied in $|\Psi_0^{(0)}\rangle$ and the sums over a and b are over the unoccupied virtual orbitals, with ε_k being the eigenvalue of orbital k in Eq. (3.5). Similarly, higher order corrections can also be expressed as sums over two-body matrix elements with the Hartree-Fock orbitals. The equations for all of the terms up to partial fourth order Møller-Plesset perturbation theory can be found in Appendix A.

A possible disadvantage of many-body perturbation theory is that it is not variational. The approximate energy is not guaranteed to be an upper bound of the real energy eigenvalue and as higher and higher orders are included it usually oscillates

around the correct value. However, an advantage of the Rayleigh-Schrödinger type of perturbation theory, which in some instances can be more desirable than using a variational method, is that the perturbation theory is size extensive at all orders. Being size extensive means that the energy scales correctly with the size of the system [92]. If the energy is not scaling correctly, the method will not include the same amount of correlations as the system size is changed [88]. Thus, if one wants to compare systems of different sizes a method that is size extensive is preferred.

3.3 Exact diagonalization and quadratic configuration interaction

In many-body perturbation theory the eigenstates $|\Psi\rangle$ and their energy eigenvalues E are expanded in orders of the perturbation $\hat{H}_p$. As higher and higher orders are considered, states with more and more substitutions of orbitals compared to the reference state $|\Psi_0\rangle$ are included. Alternatively to expanding $|\Psi\rangle$ in terms of $\hat{H}_p$ one may consider the eigenstate consisting of some certain classes of substitutions instead. One then uses the substitution operators $\hat{T}_n$

$$\hat{T}_1 = \sum_{i}^{\text{occ}} \sum_{a}^{\text{vir}} a_i^a \hat{t}_i^a, \quad \hat{T}_2 = \frac{1}{4} \sum_{ij}^{\text{occ}} \sum_{ab}^{\text{vir}} a_{ij}^{ab} \hat{t}_{ij}^{ab}, \quad \hat{T}_3 = \frac{1}{36} \sum_{ijk}^{\text{occ}} \sum_{abc}^{\text{vir}} a_{ijk}^{abc} \hat{t}_{ijk}^{abc} \quad \ldots, \tag{3.9}$$

where n is the number of substitutions, $\hat{t}_{ij\ldots}^{ab\cdots}$ are elementary substitution operators moving particles occupying the orbitals $i, j, \ldots$ to the unoccupied orbitals $a, b, \ldots$ and $a_{ij\ldots}^{ab\cdots}$ are expansion coefficients. The eigenstate $|\Psi\rangle$ is then assumed to be of the form

$$|\Psi\rangle = f(\hat{T}_1, \hat{T}_2, \hat{T}_3, \ldots)|\Psi_0\rangle, \tag{3.10}$$

where f is some function of the substitution operators in Eq. (3.9). Making suitable projections by the states $|\Psi_0\rangle, |\Psi_i^a\rangle, |\Psi_{ij}^{ab}\rangle, \ldots$ onto the equation $(\hat{H}-E)|\Psi\rangle = 0$ give a series of coupled equations that can solved in order to obtain E and the coefficients a. Using a linear function f of the $\hat{T}_n$ operators leads to the method of configuration interaction [87, 88]. The equations for E and the coefficients a can then be recast into a matrix eigenvalue equation.

Including all $\hat{T}_n$ up to $n = N$ using a linear f gives the so called full configuration interaction method. All possible substitutions in the single-particle basis set are then considered. It is then not necessary to order the different states according to their substitutions as they are all used. Expanding the sought eigenstate in the Fock states $|\Phi_n\rangle$ according to $|\Psi\rangle = \sum_n c_n |\Phi_n\rangle$ gives the matrix eigenvalue problem

$$\begin{bmatrix} \langle\Phi_0|\hat{H}|\Phi_0\rangle & \langle\Phi_0|\hat{H}|\Phi_1\rangle & \langle\Phi_0|\hat{H}|\Phi_2\rangle & \cdots \\ \langle\Phi_1|\hat{H}|\Phi_0\rangle & \langle\Phi_1|\hat{H}|\Phi_1\rangle & \langle\Phi_1|\hat{H}|\Phi_2\rangle & \cdots \\ \langle\Phi_2|\hat{H}|\Phi_0\rangle & \langle\Phi_2|\hat{H}|\Phi_1\rangle & \langle\Phi_2|\hat{H}|\Phi_2\rangle & \cdots \\ \vdots & \vdots & \vdots & \ddots \end{bmatrix} \begin{bmatrix} c_0 \\ c_1 \\ c_2 \\ \vdots \end{bmatrix} = E \begin{bmatrix} c_0 \\ c_1 \\ c_2 \\ \vdots \end{bmatrix}. \tag{3.11}$$

By diagonalizing this matrix one then obtains the eigenstates and their corresponding energies. This method is commonly referred to as full configuration interaction in quantum chemistry [87, 88], no core shell model in nuclear physics [95], or, as it is in principle just a diagonalization of the system Hamiltonian in a set of many-body states, exact diagonalization.

The method of exact diagonalization has some advantages over other methods for describing a quantum many-body system, such as, as its name suggests, it is exact. In the case of numerical diagonalization it is exact to the desired numerical precision, in the subspace that is spanned by the states used. As we are here only interested in systems with only one-body and two-body operators the different Fock states can only couple to other states which differ by at most two orbitals. The resulting matrix will then be rather sparse and this sparseness can be used to efficiently calculate the low-lying eigenstates with e.g. the Lanczos method [96, 97]. The precise numerical implementation used in Papers I-IV is described in more detail in [98].

In principle exact diagonalization allows one to access the whole excitation spectrum and all excited states. It is also variational, i.e. the energy obtained for the ground state is an upper bound for the true ground state energy. Another advantage is that the method is very general and can be applied to a wide variety of systems. It can e.g. be used for both fermions and bosons, different types of potentials and different types of interactions or other operators. The major disadvantage being that the size of the matrix needed to be diagonalized, and thus the computational complexity, is increasing extremely fast with the number of particles and orbitals used, limiting the method to be useful only for very small systems.

Similar to the previously discussed many-body perturbation theory, full configu-

ration interaction is size extensive. However, due to the very fast growth of the numerical complexity as the basis or system size is increased, one might be tempted to truncate the function $f = 1 + \hat{T}_1 + \hat{T}_2 + \cdots + \hat{T}_n$ at some $n < N$ to get a more manageable problem. Although it appears to be very similar to perturbation theory and would be a very systematic way of including more and more correlation, the resulting method will not be size extensive. There exists simple corrections to make such truncated configuration interaction results approximately size extensive, e.g. Davidson corrections, but these methods have many drawbacks on their own, such as not giving the correct value even for a two-particle system [88].

In the related method of "coupled clusters" the function f is taken to be an exponential of substitution operators $\hat{T}_n$ [92]. This method can be seen as including all substitutions of a given type to all orders. Such a construction can be shown to give a size extensive result [92]. A method that can be seen as something in between truncated configuration interaction and coupled-cluster theory can be constructed by including only the smallest number of terms needed to make the results size extensive into the projection equations. This is known as the quadratic configuration interaction method [99].

Using the Hartree-Fock ground state as the reference state $|\Psi_0\rangle$ the correct energy will be $E = E_{HF} + E_{\mathrm{QCISD}}$ where E_{HF} is the Hartree-Fock energy and E_{QCISD} is the sought-after correction. Including up to double substitutions the projection equations become

$$\langle \Psi_0 | \hat{H} \hat{T}_2 | \Psi_0 \rangle = E_{\mathrm{QCISD}}, \tag{3.12}$$

$$\langle \Psi_i^a | (\hat{H} - E_{HF})(\hat{T}_1 + \hat{T}_2 + \hat{T}_1 \hat{T}_2) | \Psi_0 \rangle = a_i^a E_{\mathrm{QCISD}}, \tag{3.13}$$

$$\langle \Psi_{ij}^{ab} | (\hat{H} - E_{HF})(1 + \hat{T}_1 + \hat{T}_2 + \hat{T}_2^2/2) | \Psi_0 \rangle = a_{ij}^{ab} E_{\mathrm{QCISD}}, \tag{3.14}$$

where the coefficients $a_{ij\cdots}^{ab\cdots}$ are the ones from Eq. (3.9), and the additional terms for size extensivity are $\hat{T}_1 \hat{T}_2$ in Eq. (3.13) and $\hat{T}_2^2/2$ in Eq. (3.14). These equations are then not linear in the coefficients a such that they can not be written as a matrix eigenvalue equation. They can however be solved iteratively until self-consistency is achieved.

Similar to many-body perturbation theory Eqs. (3.12)-(3.14) can be expressed in terms of two-body matrix elements. Including also triple substitutions is straightforward, but as in many-body perturbation theory it might become unfeasible for larger systems. A common way to incorporate some of the effects of triple substitutions is to treat them only as a perturbation on top of the solution to the full

problem with single and double substitutions. Here some care must be given to what terms are included as some have already been considered in Eq. (3.13). The full equations for quadratic configuration interaction including triple substitutions perturbations expressed in two-body matrix elements are given in App. B.

3.4 Time-evolution

The dynamical behavior of a quantum system is governed by the time-dependent Schrödinger equation, Eq. (2.1). If the system is in the state $|\Psi(t_0)\rangle$ at time t_0, at a later time $t_0 + \Delta t$ it is in a state $|\Psi(t_0 + \Delta t)\rangle = \hat{U}(t_0, \Delta t)|\Psi(t_0)\rangle$ where the time-evolution operator $\hat{U}(t_0, \Delta t)$ can be expressed e.g. as a Dyson series [25], or as an exponential $e^{\hat{\Omega}(t_0,\Delta t)}$, where $\hat{\Omega}$ can be written as a series expansion $\hat{\Omega}(t_0, \Delta t) = \sum_{k=1}^{\infty} \hat{\Omega}_k(t_0, \Delta t)$ [100, 101]. If the Hamiltonian is independent of time, the series expansion of $\hat{\Omega}$ is reduced to a single term such that

$$|\Psi(t_0 + \Delta t)\rangle = e^{-i\hat{H}\Delta t/\hbar}|\Psi(t_0)\rangle \tag{3.15}$$

which can be easily calculated if one expands the state in eigenvectors to $\hat{H}$. In the case of a time-dependent Hamiltonian the series expansion is more complicated. The first term in the expansion of $\hat{\Omega}$ is given by

$$\hat{\Omega}_1(t_0, \Delta t) = -\frac{i}{\hbar}\int_{t_0}^{t_0+\Delta t} \hat{H}(\tau)\mathrm{d}\tau \tag{3.16}$$

which is also the only term needed if the Hamiltonian at different times commutes [25]. In case of a time-dependent Hamiltonian that does not commute for different times, the whole expansion needs to be considered. However, if the time-step is sufficiently small, higher terms should be negligible and one may approximate the time-evolution operator with only the first order term $\hat{\Omega}_1$ or even take the Hamiltonian to be constant over the time-interval.

Calculating the operator exponential by diagonalizing the Hamiltonian can be computationally expensive if the basis used is large. The Lanczos algorithm [96] can then be used to efficiently create a good approximation. Starting from an initial state $|\Psi\rangle$, after performing the Lanczos iteration m times, one obtains a set of m orthogonal states $|\Lambda_i\rangle$ that span the Krylov subspace, a space that is also spanned by the states $|\Psi\rangle$, $\hat{H}|\Psi\rangle$, $\hat{H}^2|\Psi\rangle$ up to $\hat{H}^{m-1}|\Psi\rangle$ [102]. The time-independent

Hamiltonian $\hat{H}_K$ within the Krylov space is also obtained. This Hamiltonian can be diagonalized, producing an orthonormal set of eigenvectors $|\Upsilon_k\rangle$ with eigenvalues ε_k. By projecting the initial state $|\Psi(t_0)\rangle \equiv |\Lambda_0\rangle$ onto the eigenvectors $|\Upsilon_k\rangle$, propagating the state one time step forward becomes

$$|\Psi(t_0+\Delta t)\rangle = \sum_{i=0}^{m-1}\sum_{k=0}^{m-1}|\Lambda_i\rangle\langle\Lambda_i|\Upsilon_k\rangle e^{-\frac{i}{\hbar}\varepsilon_k\Delta t}\langle\Upsilon_k|\Lambda_0\rangle, \tag{3.17}$$

where it is then used that the Hamiltonian is diagonal in $|\Upsilon_k\rangle$, i.e. $\langle\Upsilon_k|\hat{H}_K|\Upsilon_l\rangle = \varepsilon_k\delta_{kl}$. The performance gain here is that the dimension m of the Krylov space can be taken to be very small compared to the full basis size [102]. This can be made plausible by considering that the exponential in Eq. (3.15) can be expanded as a power series $\sum_n(-i\Delta t/\hbar)^n\hat{H}^n/n!$ such that when Δt is small only $\hat{H}^n$ with small n has any appreciable impact. As m is small the diagonalization of $\hat{H}_K$ can be performed quickly for each time-step. Another advantage of this method is that the Lanczos algorithm only involves matrix-vector multiplications, an operation where one can use the sparseness of the matrix to reduce the workload.

We have also considered a different numerical approach for performing time-propagation. Using the expansion $|\Psi(t)\rangle = \sum_n c_n(t)|\Phi_n\rangle$ in the Schrödinger equation one obtains a set of coupled differential equations for the coefficients $c_n(t)$. There exists many numerical scheme to integrate these coupled differential equations, e.g. the Runge-Kutta methods [103]. If the Hamiltonian is dominated by a diagonal time-independent part $\hat{H}_0$ as compared to a time-dependent, possibly non-diagonal, part $\hat{H}_I(t)$ one may perform this integration efficiently using the method of exponential time differencing [104]. We then start with the matrix representation of the Schrödinger equation for the state vector $\mathbf{c}(t) = \{c_0(t), c_1(t), \dots\}$

$$i\hbar\frac{\partial}{\partial t}\mathbf{c}(t) = [\mathbf{H}_0 + \mathbf{H}_I(t)]\mathbf{c}(t), \tag{3.18}$$

where $\mathbf{H}_0$ and $\mathbf{H}_I(t)$ are the matrix representations of $\hat{H}_0$ and $\hat{H}_I(t)$ respectively. Multiplying with the integrating factor $e^{\frac{i}{\hbar}\mathbf{H}_0 t}$ and integrating from t to $t+\Delta t$, i.e. one time-step yields the exact equation

$$\begin{aligned}\mathbf{c}(t+\Delta t) = {} & e^{-\frac{i}{\hbar}\mathbf{H}_0\Delta t}\mathbf{c}(t) \\ & - \frac{i}{\hbar}e^{-\frac{i}{\hbar}\mathbf{H}_0(t+\Delta t)}\int_t^{t+\Delta t} e^{\frac{i}{\hbar}\mathbf{H}_0(t+\tau)}\mathbf{H}_I(t+\tau)\mathbf{c}(t+\tau)\mathrm{d}\tau.\end{aligned} \tag{3.19}$$

Typically, the part $\mathbf{I}(\tau) = -\frac{i}{\hbar}\mathbf{H}_I(t+\tau)\mathbf{c}(t+\tau)$ of the integrand is nicely behaving in time when dominated by the low-energy states. Such a scenario is common when, e.g., starting the simulation from the ground state. The numerically problematic part comes when multiplying with the factor $e^{\frac{i}{\hbar}\mathbf{H}_0(t+\tau)}$, which induces fast oscillations for the high-energy components. However, the integral in Eq. (3.19) can be solved exactly if $\mathbf{I}(\tau)$ is approximated by a finite polynomial. This is the method of exponential time differencing [104]. As $\mathbf{I}(\tau)$ is nicely behaving, the polynomial should not require a high degree for a good approximation. In Sec. 4.4 we will use a method utilizing the approximation

$$\mathbf{I}(\tau) \equiv \sum_{k=0}^{m-1} \frac{\tau^k}{k!}\mathbf{b}_k, \tag{3.20}$$

and where the coefficients $\mathbf{b}_k$ are found by a continuous Runge-Kutta method, as given in [105]. The full expression for propagating a time-step using the method of Ref. [105] can be found in Appendix C.

Chapter 4

Finite-size physics with ultracold atoms

In this chapter the five papers on which this thesis is based on will be given a somewhat more extended introduction together with a summary of the main results. The focus of these works has been on small droplets of quantum liquids recently made possible using ultracold atoms, introduced in Chap. 2. In the limit of large particle numbers, these systems are known to exhibit a wide variety of different phenomena related to their quantum mechanical nature, such as solitary waves and quantized vortices. Using the methods outlined in Chap. 3, we have investigated how some of these phenomena are affected by a finite system size and how this scales with the number of particles.

Section 4.1 will introduce solitary waves which are known to form in nonlinear differential equations such as the Gross-Pitaevskii equation. The results from Paper I about the effects of a finite sized system and how those scale with the number of particles will also be presented. Moving on to two-dimensional systems, Sec. 4.2 discusses the problem of using a contact-type pseudopotential in exact diagonalization and presents the scheme to handle this which was analyzed in Paper II. The well known phenomenon of quantized vortices and their formation in superfluid condensates will then be discussed in Sec. 4.3. Here the results from Paper III about correlated states during the formation of the first vortex in a finite-size system and how this scales with the number of particles will also be summarized. These correlated states appear to be related to the hysteretic behavior observed in

the mean-field treatment, leading to the discussion in Sec. 4.4 about the driving of such a system across the transition for both a finite and infinite system. Vortices can be found in repulsive fermionic systems as well, drawing many connections to the quantum Hall effect. This will be introduced in Sec. 4.5 together with the vortices of a dipolar fermionic droplet found in Paper IV. Finally, shell structure in fermionic systems and how the anisotropy of the dipole-dipole interaction affects this phenomenon in small droplets, which was analyzed in Paper V, will be explained in Sec. 4.6.

4.1 Finite-size effects in solitary wave dynamics

In the thermodynamic limit the Gross-Pitaevskii energy functional in many cases gives the correct ground state energy [106]. The extent of the validity for smaller, finite, stationary systems has been the topic of several previous investigations, see e.g. [107–109]. Here we are instead interested in the finite-size effects in the dynamical behavior. For this we used solitary wave states as their time-evolution within the mean-field approximation is very simple, and thus easy to use for comparison. On the other hand, for a finite system where one would use the Schrödinger equation to predict the exact many-body dynamics, such states are not supported. As the particle number is reduced from infinity, there must then be differences between the two approaches. To quantify these differences, in Paper I we compared the dynamics of a solitary-wave state predicted by the Gross-Pitaevskii equation to that of a many-body state where all N particles initially are in the same solitary-wave orbital as in the mean-field calculation, but propagated in time using the Schrödinger equation.

A solitary wave is a solution $\phi(x, t)$ to a wave equation that only depends on the position x and the time t in the combination $z = x - vt$. It is thus a traveling wave that does not change its shape as it travels forward with a constant velocity v. Furthermore, the region of the wavefront should be localized. If a solitary wave has not changed its shape or velocity after colliding with another solitary wave, it is said to be a soliton. The linear Schrödinger equation does not support solitary waves, but the Gross-Pitaevskii equation, Eq. (3.2), supports them as the nonlinear term compensates the dispersion [110–112]. Solitary waves were first observed in 1834 in water waves in a canal, but have since been found in a large variety of physical systems [112]. Just a few years after the first realization of a Bose-Einstein

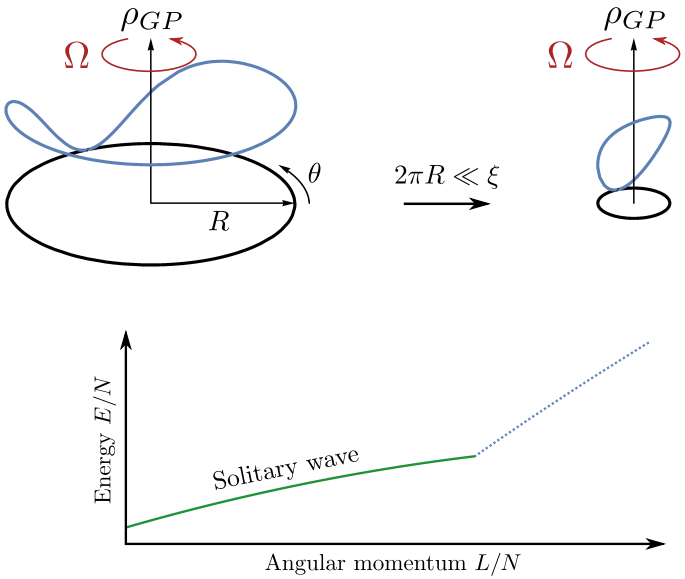

Figure 4.1: The upper part shows a schematic picture of the one-dimensional ring with bosons interacting via a contact-type interaction considered in Paper I and how the solitary wave solution becomes sinusoidal as the radius of the ring is decreased. The black curves show the ring in the plane. Blue curves are the particle density ρ_{GP} for the solitary wave solutions to Eq. (4.1) according to [121]. Lower part shows the dispersion relation for the mean-field yrast state. The solitary-wave solutions are marked by the solid green line, which starts at $L/N = 0$ and ends at the cusp at $L/N = 1$. The blue-dotted line shows the continuation of the dispersion relation.

condensate, solitary waves were observed in ultracold atomic systems [113, 114]. For a review of solitary waves and solitons in condensates, see e.g. [115].

With the realization of atomic condensates in ring shaped potentials, e.g. [11, 116–120], one may study solitary waves in a quasi-one-dimensional system with periodic boundary conditions. The Gross-Pitaevskii equation for a condensate of N particles of mass M interacting with a contact pseudopotential of strength g on a ring with radius R is

$$i\hbar\frac{\partial\psi(\theta,t)}{\partial t} = -\epsilon\frac{\partial^2\psi(\theta,t)}{\partial\theta^2} + 2\pi\epsilon\gamma|\psi(\theta,t)|^2\psi(\theta,t), \tag{4.1}$$

where θ is the position along the ring, $\epsilon = \hbar^2/(2MR^2)$ is the kinetic energy per particle and $\gamma = g(N-1)/(2\pi\epsilon)$ is the ration between the interaction and kinetic energy.

For Eq. (4.1) there are traveling wave solutions [121]. These solutions are given by the so called Jacobi elliptic functions and the shape will depend on the size of the ring. The size is characterized by the ratio of the circumference of the ring $L_{ring} = 2\pi R$ and the healing length $\xi = \hbar/\sqrt{2Mgn}$ of the condensate, where n is the particle density. In the limit of a large ring, where $L_{ring} \gg \xi$, the wavefront is localized to a specific region on the ring. In the opposite limit, for small rings, $L_{ring} \ll \xi$, the wave is instead sinusoidal. The two different limits of the solution are illustrated in the upper part of Fig. 4.1. It also turns out that the solitary wave states are equivalent to the yrast states [122, 123], i.e. the state with the lowest energy for a given value of the angular momentum. These states can thus be found by minimizing the energy functional Eq. (3.4) under the constraint of fixed angular momentum ℓ. The dispersion relation for the ring system is sketched in the lower part of Fig. 4.1. Solitary waves can also be created by stirring the condensate using a potential barrier [124].

In Paper I we solved Eq. (4.1) for weak interactions, $\gamma \ll 1$, and angular momentum per particle $\ell = L/N$ such that $0 \leq \ell \leq \hbar$. The single-particle density $\rho_{GP}(\theta, t)$ predicted by the Gross-Pitaevskii equation was found to be

$$2\pi\rho_{GP}(\theta, t) = 2\pi|\psi(\theta, t)|^2 = 1 + 2\sqrt{\ell(1-\ell)}\cos(\theta - \Omega_{GP}t), \tag{4.2}$$

where

$$\Omega_{GP} = [1 + \gamma(1 - 2\ell)]\,\frac{\epsilon}{\hbar} \tag{4.3}$$

is the angular frequency of rotation of the solitary wave solution. As the interactions are weak, the healing length is long and the ring is thus considered to be small. Hence, the sinusoidal form of the solution. Similarly, we were also able to solve the time-evolution of the corresponding full many-body state. The single-particle density $\rho(\theta, t)$ for the finite system is

$$2\pi\rho(\theta, t) = 1 + 2\sqrt{\ell(1-\ell)}A(t)\cos[\theta - \Omega(t)t] \tag{4.4}$$

with

$$A(t) = \left[1 - 4\ell(1-\ell)\sin^2\left(\frac{gt}{2\pi\hbar}\right)\right]^{(N-1)/2}, \tag{4.5}$$

$$\Omega(t) = \frac{\epsilon}{\hbar} + \frac{(N-1)\omega(t)}{t}, \tag{4.6}$$

$$\tan[\omega(t)] = (1 - 2\ell)\tan\left(\frac{gt}{2\pi\hbar}\right). \tag{4.7}$$

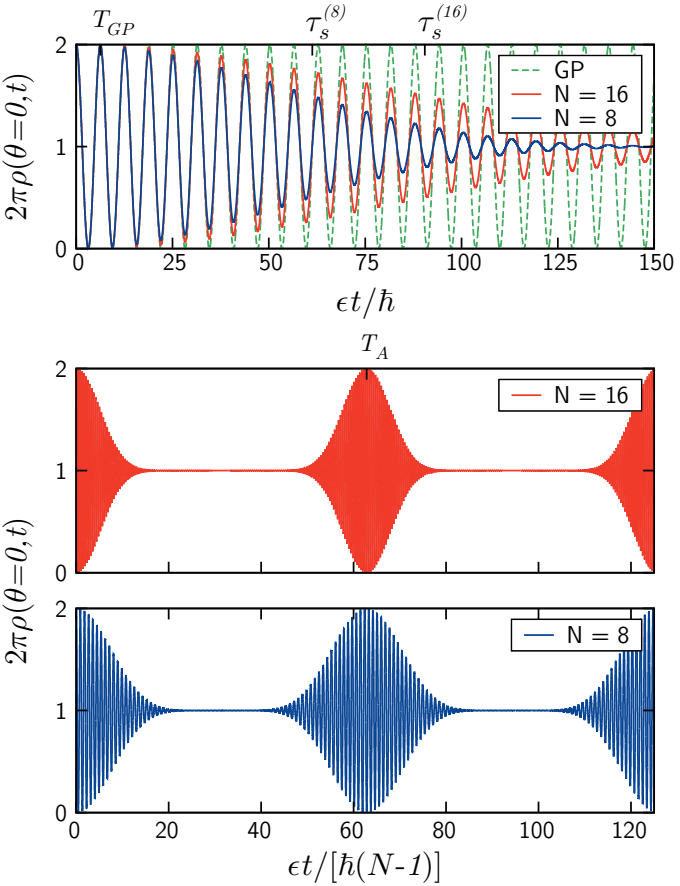

Figure 4.2: Time-evolution of the particle density at $\theta = 0$ of a solitary-wave state in a ring potential according to Eqs. (4.2) and (4.4). Here $\gamma = 0.05$ and $\ell = 1/2$. In the top panel the collapse of the solitary wave for finite-size systems is shown for both $N = 8$ and $N = 16$ as well as the corresponding mean-field solution. The two lower panels show revivals of the solitary wave at longer times. Note here that the unit of time is scaled by a factor of $(N - 1)$. Taken from Paper I where it is Figure 1.

A comparison of the resulting time-evolution of the particle density for a system with $N = 8$ or $N = 16$, $\ell = 1/2$ and $\gamma = 0.05$ using Eqs. (4.2) and (4.4) is shown in Fig. 4.2. Although the sinusoidal structure is the same, the finite-size system experiences periodic collapses and revivals of the wavefront in the particle density. Starting out clearly visible, the wavefront gradually becomes less pronounced until it completely disappears. However, after some more time the wavefront begins to appear again. This cycle then repeats forever. Collapses and revivals of a quantum system are to be expected in the time-evolution of a system with discrete energy

spectrum and a time-independent Hamiltonian, as has been observed in e.g. simulations of the Jaynes-Cummings model [125] or experimentally using ultracold atoms in optical lattices [126, 127].

The specific properties of this system lead to a highly regular periodicity of the collapses and revivals. Examining the expression for the particle densities, we found a hierarchy of timescales when N is large, but finite, together with γ and ϵ fixed, as

$$T_{GP} \ll \tau_s \ll T_A, \tag{4.8}$$

separated by a factor $\sqrt{N}$. Here T_{GP} is the time it takes for the wavefront to travel around the ring once, τ_s is the time it takes for $A(t)$ to go from its largest value to half of that, i.e. an estimate for the width of the region where the solitary wave behavior is present, and T_A the time between the revivals. These scalings were also found to hold for stronger interactions. We can also see that in the limit $N \to \infty$, with γ and ϵ fixed, $A(t) \to 1$ and $\Omega(t) \to \Omega_{GP}$, such that the two approaches agree in the large-N limit.

The parameter regime considered in Paper I should be within reach of current experimental setups [11, 116–120], although the very low particle number presents a difficult experimental challenge. If such low numbers could be achieved and the collapses and revivals are observed, they could together with the hierarchy of the scaling of the different timescales e.g. be used to give an estimate of the particle number. The exact solution could also be used to further study the build-up of the nonlinear term in the Gross-Pitaevskii equation and the scalings found could give an estimate of how long these nonlinear effects might survive. Additionally, the exact solution could potentially also be analyzed further by e.g. examining its density matrix and natural orbitals in order to get a better understanding of the connection and differences between the Schrödinger equation and Gross-Pitaevskii equation dynamics.

4.2 Renormalization of contact interactions in two dimensions

In Sec. 2.3 it was shown that in the limit of low energy, the scattering is determined by only one parameter of the scattering potential, the scattering length a.

One may then replace the true potential with a pseudopotential that will give the same scattering length but is easier to use in calculations and still get the correct results. Ultracold atomic systems are usually in the regime of low-energy scattering and the contact-type pseudopotential in Eq. (2.12) has been successfully used in many investigations of these systems. There, the pseudopotential can be seen as an effective interaction where effects of the short-range correlations from the interactions have already been incorporated. This works well when combined with a mean-field treatment, where only long-wavelength effects are considered [29].

When studying few-particle systems, it is feasible to not just rely upon the mean-field approximation, but to also utilize the full Schrödinger equation. However, using the delta function potential directly in the Hamiltonian of the system is problematic, as was noted already in the scattering problem in Sec. 2.3. It turns out that in two or three dimensions, the resulting Hamiltonian operator is not self-adjoint [37] and, as the spectral theorem is then not applicable, one is not guaranteed to be able to find eigenvectors with real, i.e. physical, energy eigenvalues.

There exists a plethora of different ways to try to remedy this problem. As one is typically only interested in the low-energy behavior, one way is to make a cut-off in the integrals over all momenta. Another way is to use a well-behaving modified, regularized, potential. E.g. it turns out that the boundary conditions of hard spheres, requiring that the wave function is identically zero for relative distances less than the diameter of the spheres, can be rewritten as a regular contact interaction [128–130]. This potential,

$$V(\mathbf{r})(\dots) = \frac{4\pi\hbar^2 a}{m}\delta(\mathbf{r})\frac{\partial}{\partial r}r(\dots), \tag{4.9}$$

where the dots indicate that this is an operator that needs to act on a wave function, can be shown to exactly give the s-wave scattering amplitude in Eq. (2.9) [128, 129]. It can also be shown that such a potential can be extended to a family of regularized contact pseudopotentials given by

$$V_{reg}(\mathbf{r}) = -\frac{2\pi\delta(\mathbf{r})}{\ln(\mathcal{A}a\Lambda)}\left[1 - \ln(\mathcal{A}\Lambda r)r\frac{\partial}{\partial r}\right], \tag{4.10}$$

where Λ is a arbitrary constant for which no observable will depend on and $\mathcal{A} = e^{\gamma}/2$ with γ being the Euler-Mascheroni constant [130].

Regularized potentials have been used to solve few-body systems analytically, e.g. two and three particles in a harmonic trap [37, 131, 132]. For two particles in a harmonic trap we can transform the problem to the center-of-mass and relative motion coordinates. The center-of-mass problem is just a normal harmonic oscillator for which the solutions are well known, but for the relative coordinate $\mathbf{r}$ we have a non-trivial Hamiltonian H_{rel}^{reg} including the regularized interaction potential $V_{reg}(\mathbf{r})$. Expanding the solution in the harmonic oscillator eigenstates together with the requirement of normalization, one may rewrite the eigenvalue problem for H_{rel}^{reg} into the equation

$$\psi(1/2 - E_{rel}^{reg}/2) = \ln(2/a^2), \tag{4.11}$$

where E_{rel}^{reg} is the eigenstate energy and ψ here is the digamma function [37]. Combined with the center-of-mass system, the total energy is given by

$$E^{reg} = E_{com} + E_{rel}^{reg}, \tag{4.12}$$

where E_{com} is the energy associated with the center-of-mass system. If the angular momentum for the relative motion is even, the solution is valid for both two spin-polarized bosons and a singlet state of two fermions.

Although regularized potentials can be used successfully in analytical treatments, to use them in numerical calculations, e.g. if one would try to solve the eigenvalue problem by constructing a matrix representation of the Hamiltonian, is not straightforward [129]. Using basis functions that do not explicitly take into account the corresponding boundary conditions, the matrix might not be Hermitian [38]. Thus, it is again not guaranteed to give a reasonable result. On the other hand, using the bare contact potential on a finite basis of well-behaved functions will produce a Hermitian matrix that can be diagonalized. Here, the problem is instead that the obtained eigenvalues will not converge as the size of the finite basis is increased.

In some instances it could still be desirable to be able to use the contact interaction in exact diagonalizations of few-particle systems, e.g. for its simplicity or for direct comparisons to mean-field simulations. To this end, in Paper II we investigated a scheme where one does not view the coupling constant of a bare delta potential in the many-body Hamiltonian to be directly given by the scattering length. Instead, the coupling strength, for the specific model space basis considered, is linked to its corresponding physical value of the scattering length by comparison of the two-particle ground state energy in the exact regularized problem, Eq. (4.12), and the diagonalized value.

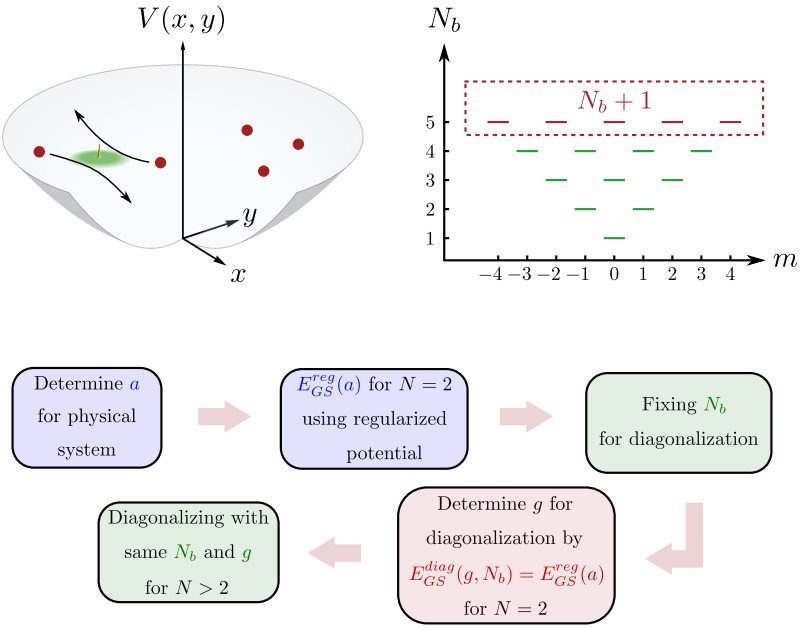

Figure 4.3: The upper left part shows a schematic picture of the system considered in Paper II, a harmonically trapped and few-body system with contact type interactions in two dimensions. In the upper right corner the single-particle spectrum and its relation to the basis size parameter N_b and angular momentum quantum number m is shown. The addition of another oscillator shell to the diagonalization basis is sketched. The lower part of the figure briefly describes the algorithm for connecting the physical scattering length parameter a to the diagonalization coupling strength g used in Paper II.

If one would like to numerically diagonalize a system of N particles in a harmonic trap with contact interactions with strength g one needs to specify a basis of the finite-dimensional Hilbert space to be used. The size of this space is characterized by a parameter N_b and the obtained eigenvalues will then depend on both g and N_b. The system and the single-particle spectrum together with the basis size parameter N_b are illustrated in the top part of Fig. 4.3. For such a system we then say that the coupling strength in this truncated space corresponds to the system with a scattering length a according to

$$E_{GS}^{diag}(N=2,g,N_b) = E_{GS}^{reg}(N=2,a), \tag{4.13}$$

where E_{GS}^{diag} is the ground state energy for two particles obtained by the numerical diagonalization and E_{GS}^{reg} is the ground state energy of the regularized problem,

Eq. (4.12). A flow chart of this algorithm is shown in the lower part of Fig. 4.3.

The analysis in Paper II showed that this scheme does indeed give converging eigenvalues as the basis size is increased. The results are also consistent with the analytical solutions for two and three particles. It was also determined that the truncation of the basis can be seen as a cut-off parameter in real space, limiting the resolution of short-range features. Thus, the method is more suitable for unpolarized fermionic systems compared to bosonic ones due to the repulsion coming from the Pauli principle. Finally it was also demonstrated that the convergence persists for larger particle numbers, validating the results of e.g. Refs. [133, 134] obtained using this scheme.

4.3 Correlated states during the nucleation of a vortex

One of the peculiar features of Bose-Einstein condensates are the so called quantized vortices, in analogy to the vortex patterns that were found in liquid Helium [64]. The occurrence of vortices is often associated with the rotation of the superfluid. Likewise, such as the critical velocity [135] and the non-classical rotational inertia [32, 64], the so called Hess-Fairbank effect [136] are consequences of the superfluid flow. In ultracold atomic systems, such quantized vortices can become macroscopically observable [137].

As the wave function Ψ is complex valued, one may write it as an amplitude n and a phase S according to

$$\Psi(\{\mathbf{r}_i\}, t) = \sqrt{n(\{\mathbf{r}_i\}, t)} e^{iS(\{\mathbf{r}_i\}, t)}, \tag{4.14}$$

where $\mathbf{r}_i$ is the position of particle i and t is the time. Inserting this into the Schrödinger equation, we instead obtain two alternative equations similar to classical hydrodynamics. For a condensate this becomes particularly simple as one can do the same reformulation with the macroscopic wave function, which is a single-particle object, together with the time-dependent Gross-Pitaevskii equation. The first equation one then obtains is a Bernoulli-type equation that is appropriate to use when describing a superfluid [137]. The second equation is a continuity equation

$$\frac{\partial n}{\partial t} + \nabla \cdot \mathbf{j} = 0 \tag{4.15}$$

relating the probability density $n = |\Psi|^2$ to the probability current $\mathbf{j}$, which is given by

$$\mathbf{j} = \frac{i\hbar}{2m}\left(\Psi\nabla\Psi^* - \Psi^*\nabla\Psi\right). \tag{4.16}$$

Applying this to Ψ in the form Eq. (4.14), we immediately get

$$\mathbf{j}(\mathbf{r},t) = n(\mathbf{r},t)\frac{\hbar}{m}\nabla S(\mathbf{r},t) \equiv n(\mathbf{r},t)\mathbf{v}(\mathbf{r},t), \tag{4.17}$$

where we have identified a velocity $\mathbf{v} = \frac{\hbar}{m}\nabla S$. That the fluid velocity is given by the gradient of the phase has the consequence that the flow must be irrotational, i.e. the vorticity $\nabla \times \mathbf{v} = 0$. This implies that a line integral of the velocity field over a closed curve is identically zero. Such a line integral is called the circulation. However, if there are singularities inside the region encircled by the curve, the line integral need not to be zero. Since the phase is only defined modulo 2π, we get that the circulation around a singularity is quantized according to

$$\oint_{\mathcal{C}} \mathbf{v}\cdot d\mathbf{l} = \frac{\hbar}{m}2\pi k, \tag{4.18}$$

where $\mathcal{C}$ is the curve and k is an integer. In the region near the singularity, the velocity goes as $1/r$, where r is the distance to the singularity, and in order for the energy of this solution not to diverge the particle density must vanish at the center [32]. Thus, the quantized phase-singularity is accompanied by a node in the density, around which there is a circular flow, forming a quantized vortex.

Early on in the studies of ultracold atomic gases several different ways of creating quantized vortices were developed. The first reported vortices were created in a two-component gas using a method of imprinting the phase by a moving laser [138], driving the transition between the two different components [139]. Later, vortices were also created by stirring the condensate using a rotating potential. Such stirring has now been achieved using both optical [140] and magnetic [141] traps.

The nucleation, stability and dynamical behavior of vortices in ultracold atomic gases have since been extensively investigated both theoretically and experimentally. See e.g. [137, 142] for reviews. Below a certain rotational frequency of the system, the configuration with no vortex is found to be the lowest in energy. Increasing the rotational frequency to above the critical frequency the configuration

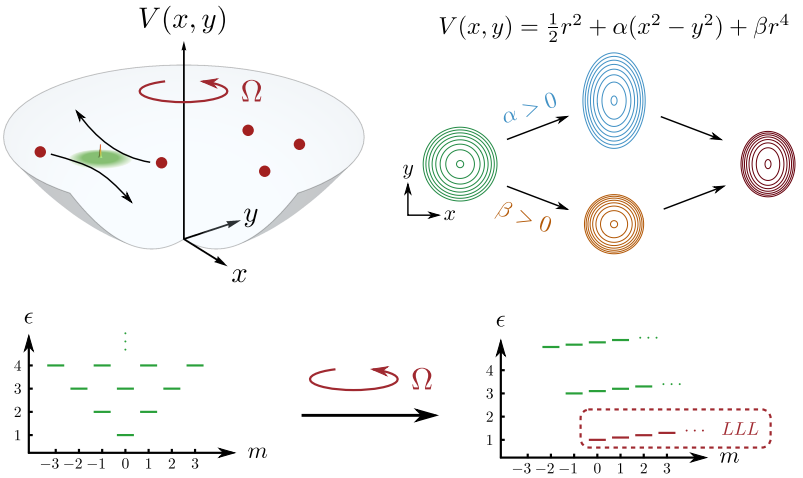

Figure 4.4: Upper left part shows a schematic picture of the system considered in Paper III, a harmonically trapped few-body system with contact type interactions rotating with angular velocity Ω around the z-axis. Contours of the trapping potential with the different deformations used are shown in the upper right part of the figure. The lower part sketches the single-particle spectrum and the formation of Landau levels, and in particular the lowest Landau level used as the basis in the calculation, as the rotation is increased.

of a vortex with one quantum of circulation becomes the lowest in energy instead. Thus, for such rotations the vortex is energetically stable. Within the mean-field approximation this has been found to be valid in both the strong-coupling limit [143, 144], where the first experiments were performed, as well as in the weakly interacting regime [145, 146]. Going beyond the mean-field approach, similar results have also been found when examining the full many-body eigenstates where the analysis is greatly simplified by the grouping of the single-particle orbitals into Landau levels, as depicted in the lower portion of Fig. 4.4. Due to the weak interactions it is sufficient to consider the lowest Landau level, within which this problem is exactly solvable [147–149].

In the experiments where the gas was stirred by a rotating elliptic trap however, the vortex did not enter the particle cloud at the value where a single vortex is predicted to become energetically stable. To resolve this discrepancy the whole dynamical process had to be considered [150–153]. Mean-field studies in the strong-coupling regime have shown that an elliptic stirring deformation of quadrupolar form, $\propto x^2 - y^2$, at some critical rotation resonantly excites a quadrupole mode in the condensate [150]. If the deformation is larger than a specific value, the quadrupole

mode becomes unstable. This leads to a so called dynamical instability, meaning that the system exhibits turbulent and chaotic dynamics [150].

It has been suggested that chaotic mean-field dynamics could be a sign of quantum entanglement [154]. Indeed, this seems to be the case for the nucleation of vortices by a quadrupolar stirrer. A system consisting of a small, but even, number of weakly interacting bosons, sketched in the upper left of Fig. 4.4, shows large differences compared to the mean-field results [155]. Due to the symmetries of the system, it was found that the system passes through a point during the nucleation process where the density matrix has two equally large eigenvalues. At this critical frequency Ω_c the ground state is entangled and strongly correlated [156]. There is however a significant difference in the reported behavior of this system when the system size is small, $N \leq 20$ as in [156, 157], and when the system is large, $N > 160$ as in [155]. There has recently been an increasing interest in correlated macroscopic quantum states, see e.g. [158] for a review. We thus characterized this system at the critical point for an intermediate range of sizes in Paper III and reconcile the different results previously reported.

At the critical point Ω_c, most of the weight of the ground state can be found in the subspace spanned by the Fock states $|N-n,n\rangle = |\psi_1\rangle^{\otimes N-n} \otimes |\psi_2\rangle^{\otimes n}$ containing particles only in the two natural orbitals $|\psi_1\rangle$ and $|\psi_2\rangle$ with the largest associated eigenvalues of the density matrix [156]. We constructed a two-mode model and solved it in the semiclassical approximation similar to [159], giving an energy of $\tilde{E} = \tilde{E}_0(\phi) + \frac{f_1(\phi)}{2}\cos\theta + \frac{f_2}{2}\cos^2\theta$, where f_1 and f_2 are terms constructed using the interaction matrix elements and ϕ and θ are spherical angles characterizing where on the Bloch sphere the state is found [160]. The minimum was found to be for $\phi = 0$ and, depending on the sign of the quantity f_1 , either $\cos\theta = 0$ or $\cos\theta = \pm 1$. This implies that the ground state is either of the form $|N/2, N/2\rangle$ or $(|0,N\rangle + |N,0\rangle)/\sqrt{2}$ for $f_1 > 0$ or $f_1 < 0$ respectively.

Our numerical analysis in Paper III confirmed this behavior and we were able to identify the few-body precursor states to the two different types of states mentioned in the previous paragraph, as shown in Fig. 4.5. However, we were not able to obtain a state on the form $(|0,N\rangle + |N,0\rangle)/\sqrt{2}$ using only a quadrupole deformation $\alpha(x^2 - y^2)$. This could however be achieved by adding an additional quartic potential βr^4. Contour plots of the different potentials used can be seen in the top right of Fig. 4.4. In addition, we also found that as both f_1 and f_2 scale roughly linear with N the behavior predicted in Paper III becomes more

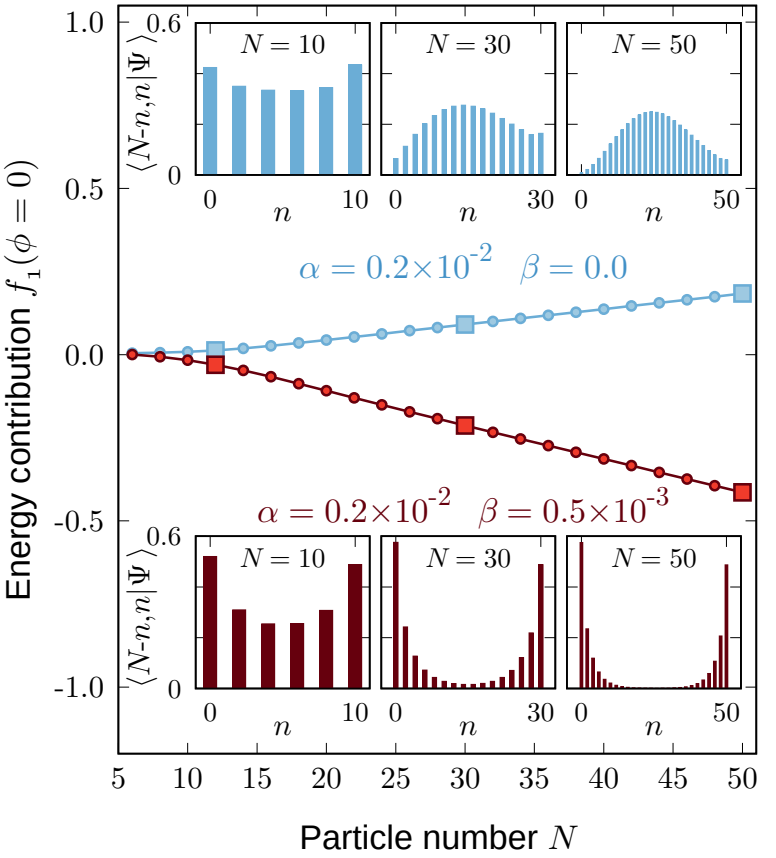

Figure 4.5: The energy term f_1 in the semi-classical ground state energy for different system sizes. The top part, in blue, shows the behavior of the system with a small quadrupole deformation of the form $\alpha(\hat{x}^2 - \hat{y}^2)$, and the bottom part, in red, is for a system with the same quadrupole deformation together with a small extra quartic potential of the form βr^4. The squares mark the systems whose expansion coefficients $\langle N - n, n|\Psi\rangle$ are shown in the insets at the top and bottom. Taken from Paper III where it is Fig. 2.

pronounced as N is increased. This also means that if N is decreased, the system starts to deviate from the behavior of the semiclassical solution and it was found that the ground state starts to resemble the form $(|N, 0\rangle + |N-2, 2\rangle + \cdots + |0, N\rangle)/\sqrt{N/2+1}$, linking together the results of the previous studies [156] and [155].

As the matrix elements used in the above two-mode model are constructed from the natural orbitals, they require a diagonalization of the full many-body problem

to be performed. Therefore it would be desirable if a way to approximate the orbitals was conceived, giving the model some predictive power. As the mean-field approximation does not distinguish between even and odd N for this parity-conserving potential, investigating the effects of a parity-breaking perturbation and the behavior of a system with N odd is however a straightforward extension. The addition of a quartic perturbation causes the vortex nucleation to experience hysteresis and the difference between the mean-field behavior and the full many-body dynamics will be discussed in Sec. 4.4.

4.4 Hysteresis in vortex nucleation for a deformed trap

When a system experiences hysteresis the current state depends on the history of the system. A well known example is the response of a ferromagnet to an external magnetic field. After becoming magnetized, up to a point, the magnetization will stay pointing in that direction even if the external field is reversed to the opposite direction. Going back to the first orientation also requires the strength of the field to reach a certain value before the flip happens. In a bosonic condensate the persistent currents can be seen as a hysteretic response to rotation [161]. It has been observed and investigated both experimentally [162] and theoretically [163] for a condensate in a ring-like potential.

A hysteretic behavior can be explained if the energy landscape as a function of an order parameter has more than one minimum for some strength of an external field [161]. This is illustrated in Fig. 4.6 where two cases are considered, either an energy landscape with one or two local minima. When there is only one minimum the system will stay there as the field is changed at a slow speed. In the case of two local minima separated by a barrier between them, the system will instead stay in the minimum it was in at the beginning even though it is no longer the global minimum. Only when this minimum ceases to exist will the system jump to the other. This will be indicated by a structure similar to a swallow tail in the energy when viewed as a function of the external field.

The phenomenon of hysteresis is more complicated to describe using the full many-body Schrödinger equation. When doing so one cannot get a simple energy surface as a function of an order parameter. There might not be eigenstates corresponding to such configurations [161]. Furthermore, if the change of the driving field is done very slow, the system should stay in the ground state and only

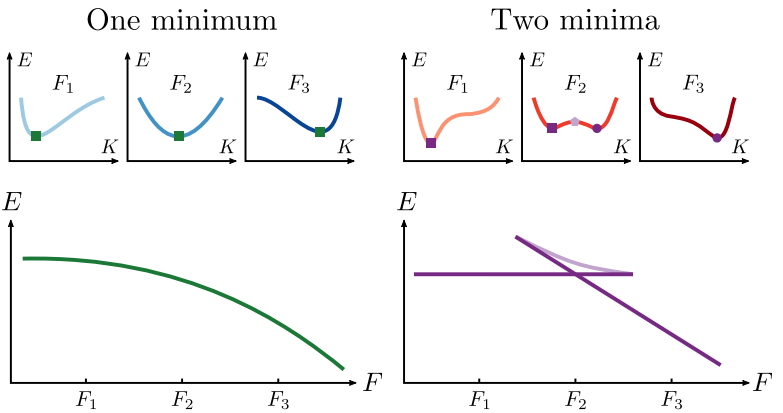

Figure 4.6: Schematic picture of hysteresis when the energy landscape has two local minima. The panels to the left shows the situation when there is only one local minimum at each value of an external field F. In the panels to the right the mean-field energy has as region where there are two local minima. The top panels schematically sketch the mean-field energy E as a function of the order parameter K at three different values of F, for the both the cases of one and two local minima. Squares and dots indicate minima and the pentagon indicates the local maximum. In the lower panels the minima and maxima are shown as a function of F. For the case of two minima the energy exhibit the swallow tail structure, leading to a hysteretic behavior.

acquire the normal phase factor of time-evolving an eigenstate. In order to facilitate the memory effect of the hysteresis, the system is thought to pass through a very narrow avoided crossing in the many-body energy spectrum as it is driven through the transition [162].

In Sec. 4.3 we observed two different types of avoided crossings in the formation of vortices in a rotating Bose-Einstein condensate depending on the shape of a rotating perturbation. Thus, we here investigate if these different systems exhibit hysteresis when ramping the rotational frequency up and down through the avoided crossing. Starting off, we numerically minimize the Gross-Pitaevskii energy functional, Eq. (3.4), for a fixed value of the order parameter, here the angular momentum per particle L/N. The results are shown in the upper panels of Fig. 4.7. The energy surface is shown as a function of L/N and the rotational frequency Ω, obtain through $E(\Omega) = E_0 - \Omega L$, where E_0 is the minimum energy for zero rotation. For the pure quadrupolar deformation we observe only one energy minimum for all values of Ω close to the critical frequency Ω_c of the many-body system, defined in the previous section. However, when adding an

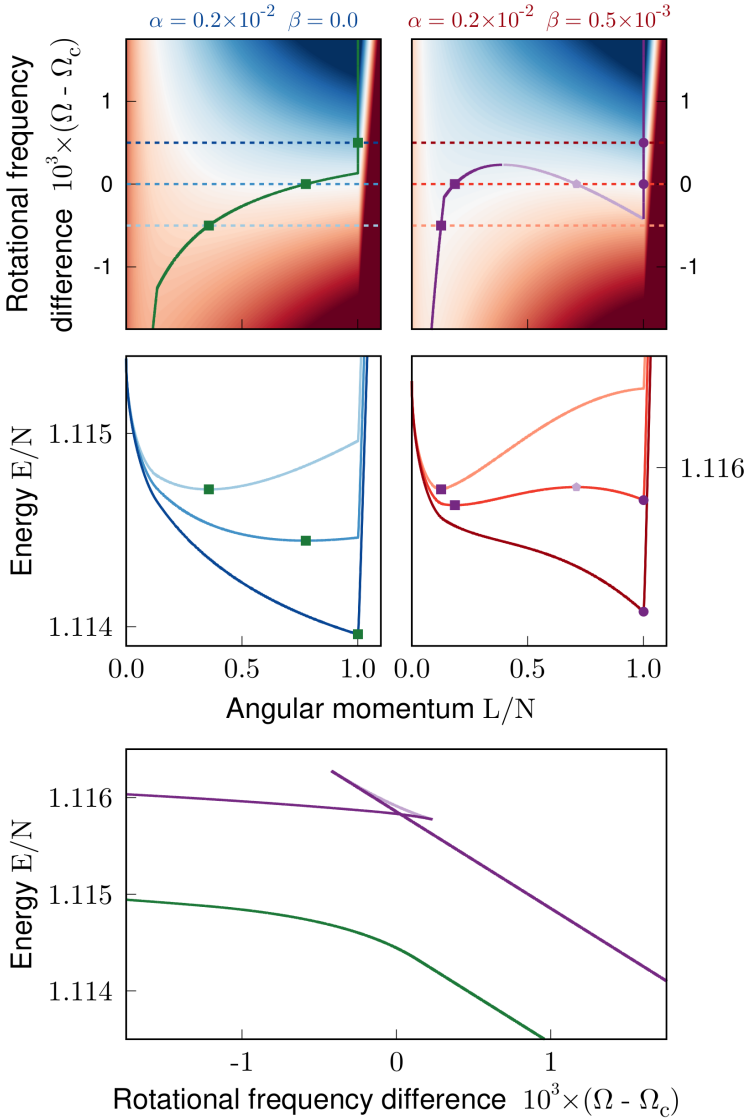

Figure 4.7: The upper panels show the minimum energy surfaces for the two different deformations considered, as a function of angular momentum and rotational frequency. The dark curve marks the local minima at each Ω. In the upper right panel the lighter curve marks the local maximum in the region where there are two local minima. In the middle panels the minimum energy for each value of L/N is shown for the three values of Ω marked by dashed lines in the upper panels. Squares and circles indicate the local minima and the pentagon marks the maximum. The lower panel shows as a function of Ω, in relation to Ω_c, the energy of the extreme points.

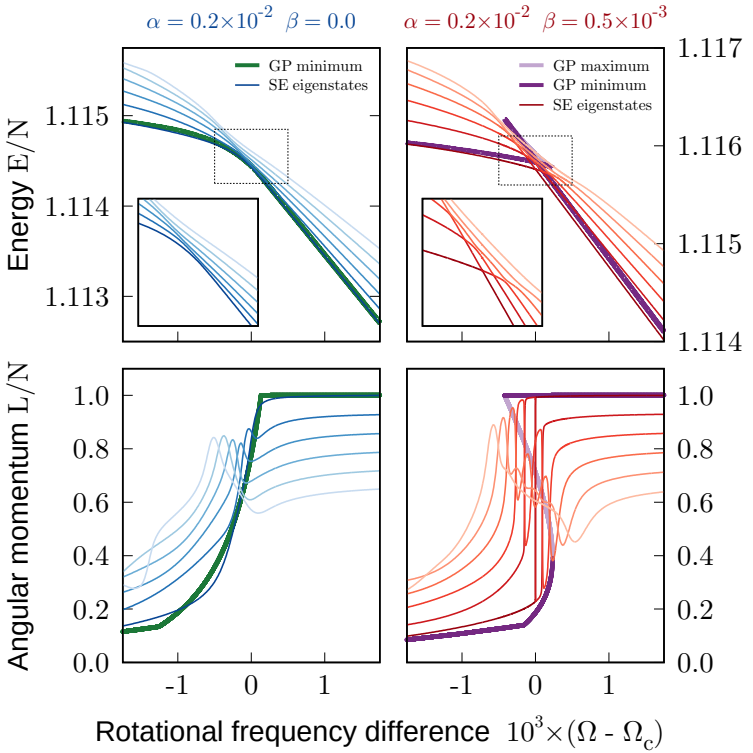

Figure 4.8: Spectrum for both the system with only a quadrupolar deformation and the one with both a quadrupolar, on the left, and an additional quartic deformation, on the right. The upper panels show the energy of the six lowest eigenstates with even parity of the systems with $N = 30$ and $gN = 1.5$ for the two different types of deformations considered. Thicker lines in a darker are the energy minima in the mean-field treatment shown in Fig. 4.7. The insets show the region marked with the dashed border which is around the avoided crossing of the ground state. The lower panels show in a similar way to the upper panels the angular momentum for the eigenstates and mean-field energy minima. Both energy and angular momentum are shown as functions of Ω in relation to the critical rotational frequency.

additional quartic deformation there appears a region with two energy minima. The middle panels of Fig. 4.7 show the energy as a function of L/N for the three rotational frequencies marked by dashed lines in the upper panels. The region with two minima can clearly be seen for the system with $\beta > 0$. We also observe a difference in the two minima where the energy surface is smooth around the minima for L/N close to zero, but a very sharp cusp at $L/N \approx 1$. In the lower panel the energy as a function of the external field Ω is shown and we clearly see the swallow tail structure when adding the quartic deformation.

A direct comparison of the stationary states of the Gross-Pitaevskii equation in Fig. 4.7 and the low-lying energy eigenstates for a system with $N = 30$ can be seen in Fig. 4.8. Here the mean-field results have been shifted in Ω to fit the many-body spectrum due to the vortex formation being dependent on the interaction energy, which will be different compared to the full many-body state. With this shift we observe a reasonable agreement between the full many-body ground state and the minimal energy state of the mean-field, despite there being a correlated state the mean-field equation should not be able to reproduce at Ω_c. We can also see that the minimum at $L \approx N$ ceases to be a minimum very abruptly. This is the case for both types of deformations, although for the additional quartic deformation the mean-field minimum does overshoot the eigenstates angular momentum before vanishing. The region of the hysteresis loop when $\beta > 0$ can be seen to roughly correspond to the region of the many-body spectrum where the avoided crossings are much sharper and are described by states on the form $(|N,0\rangle + |0,N\rangle)/\sqrt{2}$, shown in the inset of the upper right panel in Fig. 4.8.

As hysteresis is a dynamical phenomenon, we would like to calculate the time-evolution when driving these systems through the critical points. Such a driving can be done by ramping up, and down, the rotational frequency past Ω_c. All the time-dependence will then be in the Coriolis term, i.e. the Hamiltonian will be of the form $\hat{H}(t) = \hat{H}_0 - \Omega(t)\hat{L}_z$. The ramping is further assumed to be linear such that $\Omega(t) = \Omega_i + \gamma t$, where Ω_i is the initial rotational frequency and γ is the driving speed. We can then get an approximate value of the driving speed needed to achieve an adiabatic transition from the full many-body solution [156]. The probability of a transition $p_{0\to j}$ from the ground state $|\Psi_0\rangle$ to another eigenstate $|\Psi_j\rangle$ can be approximated using a perturbative calculation as

$$p_{0\to j} \leq \max\left(\frac{\alpha_{j0}}{\omega_{j0}}\right)^2, \tag{4.19}$$

where $\alpha_{j0} = \langle\Psi_j|(d|\Psi_0\rangle/dt)$ and $\omega_{j0} = E_j - E_0$ is the difference in energy of the two eigenstates [164]. The chain rule gives us $d|\Psi_0\rangle/dt = \dot{\Omega}d|\Psi_0\rangle/d\Omega$, where $\dot{\Omega}$ is the time-derivative of the rotational frequency, which here is γ. Using the instantaneous time-independent Schrödinger equation and projecting onto $|\Psi_j\rangle$ we get $\alpha_{j0} = \dot{\Omega}\langle\Psi_j|\hat{L}_z|\Psi_0\rangle/\omega_{j0}$, such that the driving speed in order to achieve an adiabatic passage is given by

$$\gamma_{adiabatic} \ll \frac{\omega_{j0}^2}{\langle\Psi_j|\hat{L}_z|\Psi_0\rangle} \equiv \eta. \tag{4.20}$$

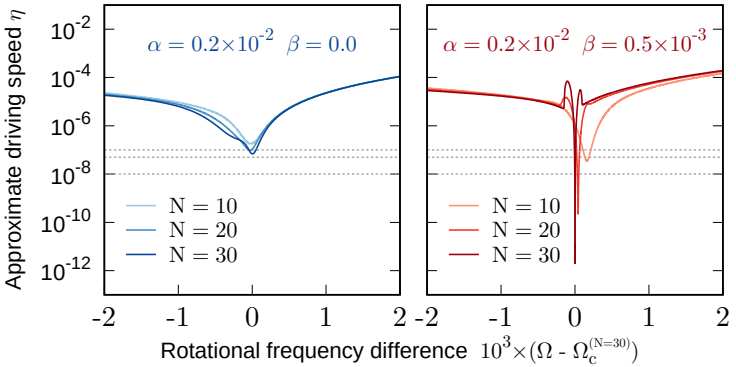

Figure 4.9: Approximate driving speed for a adiabatic transition calculated using Eq. (4.20) on the full many-body states. Three different particle numbers are given for the two types of deformations considered, shown in the left and right panel separately. The rotational frequency Ω is in relation to the critical frequency for $N = 30$ for all systems in order to separate the curves. Gray lines show the three driving speeds considered in Fig. 4.10 and Fig. 4.11.

The result of Eq. (4.20) when applied to the two systems we here consider is shown in Fig. 4.9 for three different particle numbers N. We clearly see that when the crossing starts to be described by the state $(|N,0\rangle + |0,N\rangle)/\sqrt{2}$, at $N > 20$ from Sec. 4.4, the driving of the system has to be done incredibly slow for an adiabatic sweep. Thus, for large particle numbers and experimentally realistic driving speeds the system will not stay in the ground state, but instead make a transition to and follow an excited state on the other side of Ω_c. This excited state would have a different angular momentum compared to the ground state and the time-evolution of L would show a hysteresis loop.

Performing the time-evolution with the full many-body state is challenging. The number of orbitals, and thus in the end also the Fock state basis size, needed to describe the many-body states at the crossing increases rapidly with N. In order to facilitate the calculation of the time-evolution when driving the system as slow as η, we instead diagonalize the system at Ω_c using the appropriate number of Fock states from which we then use the 200 lowest energy eigenstates as a basis for the propagation. This turns out to be adequate for the low-energy spectrum around Ω_c as the crossings we are interested in are these states coupled to each other. Thus, the Hamiltonian we use can be written as

$$\hat{H}(t) = \underbrace{\hat{H}_{sp} + \hat{V}_{int} - \Omega_c \hat{L}_z}_{\hat{H}_0} \underbrace{-(\Omega(t) - \Omega_c)\hat{L}_z}_{\hat{H}_I(t)}, \tag{4.21}$$

where $\hat{H}_{sp}$ is the single-particle part, $\hat{V}_{int}$ is the interactions and $\hat{L}_z$ is the angular momentum. The operator $\hat{H}_0$ is diagonal in the basis used and all time-dependence is in $\hat{H}_I(t)$. This system can then be propagated using the method of exponential time differencing discussed in Sec. 3.4. Similarly, the corresponding Gross-Pitaevskii equation can be time-evolved using the same method, but can directly use the single-particle orbitals making up the Fock states of the full many-body state.

In Figures 4.10 and 4.11 the time-evolutions of the systems with only quadrupolar deformation and the one with both quadrupolar and quartic deformations respectively are shown. Here a system of $N = 30$ particles is used, three different driving speeds γ are considered and both the exact dynamics and the mean-field dynamics is presented. We can see that the system without the quartic deformation can be made to stay almost entirely in the ground state at the driving speeds predicted by Eq. (4.20). At similar driving speeds we instead see the separation of the angular momentum curves when ramping up and when ramping down Ω with the additional quartic deformation added. The angular momentum also does not fully reach N or 0 when ramping up or down respectively, consistent with a transition to an excited state as predicted by Fig. 4.9. This is also supported by the expectation value of the energy which shows that the system is not in the ground state after the transition.

Comparing the dynamics of the full many-body state with the corresponding mean-field time-evolution we observe a surprisingly good agreement for the slowest driving speed considered. Perhaps the most prominent difference is the tendency for the Gross-Pitaevskii equation to predict the system to stay in the vortex state when ramping down the rotation. This can be seen in both the angular momentum and in the energy expectation value. This is noticeable for both types of deformations and is likely to be caused by the the very sharp cusp in the energy surface at that point, as was seen in Fig. 4.7.

In conclusion we have seen that the systems considered in Sec. 4.3 shows hysteresis only when the quartic deformation is added. This can be traced back to the region of avoided crossings that are of the cat-like type. In such avoided crossings the coupling is very strong between the ground state on one side of the transition and the excited states on the other. The driving can thus not be done adiabatically for realistic speeds and the angular momentum will trace out a loop when plotted against Ω. These results are similar for both the full many-body simulations

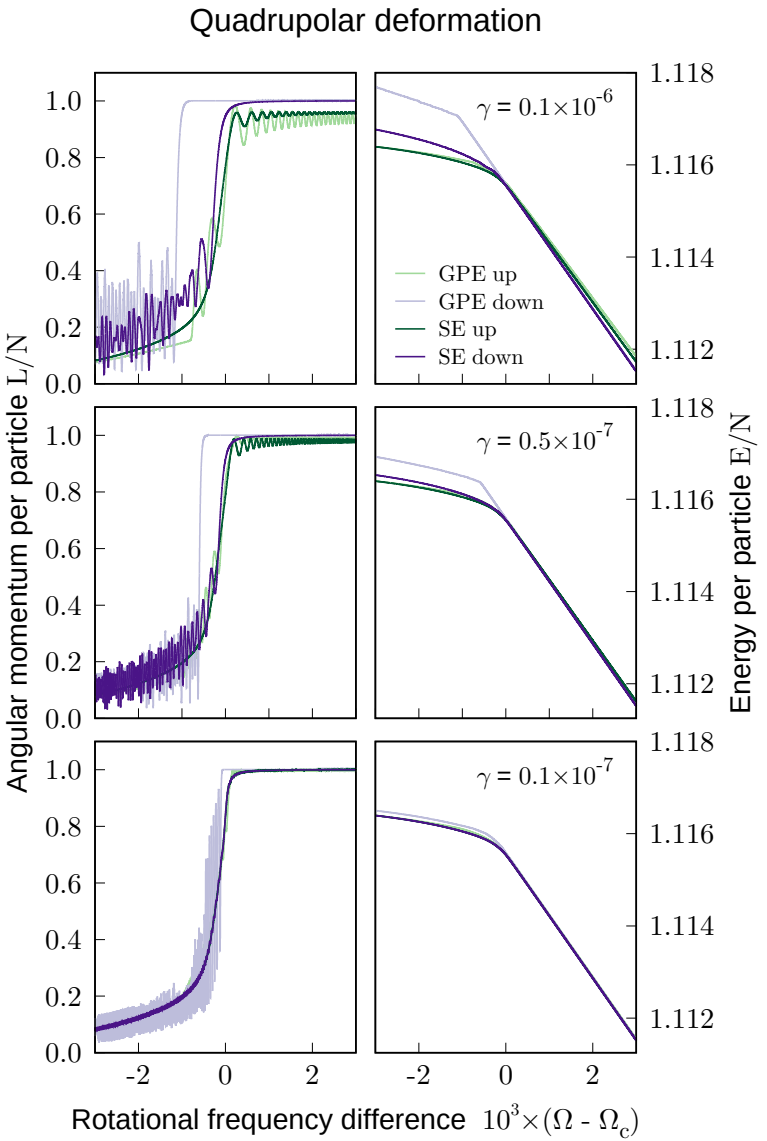

Figure 4.10: Time-evolution using both the Gross-Pitaevskii equation, lighter curves, and the Schrödinger equation, darker curves, for the system with only a quadrupolar deformation. Left panels show the evolution of the angular momentum expectation value and the right panels show the energy expectation value as Ω is ramped both up and down through the critical point. The different rows correspond to different ramping speeds γ with the fastest being in the top row and the slowest on the bottom row.

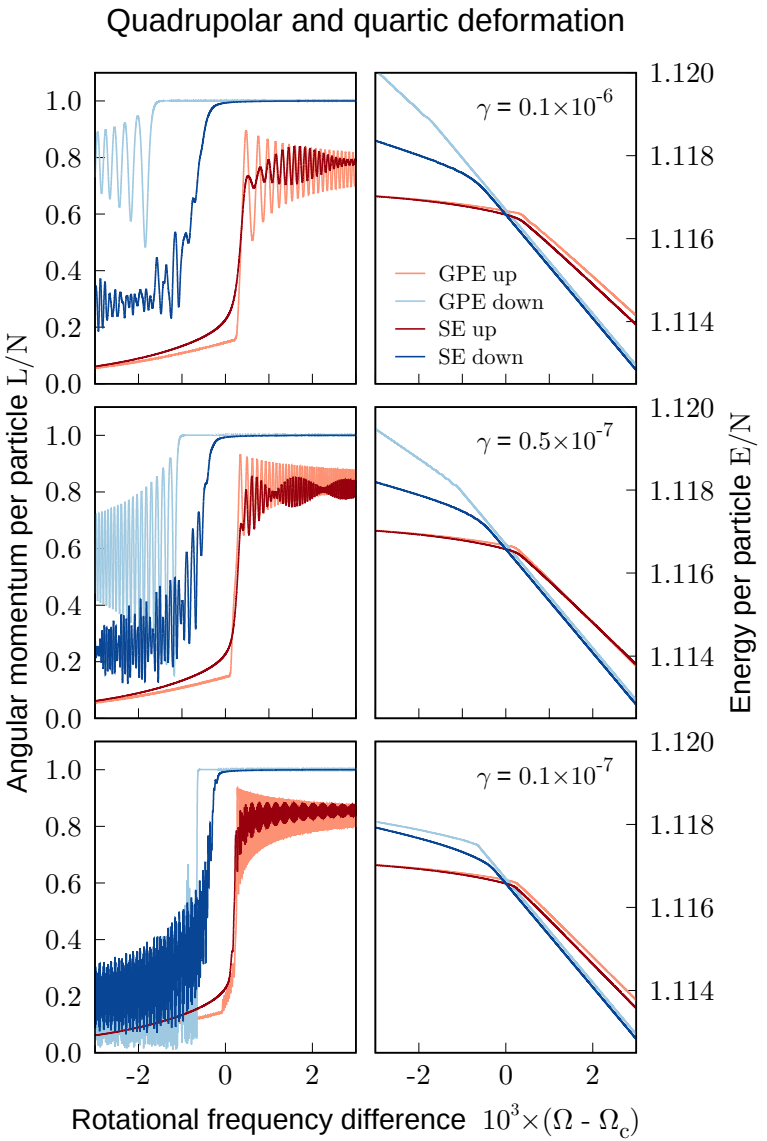

Figure 4.11: Same as Fig. 4.10 except here the trapping potential also contains a quartic term, giving rise to a hysteretic behavior.

and the mean-field treatment. The mean-field approximation can however not describe the correlated states making up these avoided crossings and the energy surface will not go any lower. In the dynamics study we observe that the mean-field simulations overestimate the time the system stays in the vortex state when ramping down, potentially due to the very sharp cusp in the energy surface for the vortex state. This will then cause the hysteresis loop to appear larger than it should be and might help explain the discrepancy between simulations and the experiments in [162].

In order to remove the residual angular momentum after the ramping is done to get a clearer hysteresis loop, more dissipation could potentially be phenomenologically included in the simulations. Despite the energy changing by the time-dependent Hamiltonian, the system can not get rid of enough energy for it to drop down to the instantaneous ground state. However, such a phenomenological approach has already been tested in mean-field simulations, but the agreement has so far not been very good [162, 165]. This study is a bit further along the way in order to understand the emergence of hysteresis in a quantum mechanical systeme, but many questions about what happens to these states in the limit of large N remain to be answered.

4.5 Vortices in fermionic droplets with dipole-dipole interactions

The quantized circulation in a superfluid previously introduced in Sec. 4.3 also has implications for faster rotation. If one continues to increase the rotational frequency after the vortex has been nucleated, the size or the circulation of the vortex does not increase. The system only picks up more circulation after another critical frequency is reached. However, this circulation is in many cases not added to the existing vortex, but instead a new one is formed. It turns out that in these cases it is energetically favorable for a condensate to have several singly-quantized vortices compared to having fewer, but multiply-quantized, vortices [29, 64, 137]. Particularly, this is the case for a harmonically trapped condensate [144]. The presence of multiple singly-quantized vortices in a trapped condensates were observed already in one of the first experiments demonstrating vortices in atomic gases [140]. The decay of a doubly-quantized into two singly-quantized vortices has also been experimentally observed in harmonically trapped atomic condensates [166].

As more and more vortices enter the system, they start to arrange in ordered shapes. For sufficiently high rotations the particle cloud becomes pierced by a lattice of quantized vortices. Such vortex lattices were first seen in superfluid Helium and have been experimentally observed in ultracold atomic condensates as well [167]. The existence of vortex lattices in Fermi gases with attractive interactions have also been experimentally verified [75]. Other examples of attractive fermionic systems that exhibit vortices include type-II superconductors in magnetic fields, as rotation and charged particles in magnetic fields give rise to a similar Hamiltonian [168].

At very high rotation of a bosonic condensate there comes a point when the number of vortices in the system starts to become larger than the number of particles. It was realized that at this point the system would transition into a new regime where the mean-field approximation would not be valid anymore [169, 170]. Here, the system would be described by states that were identified as the bosonic counterparts to the ones that show up in the fractional quantum Hall effects of a two-dimensional electron gas [171, 172]. Such strongly correlated states do not exhibit Bose-Einstein condensation and some even have anyon statistics, making them highly interesting in applications such as quantum computing. For more details about fractional quantum Hall states in rotating bosonic gases see e.g. the reviews [170, 173].

The regime of very fast rotating ultracold atomic systems has however been difficult to achieve experimentally, one problem being that the rotation effectively lowers the harmonic trapping potential and the gas becomes almost untrapped at the transition. However, the use of an additional quartic trapping potential has been shown to stabilize the system around these frequencies [174]. Another way that has been proposed is to try to go around this problem by using artificial gauge fields [137], i.e. using other processes that also have equivalent effects on the equation of motion. It has also been suggested to use spin-flips induced by dipole-dipole interactions to reach the quantum Hall regime [175].

Let us now finally comment on a remarkable similarity between slowly rotating condensates, and the quantum Hall effect in electron systems. For electrons in semiconductor devices, the integer quantum Hall effect is also interesting in the context of finite-size systems. A finite-size system of electrons can be created by confining the electron gas in all spatial directions. This can be done using e.g. electrodes or by the shape of the semiconductor itself. In many cases the confining potential can be approximated by a harmonic trap. Such a system is known

as a quantum dot [19]. For moderate strengths of the confinement and external magnetic fields, these quantum dots show a rich electronic structure with a wide variety of particle densities and spin configurations depending on e.g. the shape of the dot or the effective interaction strength. At strong magnetic fields, the quantum dot systems show many similarities to the quantum Hall effect in the bulk, from which many of the concepts can be generalized and utilized for finite-size systems.

In a quantum dot in a strong, uniform external magnetic field, the spins of the electrons start to align along the direction of the field. Above a certain field strength, the electrons may become spin polarized. As we here have a system of fermions, each electron is then occupying a distinct orbital. Here, the most natural single-particle orbitals to use are the lowest Landau level states, the same orbitals that were used in Sec. 4.3 to describe vortex formation in a weakly interacting bosonic gas. The many-body state with the lowest possible total angular momentum L is then the state where the N particles have occupied the lowest Landau level orbitals with angular momentum m from 0 up to $N-1$. Thus, this state has $L = N(N-1)/2$ and is called the maximum density droplet, as it also has the highest possible particle density [176]. The structure is sketched in the upper right part of Fig. 4.12. Using transport measurements, the existence of the maximum density droplet in semiconductor quantum dots has been confirmed [177].

Using $\nu = N(N-1)/2L$ as the finite-size version of the Landau level filling factor from the quantum Hall theory, one sees that the maximum density droplet corresponds to the integer quantum Hall state with unit filling. Due to the form of the lowest Landau level orbitals, this state has one vortex attached to each particle, a so called Pauli vortex, coming from the antisymmetry of the fermionic wave function. By removing these Pauli vortices, one obtains the $L = 0$ bosonic condensate state [178]. Thus, the maximum density droplet can be thought of as the fermionic counterpart to the non-rotating bosonic droplet.

For a quantum dot containing many electrons, increasing the strength of the magnetic field further the edge of the maximum density droplet may reconstruct into ring-like structures outside the droplet core [179–181]. However, for smaller dots, $N \lesssim 12$, instead a single vortex may form in the center of the electron liquid. This is a free vortex, as opposed to the Pauli vortices, and the approximate single-particle structure of this state is shown in the lower right part of Fig. 4.12. Further increasing the magnetic field, successive free vortices enter the particle cloud and arrange

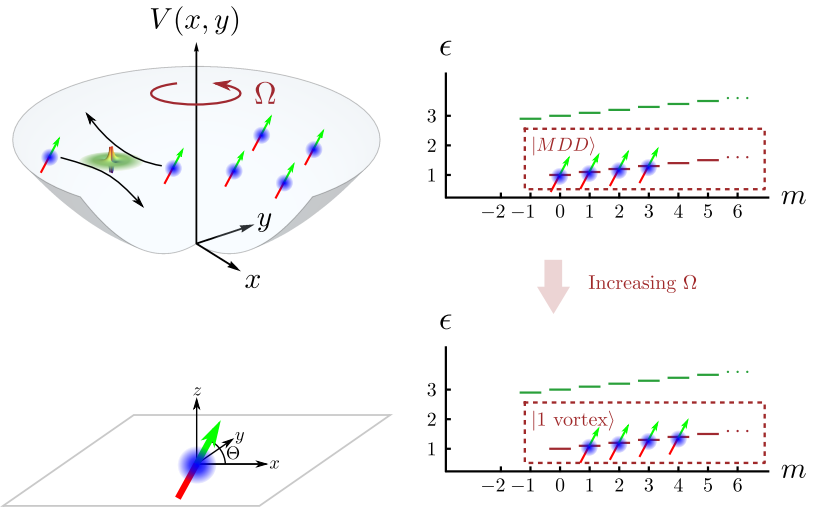

Figure 4.12: A sketch of the system considered in Paper IV is shown in the upper left part. The trapping potential is a harmonic oscillator, the fermionic particles interact via their dipole moments and the system is rotated with angular velocity Ω. In the lower left part the geometry of the dipole moments is shown. They are all aligned in the same direction, forming an angle Θ with the x-axis in the xz-plane. To the right the structure of the maximum density droplet many-body state, occupying the N lowest m-states in the lowest Landau level, is sketched. Below is a schematic picture of the structure of the unit vortex state which the system transitions into as the rotation is increased.

themselves into clusters and, if the system size and angular momentum grows even more, a lattice of vortices. Starting from the maximum density droplet and going up in field strength is thus very similar to starting from the non-rotating bosonic condensate and increasing the rotational frequency, and these two systems share much of their behavior. Such analogies exists even though the fermionic droplet here consists of particles repelling each other, thus not pairing up and forming a superfluid as in the case of a gas of attractive fermions. For a review of the analogies and the universality of vortex formation in fermionic and bosonic few-body systems see [168].

Even though the free vortices in quantum Hall droplets have been extensively investigated theoretically, and the existence of the maximum density droplet state in quantum dots was experimentally confirmed, detecting these vortices has proven to be difficult. Typically one has to rely on indirect signals in e.g. transport and magnetization measurements for these systems. The limited resolution and the large amount of noise in such measurements have not permitted a clear identifi-

cation of the vortex states [19]. The realization of few-particle fermionic systems in ultracold atomic systems [79], as discussed in Sec. 2.5, may provide new or improved types of measurements on cleaner samples.

However, atoms are charge neutral. This means that they do not interact via the long-range Coulomb interaction as electrons would do. A short-range interaction, modeled as a contact-type interaction, would not affect a spin-polarized fermionic system due to the Pauli principle and could give a different response to rotation. The use of atoms with large dipole moments, discussed in Sec. 2.3, could provide long-range interactions when trying to mimic the Coulomb interaction of electrons. Even though the dipole-dipole interaction is not exactly like the Coulomb interaction, possibly making the comparison to semiconductor quantum dots less precise, it opens up new possibilities as well. Unlike the Coulomb interaction, the dipole-dipole interaction can e.g. be made anisotropic. This will break the rotational symmetry of the system, revealing more of the internal structure, and possibly affect the rotational response in new ways.

In Paper IV we showed that vortices are indeed possible in rotating dipolar fermionic droplets, for which the system is sketched in Fig. 4.12. The response to rotation was found to be very similar to that of electrons in quantum dots in magnetic fields and rotating few-body bosonic systems with short-range interactions. Tilting the angle Θ of all dipole moments does not affect the vortices more than that they are now directly revealed in the particle density, which were not visible when the system was isotropic. As the local minima are not perfectly zero, in addition we calculated the probability current. In the current, circular flow around the density minima can be clearly seen, which is shown in Fig. 4.13. The vorticity is however not contained to a single point due to the finite size of the system and hence the circulation is not quantized either. Furthermore, we found that similar to a few electrons in quantum dots, the vortices are only the ground state for moderate rotation [168]. Increasing the rotation further, there is a transition to a crystalline state. Arrays of more vortices have since been found in dipolar fermion droplets with larger N using density-functional theory calculations [182].

The use of particles interacting with dipole-dipole interactions has also been seen to be better suitable for realizing fractional quantum Hall states [183]. The long-range interactions lift energy degeneracies prohibiting these states from become important when the size of the system is increased. How such fractional quantum Hall states would react to the anisotropy when tilting the dipole moments

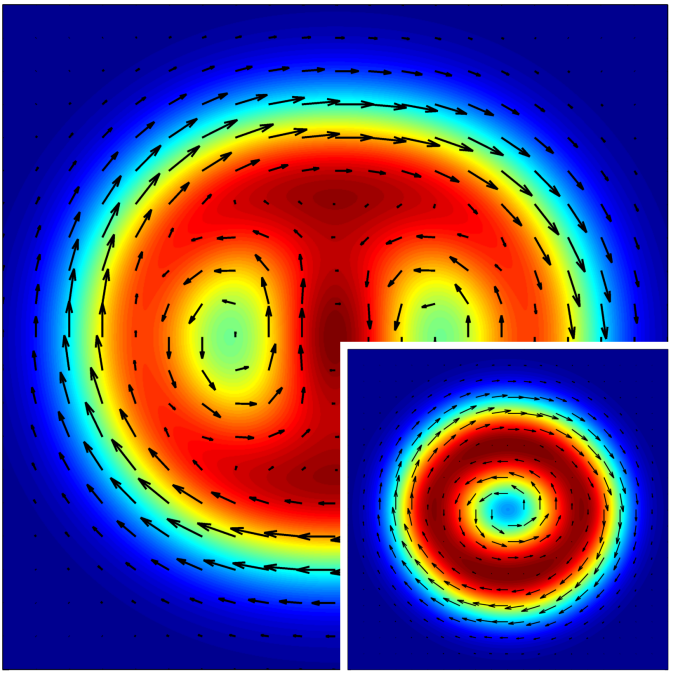

Figure 4.13: Probability current, shown as black arrows, for two and one vortex states. The color gradient from blue, indicating low values, to red, high values, represents the particle density. Both states are for tilted dipole moments, $\theta \approx 55.6^{\circ}$. The area shown goes from -4 to 4, in dimensionless units, for both directions. Taken from Paper IV where it is Fig. 3.

could possibly be an interesting direction to continue the theoretical investigation presented here.

4.6 Shell structure in fermionic droplets with dipole-dipole interactions

In a few-body system of identical fermionic particles, the Pauli exclusion principle plays an important role for the structure of the many-body state. For N non-interacting particles, the ground state fills up the N single-particle orbitals with the lowest energy. If the one-particle system possesses some symmetry, these orbitals will have degeneracies and the density of single-particle states will be high at these energies. Such a bunching of the energy levels is called a shell. A system with

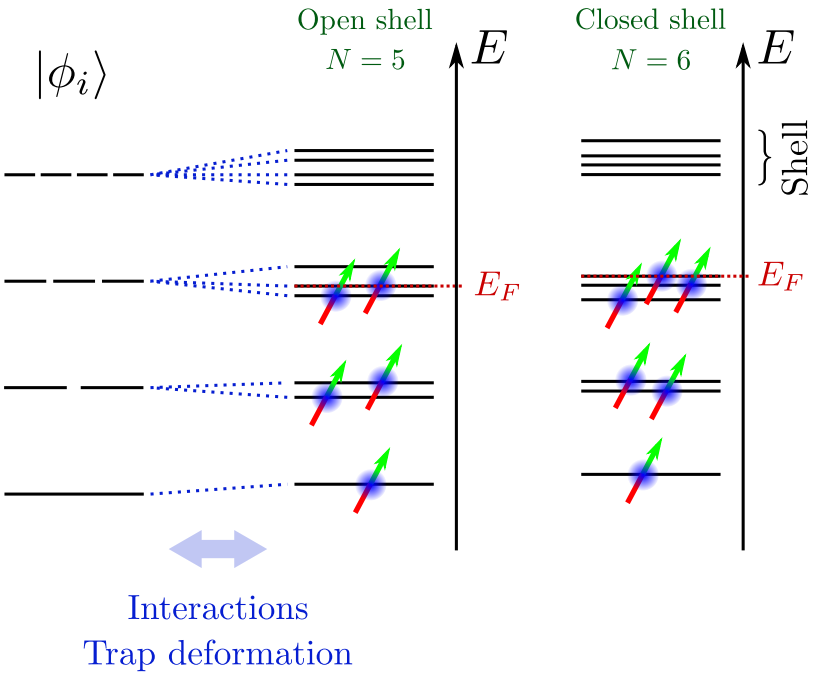

Figure 4.14: A sketch of shell structure in a fermionic system. On the left the energy of the orbitals $|\phi_i\rangle$ are shown and their degeneracy is marked by the number of segments of the lines. A splitting of these degeneracies, in the mean-field picture, can be made by both a deformation of the trap and the inclusion of interactions, indicated by the dashed blue lines. Due to the underlying symmetry of the system the mean-field orbital energies are still bunched around certain values of the energy. Such a bunching is called an energy shell. As the many-particle state is constructed by occupying the lowest orbitals different scenarios can occur. To the right are sketched the configurations for both $N = 5$ and 6. For $N = 5$ the Fermi energy E_F lies inside of a shell and for $N = 6$ E_F lies at the upper edge of a shell. The open shell configuration of the five particle system is thus less stable and more reactive compared to the system of six particles.

the Fermi energy at the energy of degeneracy will e.g. be less stable as the cost in energy of add, removing or rearranging the particles is small. The structure of these energy shells has been used to explain many properties of finite fermionic systems. Examples are the stability, ionization energy and chemical reactivity of atoms [7], a consequence of the shells of the atomic orbitals, as well as the increased stability and separation energy of atomic nuclei for some particular number of nucleons [184].

However, particles in many-body systems are usually interacting, and the single-particle orbitals have no direct physical meaning. If the interactions are weak, we

may utilize a mean-field description to obtain an approximate single-particle problem in which the orbitals of this new, approximate mean-field potential again can be used to characterize the system. The solutions to the mean-field equation might have broken the symmetries of the many-body Hamiltonian, but there might still be a significant bunching of the energy levels of the orbitals, forming a shell. Another way to split up the degenerate orbitals is if the single-particle Hamiltonian is perturbed directly, e.g. by deforming the trapping potential. The formation of energy shells is sketched in Fig. 4.14 where the solutions to the single-particle problem is split up due to interactions or a deformation of the trap, but the bunching from the underlying symmetry still persists.

Going beyond mean-field methods one may still observe the consequences of the shell structure. If the system is not very correlated and the single-particle orbital picture is still valid to some extent, one may determine if system is in an open or closed shell configuration by examining the excitation energy. The first excited state would be the configuration where the particle occupying the highest occupied energy level has been lifted up to the lowest unoccupied level. For an open shell configuration the difference in energy between the two levels is small. In comparison the energy difference is much larger for a closed shell, where the particle must be lifted up all the way to the next shell. Further signals of the shell structure can be found by studying the addition energy $\mu(N) = E_0(N) - E_0(N-1)$ and in particular the difference in addition energy

$$\begin{aligned}\Delta_2(N) &= \mu(N+1) - \mu(N) \\ &= E_0(N+1) - 2E_0(N) + E_0(N-1),\end{aligned} \tag{4.22}$$

where $E_0(N)$ is the ground state energy for a system of N particles. Similar to the first excited state, when the system has a closed shell at the Fermi energy, Δ_2 will have a peak, while it will have a low value for open shells. The shell structure of artificial many-body systems of interacting particles such as clusters of metal atoms [2, 3] and electrons in semiconductor quantum dots [19] have been studied extensively using these quantities.

The shell structure of a one-dimensional ultracold atomic system has been examined experimentally [81]. Inspired by this, in Paper V we investigated how the shell structure of a system of harmonically trapped dipolar fermionic particles, similar to the one in Sec. 4.5, behaved and could be altered. This was done by both changing the trapping potential and making the two-body interactions anisotropic by tilting the dipoles, forming an angle Θ in the xz direction as sketched in the lower

left part of Fig. 4.12. As in Paper IV, the dipolar particles are assumed to be in a quasi-two-dimensional harmonic trapping potential. The trapping potential is taken to be

$$V(x,y) = \frac{1}{2} m \omega_{\perp}^2 \left(\alpha x^2 + \alpha^{-1} y^2 \right), \tag{4.23}$$

where the deformation parameter α determines the ration between the trap frequencies ω_x and ω_y in the x and y direction respectively, and $\omega_{\perp}^2 = \omega_x \omega_y$. Thus, the area enclosed by an equipotential curve at a certain energy is independent of α. We here also keep the same trapping frequencies for all N considered, as ω_x and ω_y are set by the external laser field in experiments with ultracold atomic system. When more and more particles are added this means that the particle density is increasing and hence the interaction energy is also rapidly increasing. This is different from electrons in semiconductor quantum dots where the particle density often is observed to be constant and the confinement is weakened as N is increased [19].

Due to the increasing influence of the interactions as the particle number is increased we expect the mean-field approximation to break down for larger N and we should go beyond Hartree-Fock calculations. In order to study the shell structure we will however need to simulate systems of different number of particles and also use larger N than is feasible for full configuration interaction calculations. As was discussed in Sec. 3.2, when comparing systems of different particle numbers one would like to utilize a size extensive method in order to assure the same amount of correlations are included for all N. Thus, we have performed both Møller-Plesset perturbation theory, as described in Sec. 3.2, and quadratic configuration interaction, introduced in Sec. 3.3, for this system.

The results of both perturbation theory to different orders and quadratic configuration interaction at a moderate interaction strength and a trapping deformation of $\alpha = 1.15$ for two different angles Θ of the dipoles are shown in Fig. 4.15. As N increases the results of the different methods start to diverge. However, partial fourth order perturbation theory and quadratic configuration interaction give very similar results with an absolute difference in energy less than 0.3% for all system parameters considered. Already third order perturbation theory gives similar qualitative behavior, indicating that quadratic configuration interaction with single and double substitutions gives a proper description of the system.

The shape of the Δ_2 curve in the upper part of Fig. 4.15 indicates that the shell struc-

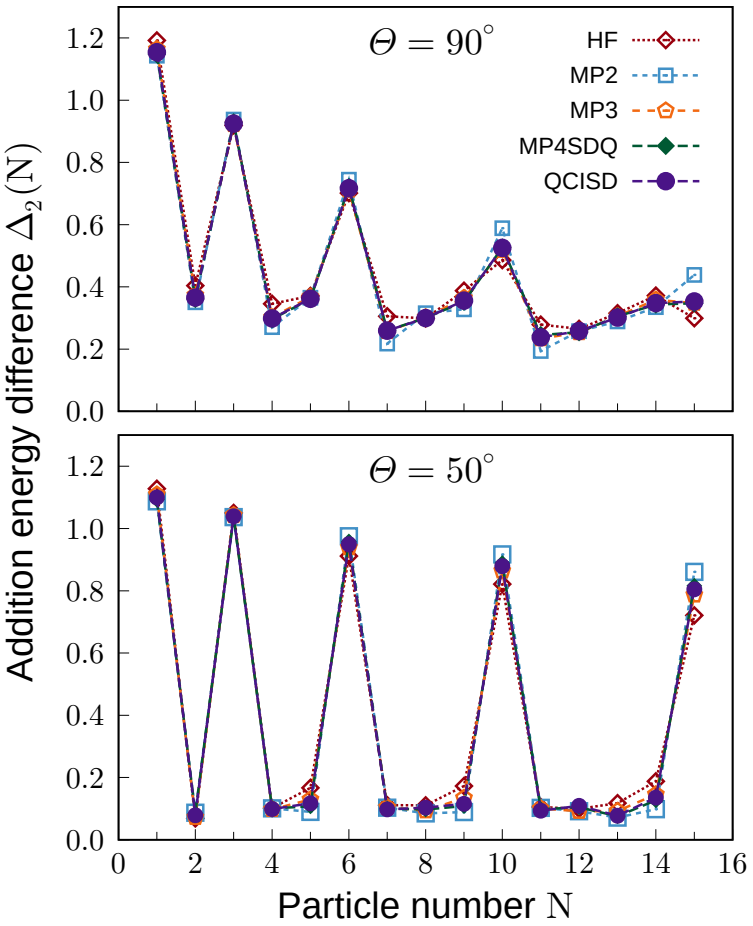

Figure 4.15: Addition energy difference Δ_2 as a function of N calculated using only Hartree-Fock, Møller-Plesset perturbation theory to second, third and partial fourth order, as well as quadratic configuration interaction with single and double substitutions. Here $\alpha = 1.15$ for both panels. Upper panel is for a system with the dipoles pointing in the direction perpendicular to the plane of the two-dimensional system. In the lower panel the dipoles are tilted to an angle $\Theta = 50^\circ$ in the xz plane.

ture is quickly lost even though the dipole-dipole interactions are kept isotropic when the trap is deformed. However, by tilting the dipoles in the same direction as the stronger trapping frequency a strong signal of shell structure can be obtained, with distinct peaks in Δ_2, as seen in the lower part of Fig. 4.15. A thorough sweep of Θ was performed in Paper v and it was found that there is indeed a region in the parameter space where the result of an anisotropic dipole-dipole interaction

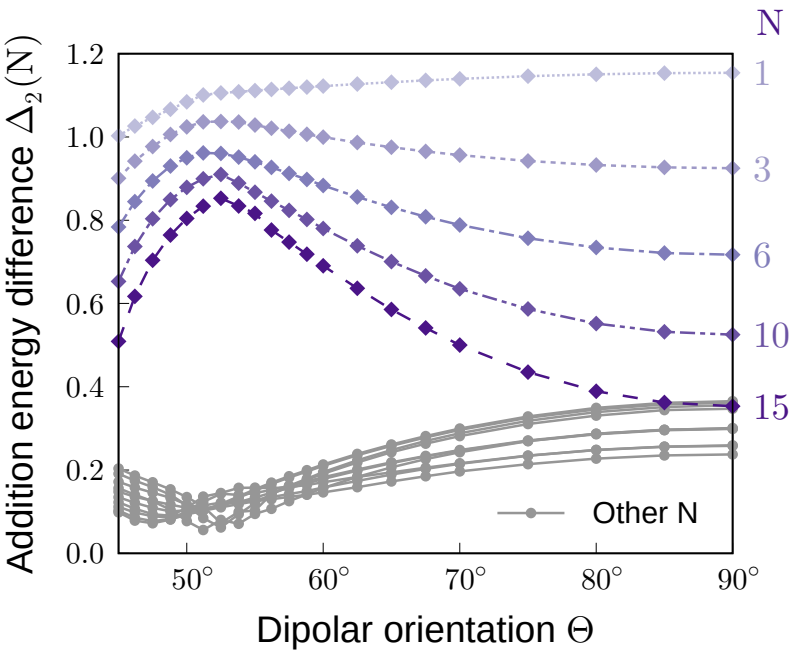

Figure 4.16: Addition energy difference as a function of the angle Θ of the dipoles. Purple curves are for the values of N indicated on the right, corresponding to the closed shells of the isotropic two-dimensional harmonic oscillator. Gray curves are for the other values of N between one and 15. For all systems $\alpha = 1.15$. Adapted from Fig.4 in Paper v.

can counter a trap deformation on the form of Eq. (4.23), restoring a strong shell structure. This is shown in Fig. 4.16.

At the point where the anisotropy of the interactions counteract the trap deformation, the system is in a situation where the symmetry breaking of the single-particle part is, almost, canceled by a two-body part. Thus, the direct correlations of the interaction, which the mean-field equations cannot describe, determines the exact point where the elongation of the particle density changes direction. While the state with a particle density elongated in the direction perpendicular to the direction of stronger trapping is not significantly affected by the anisotropic interactions, the state with the particle density elongated in the same direction as the dipoles are tilted, reduces its interaction energy. This reduction in interaction energy will be enhanced, the more correlations are included in the calculation. There will thus be a region around this point where the mean-field approach underestimates the effect of the interactions and the true many-body ground state is

approximated by an excited mean-field state.

The starting point for both the Møller-Plesset perturbation theory and quadratic configuration interaction calculations is here taken as a solution to the Hartree-Fock equations and thus care must be taken to choose the one that will actually be the ground state after the corrections have been applied. Converging to other local minima on the Hartree-Fock energy surface other than the global minimum is not trivial. In Paper v we had to utilize the method of maximum overlap in order to guide the self-consistent iterations to the nearest minimum from the initial guess [185]. This was also supported by the method of direct inversion in the iterative subspace in order to achieve convergence [186].

Shell structure in dipolar fermionic droplets could have future applications in e.g. atomtronics devices. These are devices constructed from ultracold atomic systems intended to be used the same way as ordinary electronics [187]. In a single-electron transistor made using a semiconductor quantum dot, the shell structure can e.g. be seen in the transport spectrum [19]. Similar transport experiments have already been realized in experiments with ultracold atoms [13, 24, 188, 189] and the inclusion of dipole-dipole interactions in particle transport is known to produce new behavior [190]. Increasing the strength of the interactions will also increase the effect of the behavior examined in Paper v, but in order to simulate such a system we would need to include more correlations. One immediate improvement would be to include the effect of triple substitutions in the quadratic configuration interaction calculations as described in Sec. 3.3 and App. B. This would however require a more efficient implementation which has not yet been done, or alternatively more powerful computers, as the complexity grows significantly.

Chapter 5

Outlook

Research is an evermoving process. Sometimes there is a major breakthrough, but more often the advances are made in smaller steps. This thesis represents steps forward in the understanding of some of the many different collective phenomena that are present in many-body quantum systems of ultracold atomic gases, and also how these phenomena are altered when the particle number is small. As with most basic research, the direct implications beyond the immediate increase in knowledge of the particular system in question is difficult to predict. The hope is however that it some day can be used as a building block for practical applications such as in atomtronics devices [191]. Or in the development of new fundamental concepts and approaches for collective behavior in many-body quantum systems.

Ultracold atomic systems will continue to see progress both experimentally and in the theoretical understanding, together with new predictions. With the highly adaptable technology of optical lattices quantum simulations of model systems from condensed matter physics will continue to be performed [21]. Here it might help in e.g. uncovering the mechanism for high temperature superconductors, a question that is still waiting to be answered. Other investigations could focus on the many exotic topological phases predicted to exist in many-body systems and the quasiparticles used to describe them. Utilizing the possibility to follow many-body quantum systems in time using ultracold atoms makes it possible to study questions like thermalization and opens up the possibility to perform transport measurements of neutral atoms [24].

Many of these questions could potentially benefit from the knowledge of the behavior of a similar systems, but with a finite number of particles. The separation of scales as new collective behavior emerges is a very complicated matter. Here, the recent experimental progress in achieving small particle numbers in systems of laser-trapped atoms could help us unravel the mysteries. The ability to create highly tunable artificial few-body systems could also lead to new understandings of natural finite-sized systems, with the simulation of atomic nuclei as a major goal. Together with the continued development of numerical methods and algorithms, as well as the general improvement of computational power, there will arise many possibilities for new investigations in the region between collections of very few particles and ones with infinitely many.

References

[1] P. W. Anderson, Science **177**, 393 (1972).

[2] W. A. de Heer, Reviews of Modern Physics **65**, 611 (1993).

[3] M. Brack, Reviews of Modern Physics **65**, 677 (1993).

[4] R. C. Ashoori, Nature **379**, 413 (1996).

[5] I. Bloch, J. Dalibard, and W. Zwerger, Reviews of Modern Physics **80**, 885 (2008).

[6] H. J. Metcalf and P. v. d. Straten, *Laser cooling and trapping* (Springer, 1999).

[7] C. J. Foot, *Atomic physics* (Oxford University Press, 2005).

[8] W. D. Phillips, Reviews of Modern Physics **70**, 721 (1998).

[9] D. J. Wineland, R. E. Drullinger, and F. L. Walls, Physical Review Letters **40**, 1639 (1978).

[10] W. D. Phillips and H. Metcalf, Physical Review Letters **48**, 596 (1982).

[11] S. E. Olson, M. L. Terraciano, M. Bashkansky, and F. K. Fatemi, Physical Review A **76**, 061404 (2007).

[12] S. Murmann, A. Bergschneider, V. M. Klinkhamer, G. Zürn, T. Lompe, and S. Jochim, Physical Review Letters **114**, 080402 (2015).

[13] J.-P. Brantut, J. Meineke, D. Stadler, S. Krinner, and T. Esslinger, Science **337**, 1069 (2012).

[14] P. D. Lett, R. N. Watts, C. I. Westbrook, W. D. Phillips, P. L. Gould, and H. J. Metcalf, Physical Review Letters **61**, 169 (1988).

[15] S. Chu, Reviews of Modern Physics **70**, 685 (1998).

[16] C. N. Cohen-Tannoudji, Reviews of Modern Physics **70**, 707 (1998).

[17] W. Ketterle, D. S. Durfee, and D. M. Stamper-Kurn, Proceedings of the International School of Physics "Enrico Fermi" **140**, 67–176 (1999).

[18] H. Ott, Reports on Progress in Physics **79**, 054401 (2016).

[19] S. M. Reimann and M. Manninen, Reviews of Modern Physics **74**, 1283 (2002).

[20] M. Lewenstein, A. Sanpera, V. Ahufinger, B. Damski, A. Sen(De), and U. Sen, Advances in Physics **56**, 243 (2007).

[21] C. Gross and I. Bloch, Science **357**, 995 (2017).

[22] V. Galitski and I. B. Spielman, Nature **494**, 49 (2013).

[23] T. Langen, R. Geiger, and J. Schmiedmayer, Annual Review of Condensed Matter Physics **6**, 201 (2015).

[24] S. Krinner, T. Esslinger, and J.-P. Brantut, Journal of Physics: Condensed Matter **29**, 343003 (2017).

[25] J. J. Sakurai and S. F. Tuan, *Modern quantum mechanics* (Addison-Wesley, 1994).

[26] A. Fetter and J. Walecka, *Quantum Theory of Many-Particle Systems* (Dover Publications, 2012).

[27] E. K. U. Gross, E. Runge, and O. Heinonen, *Many-particle theory* (Hilger, 1991).

[28] S. Takagi, Progress of Theoretical Physics **85**, 463 (1991).

[29] C. Pethick and H. Smith, *Bose–Einstein Condensation in Dilute Gases* (Cambridge University Press, 2008).

[30] J. R. Taylor, *Scattering theory : the quantum theory on nonrelativistic collisions* (John Wiley & Sons, 1972).

[31] H. Stoof, D. Dickerscheid, and K. Gubbels, *Ultracold Quantum Fields* (Springer Netherlands, 2008).

[32] L. Pitaevskii and S. Stringari, *Bose-Einstein condensation* (Clarendon Press, 2003).

[33] L. D. Landau and E. M. Lifshitz, *Quantum mechanics : non-relativistic theory.* (Pergamon Press, 1958).

[34] H. A. Bethe, Physical Review **76**, 38 (1949).

[35] C. Chin, R. Grimm, P. Julienne, and E. Tiesinga, Reviews of Modern Physics **82**, 1225 (2010).

[36] S. Inouye, M. Andrews, J. Stenger, H. Miesner, D. Stamper-Kurn, and W. Ketterle, Nature **392**, 151 (1998).

[37] T. Busch, B.-G. Englert, K. Rzażewski, and M. Wilkens, Foundations of Physics **28**, 549 (1998).

[38] B. D. Esry and C. H. Greene, Physical Review A **60**, 1451 (1999).

[39] T. Lahaye, C. Menotti, L. Santos, M. Lewenstein, and T. Pfau, Reports on Progress in Physics **72**, 126401 (2009).

[40] M. Baranov, Physics Reports **464**, 71 (2008).

[41] M. A. Baranov, M. Dalmonte, G. Pupillo, and P. Zoller, Chemical Reviews **112**, 5012 (2012).

[42] D. J. Griffiths, *Introduction to Electrodynamics* (Pearson Benjamin Cummings, 2008).

[43] A. Griesmaier, J. Werner, S. Hensler, J. Stuhler, and T. Pfau, Physical Review Letters **94**, 160401 (2005).

[44] M. Lu, N. Q. Burdick, S. H. Youn, and B. L. Lev, Physical Review Letters **107**, 190401 (2011).

[45] K. Aikawa, A. Frisch, M. Mark, S. Baier, A. Rietzler, R. Grimm, and F. Ferlaino, Physical Review Letters **108**, 210401 (2012).

[46] K. Aikawa, A. Frisch, M. Mark, S. Baier, R. Grimm, and F. Ferlaino, Physical Review Letters **112**, 010404 (2014).

[47] K.-K. Ni, S. Ospelkaus, M. H. G. de Miranda, A. Pe'er, B. Neyenhuis, J. J. Zirbel, S. Kotochigova, P. S. Julienne, D. S. Jin, and J. Ye, Science **322**, 231 (2008).

[48] J. G. Danzl, M. J. Mark, E. Haller, M. Gustavsson, R. Hart, J. Aldegunde, J. M. Hutson, and H.-C. Nägerl, Nature Physics **6**, 265 (2010).

[49] T. Takekoshi, L. Reichsöllner, A. Schindewolf, J. M. Hutson, C. R. Le Sueur, O. Dulieu, F. Ferlaino, R. Grimm, and H.-C. Nägerl, Physical Review Letters **113**, 205301 (2014).

[50] P. K. Molony, P. D. Gregory, Z. Ji, B. Lu, M. P. Köppinger, C. R. Le Sueur, C. L. Blackley, J. M. Hutson, and S. L. Cornish, Physical Review Letters **113**, 255301 (2014).

[51] J. W. Park, S. A. Will, and M. W. Zwierlein, Physical Review Letters **114**, 205302 (2015).

[52] M. Guo, B. Zhu, B. Lu, X. Ye, F. Wang, R. Vexiau, N. Bouloufa-Maafa, G. Quéméner, O. Dulieu, and D. Wang, Physical Review Letters **116**, 205303 (2016).

[53] R. Löw, H. Weimer, J. Nipper, J. B. Balewski, B. Butscher, H. P. Büchler, and T. Pfau, Journal of Physics B: Atomic, Molecular and Optical Physics **45**, 113001 (2012).

[54] M. Schmitt, M. Wenzel, F. Böttcher, I. Ferrier-Barbut, and T. Pfau, Nature **539**, 259 (2016).

[55] L. Tanzi, E. Lucioni, F. Famà, J. Catani, A. Fioretti, C. Gabbanini, R. N. Bisset, L. Santos, and G. Modugno, Physical Review Letters **122**, 130405 (2019).

[56] F. Böttcher, J.-N. Schmidt, M. Wenzel, J. Hertkorn, M. Guo, T. Langen, and T. Pfau, Physical Review X **9**, 011051 (2019).

[57] L. Chomaz, D. Petter, P. Ilzhöfer, G. Natale, A. Trautmann, C. Politi, G. Durastante, R. M. W. van Bijnen, A. Patscheider, M. Sohmen, M. J. Mark, and F. Ferlaino, Physical Review X **9**, 021012 (2019).

[58] R. Baierlein, *Thermal physics* (Cambridge University Press, 1999).

[59] S. N. Bose, Zeitschrift für Physik **26**, 178 (1924).

[60] A. Einstein, Sitzungsberichte der Preussischen Akademie der Wissenschaften, Physikalisch-Mathematische Klasse , 261 (1924).

[61] A. Einstein, Sitzungsberichte der Preussischen Akademie der Wissenschaften, Physikalisch-Mathematische Klasse , 3 (1925).

[62] A. Einstein, A. Beck, D. Buchwald, J. Illy, P. Havas, Z. Rosenkranz, T. Sauer, A. Hentschel, and J. James, *The Collected Papers of Albert Einstein, Volume 14 (English): The Berlin Years: Writings & Correspondence, April 1923–May 1925 (English Translation Supplement)*, Collected Papers of Albert Einstein (Princeton University Press, 2015) , available online at http://einsteinpapers.press.princeton.edu/.

[63] O. Penrose and L. Onsager, Physical Review **104**, 576 (1956).

[64] A. J. Leggett, *Quantum liquids : Bose condensation and Cooper pairing in condensed-matter systems* (Oxford University Press, 2006).

[65] E. J. Mueller, T.-L. Ho, M. Ueda, and G. Baym, Physical Review A **74**, 033612 (2006).

[66] F. London, Nature **141**, 643 (1938).

[67] W. C. Stwalley and L. H. Nosanow, Physical Review Letters **36**, 910 (1976).

[68] T. Greytak, D. Kleppner, D. Fried, T. Killian, L. Willmann, D. Landhuis, and S. Moss, Physica B: Condensed Matter **280**, 20 (2000).

[69] M. H. Anderson, J. R. Ensher, M. R. Matthews, C. E. Wieman, and E. A. Cornell, Science **269**, 198 (1995).

[70] E. A. Cornell and C. E. Wieman, Reviews of Modern Physics **74**, 875 (2002).

[71] W. Ketterle, Reviews of Modern Physics **74**, 1131 (2002).

[72] D. Schroeder, *An introduction to thermal physics* (Addison Wesley, 2000).

[73] B. DeMarco and D. S. Jin, Science **285**, 1703 (1999).

[74] J. Bardeen, L. N. Cooper, and J. R. Schrieffer, Physical Review **108**, 1175 (1957).

[75] S. Giorgini, L. P. Pitaevskii, and S. Stringari, Reviews of Modern Physics **80**, 1215 (2008).

[76] Z. Hu and H. J. Kimble, Optics Letters **19**, 1888 (1994).

[77] N. Schlosser, G. Reymond, I. Protsenko, and P. Grangier, Nature **411**, 1024 (2001).

[78] C.-S. Chuu, F. Schreck, T. P. Meyrath, J. L. Hanssen, G. N. Price, and M. G. Raizen, Physical Review Letters **95**, 260403 (2005).

[79] F. Serwane, G. Zürn, T. Lompe, T. B. Ottenstein, A. N. Wenz, and S. Jochim, Science **332**, 336 (2011).

[80] F. Serwane, *Deterministic preparation of a tunable few-fermion system*, Ph.D. thesis, Ruperto-Carola-University of Heidelberg (2011).

[81] G. Zürn, A. N. Wenz, S. Murmann, A. Bergschneider, T. Lompe, and S. Jochim, Physical Review Letters **111**, 175302 (2013).

[82] A. N. Wenz, G. Zürn, S. Murmann, I. Brouzos, T. Lompe, and S. Jochim, Science **342**, 457 (2013).

[83] S. Murmann, F. Deuretzbacher, G. Zürn, J. Bjerlin, S. M. Reimann, L. Santos, T. Lompe, and S. Jochim, Physical Review Letters **115**, 215301 (2015).

[84] G. Zürn, *Deterministic preparation of a tunable few-fermion system*, Ph.D. thesis, Ruperto-Carola-University of Heidelberg (2012).

[85] A. M. Dudarev, M. G. Raizen, and Q. Niu, Physical Review Letters **98**, 063001 (2007).

[86] G. Zürn, F. Serwane, T. Lompe, A. N. Wenz, M. G. Ries, J. E. Bohn, and S. Jochim, Physical Review Letters **108**, 075303 (2012).

[87] A. Szabo and N. S. Ostlund, *Modern quantum chemistry* (McGraw-Hill, 1989).

[88] F. Jensen, *Introduction to computational chemistry.* (Wiley, 2007).

[89] R. Martin, *Electronic structure* (Cambridge University Press, 2008).

[90] E. P. Gross, Il Nuovo Cimento **20**, 454 (1961).

[91] L. P. Pitaevskii, Soviet Physics JETP-USSR **13**, 451 (1961).

[92] I. Shavitt and R. J. Bartlett, *Many–Body Methods in Chemistry and Physics* (Cambridge University Press, 2009).

[93] D. Cremer, Wiley Interdisciplinary Reviews: Computational Molecular Science **1**, 509 (2011).

[94] C. Møller and M. S. Plesset, Physical Review **46**, 618 (1934).

[95] P. Navrátil, S. Quaglioni, I. Stetcu, and B. R. Barrett, Journal of Physics G: Nuclear and Particle Physics **36**, 083101 (2009).

[96] C. Lanczos, Journal of Research of the National Bureau of Standards **45**, 255 (1950).

[97] W. E. Arnoldi, Quarterly of Applied Mathematics **9**, 17 (1951).

[98] J. C. Cremon, *Quantum few-body physics with the configuration interaction approach*, Ph.D. thesis, Lund University (2010).

[99] J. A. Pople, M. Head-Gordon, and K. Raghavachari, The Journal of Chemical Physics **87**, 5968 (1987).

[100] W. Magnus, Communications on Pure and Applied Mathematics **7**, 649 (1954).

[101] S. Klarsfeld and J. A. Oteo, Journal of Physics A: Mathematical and General **22**, 2687 (1989).

[102] C. Moler and C. Van Loan, SIAM Review **45**, 3 (2003).

[103] E. Süli and D. F. Mayers, *An Introduction to Numerical Analysis* (Cambridge University Press, 2003).

[104] S. Cox and P. Matthews, Journal of Computational Physics **176**, 430 (2002).

[105] S. Krogstad, Journal of Computational Physics **203**, 72 (2005).

[106] E. H. Lieb, R. Seiringer, and J. Yngvason, Physical Review A **61**, 043602 (2000).

[107] A. D. Jackson, G. M. Kavoulakis, B. Mottelson, and S. M. Reimann, Physical Review Letters **86**, 945 (2001).

[108] J. C. Cremon, G. M. Kavoulakis, B. R. Mottelson, and S. M. Reimann, Physical Review A **87**, 053615 (2013).

[109] J. C. Cremon, A. D. Jackson, E. O. Karabulut, G. M. Kavoulakis, B. R. Mottelson, and S. M. Reimann, Physical Review A **91**, 033623 (2015).

[110] V. Zakharov, Sov. Phys. JETP **34**, 62 (1972).

[111] V. Zakharov and A. Shabat, Sov. Phys. JETP **37**, 823 (1973).

[112] A. C. Scott, F. Y. F. Chu, and D. W. McLaughlin, Proceedings of the IEEE **61**, 1443 (1973).

[113] J. Denschlag, J. E. Simsarian, D. L. Feder, C. W. Clark, L. A. Collins, J. Cubizolles, L. Deng, E. W. Hagley, K. Helmerson, W. P. Reinhardt, S. L. Rolston, B. I. Schneider, and W. D. Phillips, Science **287**, 97 (2000).

[114] S. Burger, K. Bongs, S. Dettmer, W. Ertmer, K. Sengstock, A. Sanpera, G. V. Shlyapnikov, and M. Lewenstein, Physical Review Letters **83**, 5198 (1999).

[115] D. J. Frantzeskakis, Journal of Physics A: Mathematical and Theoretical **43**, 213001 (2010).

[116] S. Gupta, K. W. Murch, K. L. Moore, T. P. Purdy, and D. M. Stamper-Kurn, Physical Review Letters **95**, 143201 (2005).

[117] C. Ryu, M. F. Andersen, P. Cladé, V. Natarajan, K. Helmerson, and W. D. Phillips, Physical Review Letters **99**, 260401 (2007).

[118] B. E. Sherlock, M. Gildemeister, E. Owen, E. Nugent, and C. J. Foot, Physical Review A **83**, 043408 (2011).

[119] A. Ramanathan, K. C. Wright, S. R. Muniz, M. Zelan, W. T. Hill, C. J. Lobb, K. Helmerson, W. D. Phillips, and G. K. Campbell, Physical Review Letters **106**, 130401 (2011).

[120] S. Moulder, S. Beattie, R. P. Smith, N. Tammuz, and Z. Hadzibabic, Physical Review A **86**, 013629 (2012).

[121] J. Smyrnakis, M. Magiropoulos, G. M. Kavoulakis, and A. D. Jackson, Physical Review A **82**, 023604 (2010).

[122] R. Kanamoto, L. D. Carr, and M. Ueda, Physical Review A **81**, 023625 (2010).

[123] A. D. Jackson, J. Smyrnakis, M. Magiropoulos, and G. M. Kavoulakis, Europhysics Letters **95**, 30002 (2011).

[124] M. Cominotti, D. Rossini, M. Rizzi, F. Hekking, and A. Minguzzi, Physical Review Letters **113**, 025301 (2014).

[125] J. H. Eberly, N. B. Narozhny, and J. J. Sanchez-Mondragon, Physical Review Letters **44**, 1323 (1980).

[126] M. Greiner, O. Mandel, T. W. Hänsch, and I. Bloch, Nature **419**, 51 (2002).

[127] F. Meinert, M. J. Mark, E. Kirilov, K. Lauber, P. Weinmann, M. Gröbner, and H.-C. Nägerl, Physical Review Letters **112**, 193003 (2014).

[128] K. Huang and C. N. Yang, Physical Review **105**, 767 (1957).

[129] K. Huang, *Statistical mechanics* (Wiley, 1987).

[130] M. Olshanii and L. Pricoupenko, Physical Review Letters **88**, 010402 (2001).

[131] X.-J. Liu, H. Hu, and P. D. Drummond, Physical Review B **82**, 054524 (2010).

[132] X.-J. Liu, H. Hu, and P. D. Drummond, Physical Review A **82**, 023619 (2010).

[133] M. Rontani, J. R. Armstrong, Y. Yu, S. Åberg, and S. M. Reimann, Physical Review Letters **102**, 060401 (2009).

[134] J. Bjerlin, S. M. Reimann, and G. M. Bruun, Physical Review Letters **116**, 155302 (2016).

[135] R. Feynman, Progress in Low Temperature Physics **1**, 17 (1955).

[136] G. B. Hess and W. M. Fairbank, Physical Review Letters **19**, 216 (1967).

[137] A. L. Fetter, Reviews of Modern Physics **81**, 647 (2009).

[138] M. R. Matthews, B. P. Anderson, P. C. Haljan, D. S. Hall, C. E. Wieman, and E. A. Cornell, Physical Review Letters **83**, 2498 (1999).

[139] J. E. Williams and M. J. Holland, Nature **401**, 568 (1999).

[140] K. W. Madison, F. Chevy, W. Wohlleben, and J. Dalibard, Physical Review Letters **84**, 806 (2000).

[141] E. Hodby, G. Hechenblaikner, S. A. Hopkins, O. M. Maragò, and C. J. Foot, Physical Review Letters **88**, 010405 (2001).

[142] A. L. Fetter and A. A. Svidzinsky, Journal of Physics: Condensed Matter **13**, R135 (2001).

[143] A. A. Svidzinsky and A. L. Fetter, Physical Review A **62**, 063617 (2000).

[144] Y. Castin and R. Dum, The European Physical Journal D - Atomic, Molecular, Optical and Plasma Physics **7**, 399 (1999).

[145] D. A. Butts and D. S. Rokhsar, Nature **397**, 327 (1999).

[146] G. M. Kavoulakis, B. Mottelson, and C. J. Pethick, Physical Review A **62**, 063605 (2000).

[147] A. D. Jackson and G. M. Kavoulakis, Physical Review Letters **85**, 2854 (2000).

[148] G. F. Bertsch and T. Papenbrock, Physical Review Letters **83**, 5412 (1999).

[149] R. A. Smith and N. K. Wilkin, Physical Review A **62**, 061602 (2000).

[150] S. Sinha and Y. Castin, Physical Review Letters **87**, 190402 (2001).

[151] D. L. Feder, C. W. Clark, and B. I. Schneider, Physical Review A **61**, 011601 (1999).

[152] E. Lundh, J.-P. Martikainen, and K.-A. Suominen, Physical Review A **67**, 063604 (2003).

[153] K. Kasamatsu, M. Tsubota, and M. Ueda, Physical Review A **67**, 033610 (2003).

[154] C. Weiss and N. Teichmann, Physical Review Letters **100**, 140408 (2008).

[155] M. I. Parke, N. K. Wilkin, J. M. F. Gunn, and A. Bourne, Physical Review Letters **101**, 110401 (2008).

[156] D. Dagnino, N. Barberán, M. Lewenstein, and J. Dalibard, Nature Physics **5**, 431 (2009).

[157] D. Dagnino, N. Barberán, and M. Lewenstein, Physical Review A **80**, 053611 (2009).

[158] F. Fröwis, P. Sekatski, W. Dür, N. Gisin, and N. Sangouard, Reviews of Modern Physics **90**, 025004 (2018).

[159] O. Elgarøy and C. J. Pethick, Physical Review A **59**, 1711 (1999).

[160] B. Juliá-Díaz, A. D. Gottlieb, J. Martorell, and A. Polls, Physical Review A **88**, 033601 (2013).

[161] E. J. Mueller, Physical Review A **66**, 063603 (2002).

[162] S. Eckel, J. G. Lee, F. Jendrzejewski, N. Murray, C. W. Clark, C. J. Lobb, W. D. Phillips, M. Edwards, and G. K. Campbell, Nature **506**, 200 (2014).

[163] A. Muñoz Mateo, A. Gallemí, M. Guilleumas, and R. Mayol, Physical Review A **91**, 063625 (2015).

[164] A. Messiah, *Quantum mechanics* (Dover Publications, 1999).

[165] S. Choi, S. A. Morgan, and K. Burnett, Physical Review A **57**, 4057 (1998).

[166] Y. Shin, M. Saba, M. Vengalattore, T. A. Pasquini, C. Sanner, A. E. Leanhardt, M. Prentiss, D. E. Pritchard, and W. Ketterle, Physical Review Letters **93**, 160406 (2004).

[167] J. R. Abo-Shaeer, C. Raman, J. M. Vogels, and W. Ketterle, Science **292**, 476 (2001).

[168] H. Saarikoski, S. M. Reimann, A. Harju, and M. Manninen, Reviews of Modern Physics **82**, 2785 (2010).

[169] G. Baym, Journal of Low Temperature Physics **138**, 601 (2005).

[170] N. Cooper, Advances in Physics **57**, 539 (2008).

[171] N. K. Wilkin, J. M. F. Gunn, and R. A. Smith, Physical Review Letters **80**, 2265 (1998).

[172] N. R. Cooper and N. K. Wilkin, Physical Review B **60**, R16279 (1999).

[173] S. Viefers, Journal of Physics: Condensed Matter **20**, 123202 (2008).

[174] V. Schweikhard, I. Coddington, P. Engels, V. P. Mogendorff, and E. A. Cornell, Physical Review Letters **92**, 040404 (2004).

[175] D. Peter, A. Griesmaier, T. Pfau, and H. P. Büchler, Physical Review Letters **110**, 145303 (2013).

[176] A. MacDonald, S. E. Yang, and M. Johnson, Australian Journal of Physics **46**, 345 (1993).

[177] T. H. Oosterkamp, J. W. Janssen, L. P. Kouwenhoven, D. G. Austing, T. Honda, and S. Tarucha, Physical Review Letters **82**, 2931 (1999).

[178] M. Toreblad, M. Borgh, M. Koskinen, M. Manninen, and S. M. Reimann, Physical Review Letters **93**, 090407 (2004).

[179] C. d. C. Chamon and X. G. Wen, Physical Review B **49**, 8227 (1994).

[180] E. Goldmann and S. R. Renn, Physical Review B **60**, 16611 (1999).

[181] S. M. Reimann, M. Koskinen, M. Manninen, and B. R. Mottelson, Physical Review Letters **83**, 3270 (1999).

[182] F. Ancilotto, Physical Review A **92**, 061602 (2015).

[183] M. A. Baranov, K. Osterloh, and M. Lewenstein, Physical Review Letters **94**, 070404 (2005).

[184] A. Bohr and B. R. Mottelson, *Nuclear structure* (W.A. Benjamin, 1969).

[185] A. T. B. Gilbert, N. A. Besley, and P. M. W. Gill, The Journal of Physical Chemistry A **112**, 13164 (2008).

[186] P. Pulay, Chemical Physics Letters **73**, 393 (1980).

[187] B. T. Seaman, M. Krämer, D. Z. Anderson, and M. J. Holland, Physical Review A **75**, 023615 (2007).

[188] D. Stadler, S. Krinner, J. Meineke, J.-P. Brantut, and T. Esslinger, Nature **491**, 736 (2012).

[189] S. Krinner, D. Stadler, D. Husmann, J.-P. Brantut, and T. Esslinger, Nature **517**, 64 (2015).

[190] L. H. Kristinsdóttir, O. Karlström, J. Bjerlin, J. C. Cremon, P. Schlagheck, A. Wacker, and S. M. Reimann, Physical Review Letters **110**, 085303 (2013).

[191] L. Amico, G. Birkl, M. Boshier, and L.-C. Kwek, New Journal of Physics **19**, 020201 (2017).

[192] J. A. Pople, J. S. Binkley, and R. Seeger, International Journal of Quantum Chemistry **10**, 1 (1976).

[193] J. A. Pople, R. Seeger, and R. Krishnan, International Journal of Quantum Chemistry **12**, 149 (1977).

[194] R. Krishnan and J. A. Pople, International Journal of Quantum Chemistry **14**, 91 (1978).

[195] R. Krishnan, M. J. Frisch, and J. A. Pople, The Journal of Chemical Physics **72**, 4244 (1980).

Appendix A

Møller-Plesset perturbation theory

As discussed in Sec. 3.2 using the Hartree-Fock ground state as the reference state in many-body perturbation theory for a fermionic system leads to Møller-Plesset perturbation theory [94]. After applying the formulas for Rayleigh-Schrödinger perturbation theory to the perturbation in Eq. (3.7) one may use the Slater-Condon rules [88] to express the energy corrections in terms of two-body matrix elements of the Hartree-Fock orbitals [192–195]. The first order correction is given by

$$E_{MP}^{(1)} = -\frac{1}{2}\sum_{ij}^{\text{occ}} \langle ij\,||\,ij\rangle, \tag{A.1}$$

where $\langle ij\,||\,kl\rangle = \langle ij\,|\hat{V}_{\text{int}}|kl\rangle - \langle ij\,|\hat{V}_{\text{int}}|lk\rangle$ and the sums are over the occupied orbitals. To first order, the total energy is the Hartree-Fock energy [88]. Continuing, the second order correction

$$E_{MP}^{(2)} = \frac{1}{4}\sum_{ij}^{\text{occ}}\sum_{ab}^{\text{vir}} \langle ij\,||\,ab\rangle a_{ij}^{ab} \tag{A.2}$$

with $a_{ij}^{ab} = (\epsilon_i + \epsilon_j - \epsilon_a - \epsilon_b)^{-1}\langle ab\,||\,ij\rangle$ and where the sums over a and b are over the virtual, unoccupied, orbitals. This is Eq. (3.8). The third order correction can

similarly be expressed as

$$\begin{aligned} E_{\mathrm{MP}}^{(3)} =& \frac{1}{8}\sum_{ij}^{\mathrm{occ}}\sum_{abcd}^{\mathrm{vir}}(a_{ij}^{ab})^* a_{ij}^{cd}\langle ab\,||cd\rangle \\ &+\frac{1}{8}\sum_{ijkl}^{\mathrm{occ}}\sum_{ab}^{\mathrm{vir}}(a_{ij}^{ab})^* a_{kl}^{ab}\langle kl\,||ij\rangle \\ &+\sum_{ijk}^{\mathrm{occ}}\sum_{abc}^{\mathrm{vir}}(a_{ij}^{ab})^* a_{kj}^{cb}\langle ak\,||ic\rangle. \end{aligned} \tag{A.3}$$

At the fourth order, the expressions become more cumbersome. The fourth order energy correction can be divided into five different terms according to what type of substitutions they include:

$$E_{MP}^{(4)} = E_S^{(4)} + E_D^{(4)} + E_T^{(4)} + E_Q^{(4)} + {}_R^{(4)}\,. \tag{A.4}$$

Here $E_R^{(4)}$ is the so called renormalization term. For single substitutions s of the occupied orbital i with the virtual orbital a, we have

$$E_S^{(4)} = \sum_s^{\mathcal{S}} \frac{|u_s|^2}{(E_0 - E_s)}, \tag{A.5}$$

where $\mathcal{S}$ is the set of all single substitutions and

$$u_i^a = -\frac{1}{2}\sum_j^{\mathrm{occ}}\sum_{bc}^{\mathrm{vir}}\langle ja||bc\rangle a_{ij}^{bc} - \frac{1}{2}\sum_{jk}^{\mathrm{occ}}\sum_b^{\mathrm{vir}}\langle jk||ib\rangle a_{jk}^{ab}. \tag{A.6}$$

The contributions from the double substitutions have a similar expression

$$E_D^{(4)} = \sum_t^{\mathcal{D}} \frac{|u_t|^2}{(E_0 - E_t)}, \tag{A.7}$$

where, for the double substitution $t : ij \to ab$ in the set $\mathcal{D}$ of all such substitutions,

$$\begin{aligned} u_{ij}^{ab} =& \frac{1}{2}\sum_{cd}^{\text{vir}} \langle ab||cd\rangle a_{ij}^{cd} + \frac{1}{2}\sum_{kl}^{\text{occ}} \langle kl||ij\rangle a_{kl}^{ab} \\ & - \frac{1}{2}\sum_{k}^{\text{occ}}\sum_{c}^{\text{vir}} \Big(\langle kb||jc\rangle a_{ik}^{ac} + \langle ka||jc\rangle a_{ik}^{cb} \\ & + \langle kb||ic\rangle a_{kj}^{ac} + \langle ka||ic\rangle a_{kj}^{cb} \Big) . \end{aligned} \tag{A.8}$$

The contribution from quadruple substitutions can be expressed as

$$E_Q^{(4)} = \sum_{t}^{\mathcal{D}} a_t y_t, \tag{A.9}$$

where

$$\begin{aligned} y_{ij}^{ab} =& \frac{1}{4}\sum_{kl}^{\text{occ}}\sum_{cd}^{\text{vir}} \langle kl||cd\rangle \Big(a_{ij}^{ab} a_{kl}^{cd} + a_{ij}^{cd} a_{kl}^{ab} \\ & - 2\left(a_{ij}^{ac} a_{kl}^{bd} + a_{ij}^{bd} a_{kl}^{ac} \right) - 2\left(a_{ik}^{ab} a_{jl}^{cd} + a_{ik}^{cd} a_{jl}^{ab} \right) \\ & + 4\left(a_{ik}^{ac} a_{jl}^{bd} + a_{ik}^{bd} a_{jl}^{ac} \right) \Big) . \end{aligned} \tag{A.10}$$

It can be shown that the terms $E_S^{(4)}$, $E_D^{(4)}$ and $E_T^{(4)}$ are proportional to N, i.e. they are size extensive. This is also true for the total energy corrections at all order in Møller-Plesset perturbation theory [92]. The renormalization term $E_R^{(4)}$ turns out to be proportional to N^2, such that there must be a part or the whole of $E_Q^{(4)}$ cancels it. It was found that it is the first term in Eq. (A.10) which is responsible for this [194]. By excluding the canceling terms the calculation can be performed faster. From this one may also see that excluding the term $E_T^{(4)}$ gives an approximate value of the fourth order energy contribution that is still size extensive [194].

If one would like to include also the triple substitution contributions, an expression for these can be found in [195]. Going to higher orders is straightforward, but as already the triple substitutions are difficult to include for computational reasons, the higher order terms are unlikely to be useful in general. A review of the development of higher order Møller-Plesset perturbation theory in quantum chemistry can be found in [93].

Appendix B

Quadratic configuration interaction

As mentioned in Sec. 3.3 the quadratic configuration interaction equations can be expressed using two-body matrix elements [99]. As the reference state $|\Psi_0\rangle$, the Hartree-Fock state is chosen. The energy of the eigenstate $|\Psi\rangle$ is assumed to be given by $E = E_{HF} + E_{\mathrm{QCISD}} + \Delta E_T$ where E_{HF} is the Hartree-Fock energy, E_{QCISD} is the correlation energy from the single and double substitutions and ΔE_T is the energy correction when considering triple substitutions as a perturbation.

Starting with the correlation energy from single and double substitutions, we have

$$E_{\mathrm{QCISD}} = \frac{1}{4}\sum_{ij}^{\mathrm{occ}}\sum_{ab}^{\mathrm{vir}}\langle ij\,||ab\rangle a_{ij}^{ab}. \tag{B.1}$$

This equation looks the same as the second order correction in Møller-Plesset perturbation theory, Eq. (A.2). However, the coefficients a_{ij}^{ab} are here obtained by solving the following equations iteratively

$$a_i^a = -[u_i^a + v_i^a]\,(\epsilon_a - \epsilon_i)^{-1} \tag{B.2}$$

$$a_{ij}^{ab} = -[\langle ab\,||ij\rangle + u_{ij}^{ab} + v_{ij}^{ab}]\,\left(\epsilon_a + \epsilon_b - \epsilon_i - \epsilon_j\right)^{-1}, \tag{B.3}$$

where ϵ_i is the corresponding eigenvalue for orbital i. The vectors u and v are given

by

$$u_i^a = -\sum_j^{\text{occ}} \sum_b^{\text{vir}} \langle ja||ib\rangle a_j^b - \frac{1}{2}\sum_j^{\text{occ}} \sum_{bc}^{\text{vir}} \langle ja||bc\rangle a_{ij}^{bc} - \frac{1}{2}\sum_{jk}^{\text{occ}} \sum_b^{\text{vir}} \langle jk||ib\rangle a_{jk}^{ab} \tag{B.4}$$

$$\begin{aligned} u_{ij}^{ab} = &\sum_c^{\text{vir}} \left[\langle ab||cj\rangle a_i^c - \langle ab||ci\rangle a_j^c\right] + \sum_k^{\text{occ}} \left[-\langle kb||ij\rangle a_k^a + \langle ka||ij\rangle a_k^b\right] \\ &+ \frac{1}{2}\sum_{cd}^{\text{vir}} \langle ab||cd\rangle a_{ij}^{cd} + \frac{1}{2}\sum_{kl}^{\text{occ}} \langle kl||ij\rangle a_{kl}^{ab} \\ &- \sum_k^{\text{occ}} \sum_c^{\text{vir}} \left[\langle kb||jc\rangle a_{ik}^{ac} + \langle ka||jc\rangle a_{ik}^{cb} + \langle kb||ic\rangle a_{kj}^{ac} + \langle ka||ic\rangle a_{kj}^{cb}\right] \end{aligned} \tag{B.5}$$

and

$$v_i^a = \frac{1}{2}\sum_{jk}^{\text{occ}} \sum_{bc}^{\text{vir}} \langle jk||bc\rangle \left[a_i^b a_{jk}^{ca} + a_j^a a_{ik}^{cb} + 2a_j^b a_{ik}^{ac}\right] \tag{B.6}$$

$$\begin{aligned} v_{ij}^{ab} = \frac{1}{4}\sum_{kl}^{\text{occ}} \sum_{cd}^{\text{vir}} &\left[a_{ij}^{cd} a_{kl}^{ab} - 2\left(a_{ij}^{ac} a_{kl}^{bd} + a_{ij}^{bd} a_{kl}^{ac}\right)\right. \\ &\left. -2\left(a_{ik}^{ab} a_{jl}^{cd} + a_{ik}^{cd} a_{jl}^{ab}\right) + 4\left(a_{ik}^{ac} a_{jl}^{bd} + a_{ik}^{bd} a_{jl}^{ac}\right)\right], \end{aligned} \tag{B.7}$$

where for the first iteration they are taken to be zero, i.e. $u = v = 0$.

The effect of the triple-substitutions can be calculated by

$$\Delta E_T = -\frac{1}{36}\sum_{ijk}^{\text{occ}} \sum_{abc}^{\text{vir}} \frac{\left(2\bar{u}_{ijk}^{abc} + \bar{\bar{u}}_{ijk}^{abc}\right)\bar{\bar{u}}_{ijk}^{abc}}{\epsilon_a + \epsilon_b + \epsilon_c - \epsilon_i - \epsilon_j - \epsilon_k}, \tag{B.8}$$

where

$$\begin{aligned} \bar{u}_{ijk}^{abc} = &\, a_i^a\langle jk||bc\rangle + a_i^b\langle jk||ca\rangle + a_i^c\langle jk||ab\rangle \\ &+ a_j^a\langle ki||bc\rangle + a_j^b\langle ki||ca\rangle + a_j^c\langle ki||ab\rangle \\ &+ a_k^a\langle ij||bc\rangle + a_k^b\langle ij||ca\rangle + a_k^c\langle ij||ab\rangle \end{aligned} \tag{B.9}$$

and

$$\begin{aligned}\bar{\bar{u}}_{ijk}^{abc} = \sum_{e}^{\text{vir}} \Big[& a_{ij}^{ae}\langle bc||ek\rangle + a_{ij}^{be}\langle ca||ek\rangle + a_{ij}^{ce}\langle ab||ek\rangle \\ & + a_{ki}^{ae}\langle bc||ej\rangle + a_{ki}^{be}\langle ca||ej\rangle + a_{ki}^{ce}\langle ab||ej\rangle \\ & + a_{jk}^{ae}\langle bc||ei\rangle + a_{jk}^{be}\langle ca||ei\rangle + a_{jk}^{ce}\langle ab||ei\rangle \Big] \\ + \sum_{m}^{\text{occ}} \Big[& a_{im}^{ab}\langle cm||jk\rangle + a_{im}^{bc}\langle am||jk\rangle + a_{im}^{ca}\langle bm||jk\rangle \\ & + a_{jm}^{ab}\langle cm||ki\rangle + a_{jm}^{bc}\langle am||ki\rangle + a_{jm}^{ca}\langle bm||ki\rangle \\ & + a_{km}^{ab}\langle cm||ij\rangle + a_{km}^{bc}\langle am||ij\rangle + a_{km}^{ca}\langle bm||ij\rangle \Big] . \end{aligned} \tag{B.10}$$

Appendix C

Exponential time differencing

Continuing from Sec. 3.4 we here present the complete formula for time-propagation using the method of exponential time differencing from Ref. [105]. After inserting the approximation Eq. (3.20) into Eq. (3.19) the latter can be solved exactly [104]. One then ends up with the following equation for propagating one time-step forward

$$\mathbf{c}(t+\Delta t) = e^{-\frac{i}{\hbar}\mathbf{H}_0\Delta t}\mathbf{c}(t) + \sum_{k=1}^{m} \Delta t^k \phi_k(\Delta t)\mathbf{b}_{k-1}, \tag{C.1}$$

where $\phi_k(\Delta t)$ is given by

$$\phi_k(\Delta t) = \frac{1}{\Delta t^k}\int_0^{\Delta t} \frac{\tau^{k-1}}{(k-1)!} e^{-\frac{i}{\hbar}\mathbf{H}_0(\Delta t-\tau)} \mathrm{d}\tau. \tag{C.2}$$

These can also be obtained via a recursion equation, starting from

$$\phi_1(\Delta t) = \left(e^{-\frac{i}{\hbar}\mathbf{H}_0\Delta t} - 1\right)\left(-\frac{i}{\hbar}\mathbf{H}_0\Delta t\right)^{-1} \tag{C.3}$$

which is easily computed as $\mathbf{H}_0$ is diagonal and with subsequent ϕ_k's given by

$$\phi_k(\Delta t) = \left(\phi_{k-1}(\Delta t) - \frac{1}{(k-1)!}\right)\left(-\frac{i}{\hbar}\mathbf{H}_0\Delta t\right)^{-1}. \tag{C.4}$$

Seeing that the integrand $\mathbf{I}(\tau)$ in Eq. (3.20) is a function of the variable τ, one might get the coefficients $\mathbf{b}_k$ by a Taylor expansion. However, using a fourth order continuous Runge-Kutta scheme to approximate the coefficients might lead to better properties of the algorithm [105]. Such a scheme leads to the following equations

$$
\begin{aligned}
\mathbf{c}_{(1)} &= \mathbf{c}(t) && \mathbf{k}_1 = -\frac{i}{\hbar}\mathbf{H}_I(t)\mathbf{c}_{(1)} \\
\mathbf{c}_{(2)} &= e^{-\frac{i}{\hbar}\mathbf{H}_0\frac{\Delta t}{2}}\mathbf{c}_{(1)} && \mathbf{k}_2 = -\frac{i}{\hbar}\mathbf{H}_I(t+\frac{\Delta t}{2})\mathbf{c}_{(2)} \\
&\quad + \frac{\Delta t}{2}\phi_1(\frac{\Delta t}{2})\mathbf{k}_1 \\
\mathbf{c}_{(3)} &= e^{-\frac{i}{\hbar}\mathbf{H}_0\frac{\Delta t}{2}}\mathbf{c}_{(1)} && \mathbf{k}_3 = -\frac{i}{\hbar}\mathbf{H}_I(t+\frac{\Delta t}{2})\mathbf{c}_{(3)} \\
&\quad + \frac{\Delta t}{2}\left[\phi_1(\frac{\Delta t}{2}) - 2\phi_2(\frac{\Delta t}{2})\right]\mathbf{k}_1 \\
&\quad + \Delta t\phi_2(\frac{\Delta t}{2})\mathbf{k}_2 \\
\mathbf{c}_{(4)} &= e^{-\frac{i}{\hbar}\mathbf{H}_0\Delta t}\mathbf{c}_{(1)} && \mathbf{k}_4 = -\frac{i}{\hbar}\mathbf{H}_I(t+\Delta t)\mathbf{c}_{(4)} \\
&\quad + \Delta t\left[\phi_1(\Delta t) - 2\phi_2(\Delta t)\right]\mathbf{k}_1 \\
&\quad + \Delta t\phi_2(\Delta t)2\mathbf{k}_3
\end{aligned}
\tag{C.5}
$$

and the final equation for performing a step in time

$$
\begin{aligned}
\mathbf{c}(t+\Delta t) = e^{-\frac{i}{\hbar}\mathbf{H}_0\Delta t}\mathbf{c}(t) \\
&+ \Delta t\left[4\phi_3(\Delta t) - 3\phi_2(\Delta t) + \phi_1(\Delta t)\right]\mathbf{k}_1 \\
&+ \Delta t\left[-4\phi_3(\Delta t) + 2\phi_2(\Delta t)\right](\mathbf{k}_2 + \mathbf{k}_3) \\
&+ \Delta t\left[4\phi_3(\Delta t) - \phi_2(\Delta t)\right]\mathbf{k}_4.
\end{aligned}
\tag{C.6}
$$

The papers